

GEOLOGICA ULTRAIECTINA

Mededelingen van de  
Faculteit Aardwetenschappen  
Universiteit Utrecht

No. 226

**Three-dimensional modelling of thrust-controlled  
foreland basin stratigraphy**

Quintijn Clevis

Cover illustration: Evolution of deltaic drainage patterns in the foreland basin model presented in this thesis.

This research was carried out at the Sedimentology Group,  
Faculty of Earth Sciences, Utrecht University.

*Address:*

*Budapestlaan 4  
PO Box 80021  
3508 TA Utrecht  
The Netherlands*



*Internet site: [www.geo.uu.nl/Research/Sedimentology](http://www.geo.uu.nl/Research/Sedimentology)*

ISBN: 90-5744-085-7

**Three-dimensional modelling of thrust-controlled  
foreland basin stratigraphy**

**Een drie-dimensionale modelstudie van voorlandbekken  
stratigrafie gecontroleerd door overschuivings tektoniek**

*(met een samenvatting in het Nederlands)*

Proefschrift

ter verkrijging van de graad van doctor

aan de Universiteit Utrecht

op gezag van de Rector Magnificus, Prof. Dr. W.H. Gispen,

ingevolge het besluit van het College van Promoties

in het openbaar te verdedigen

op maandag 19 mei 2003 des namiddags te 4.15 uur

door

Quintus Johannes Wilhelmus Antonius Clevis

geboren op 27 februari 1975

te Broekhuizen

Promotor: Prof. Dr. P.L. de Boer  
Faculty of Earth Sciences  
Utrecht University

Co-promotor: Dr. W. Nijman  
Faculty of Earth Sciences  
Utrecht University

*Out of theories we create a world: not the real world,  
but our own nets in which we try to catch the real world*

– Karl Popper

*Voor Saskia*

**Members of the dissertation committee:**

Prof. Dr. P.A. Burrough

Faculty of Geographical Sciences, Utrecht University  
Utrecht, The Netherlands

Prof. Dr. S.A.P.L. Cloetingh

Faculty of Earth Sciences, Free University  
Amsterdam, The Netherlands

Prof. Dr. S.B. Kroonenberg

Faculty of Applied Earth Sciences, Delft University of Technology  
Delft, The Netherlands

Dr. G.E. Tucker

School of Geography and the Environment, Oxford University  
Oxford, United Kingdom

Dr. C.J. van der Zwan

Shell International Exploration and Production  
Rijswijk, The Netherlands

## Table of contents

<b>1. Introduction</b>	<b>11</b>
1.1 General introduction	11
1.2 Foreland basins	13
1.2.1 Foreland basin definition	13
1.2.2 Underfilled versus overfilled foreland basins	13
1.2.3 Two-phase foreland basin concept	15
1.2.4 Structural segmentation of the foreland and the creation of thrust-sheet top basins	17
1.3 Stratigraphic simulation models	17
1.3.1 Why stratigraphic modelling?	17
1.3.2 Overview of modelling methods	18
1.4 Model scope and description	21
1.4.1 Model scope	21
1.4.2 Model description and flow chart	22
1.5 Aim and outline of this thesis	24
<b>2. Numerical modelling of drainage basin evolution     and three-dimensional alluvial fan stratigraphy</b>	<b>27</b>
2.1 Introduction	27
2.2 Methodology	30
2.2.1 Geomorphic and stratigraphic model	30
2.2.2 Perfect sorting	35
2.2.3 Handling depressions in the grid	35
2.2.4 Tectonic mass translation	36
2.2.5 Flexure and basin subsidence	36
2.3 Numerical experiments	38
2.3.1 The effect of variable bedrock erodability and vertical displacement rate	38
2.3.2 The effect of pulsating tectonic activity on alluvial fan stratigraphy	44
2.3.3 The effect of pulsating tectonic activity and sinuous sea-level variation	48
2.3.4 Lag time in the depositional response	48
2.4 Discussion	51
2.5 Conclusions	54

<b>3. Differentiating the effect of tectonic pulsation and eustatic sea-level fluctuation in foreland basins filled by alluvial fans and axial deltaic systems</b>	<b>55</b>
3.1 Introduction	56
3.2 Modelling method	59
3.2.1 Earlier modelling studies	59
3.2.2 Model used in this study	59
3.2.3 Surface processes	60
3.2.4 Tectonic processes	64
3.2.5 Tectonic and eustatic forcing	64
3.3 Experimental results	65
3.3.1 Geomorphic response to tectonic and eustatic change	65
3.3.2 Response of the axial-alluvial system to tectonic and eustatic change	67
3.3.3 Foreland basin landscapes	67
3.3.4 Three-dimensional basin fill	70
3.3.5 Three-dimensional visualization of subsurface channel belts	77
3.4 Discussion	79
3.5 Conclusions	81
<b>4. Stratigraphic signatures of translation of thrust-sheet top basins over low-angle detachment faults</b>	<b>83</b>
4.1 Introduction	83
4.2 Numerical model	85
4.2.1 Basin geometry	85
4.2.2 Horizontal translation of thrust-sheet top stratigraphy	87
4.2.3 Three-dimensional flexure	89
4.2.4 Submarine slope collapse and mass-flow deposition	90
4.2.5 Model scenarios	91
4.3 Experimental results	92
4.3.1 Thrust-sheet top basin landscape evolution	92
4.3.2 Evolution of the accommodation space	93
4.3.3 Thrust-sheet top basin sequence architecture	98
4.3.4 The delta-slope stratigraphy in the adjacent basin	99
4.3.5 Correlation of mass-flow events to the eustatic signal	99



4.4 Discussion	101
4.4.1 Fluvial patterns	101
4.4.2 Stratigraphy	102
4.4.3 Temporal sediment storage on thrust-sheet top basins	103
4.5 Conclusions	104
<b>5. Stratigraphic modelling using CHILD</b>	<b>105</b>
5.1 Triangular irregular network	105
5.1.1 Reduction of artificial symmetry in stream networks	106
5.1.2 Representation of complex geometries	106
5.1.3 Horizontal translation	106
5.2 Channel Hillslope Integrated Landscape Development model, CHILD	107
5.2.1 Alluvial fans	107
5.2.2 River meandering	108
5.2.3 Basin fill	108
5.3 Conclusions	112
<b>6. Conclusions</b>	<b>113</b>
6.1 Drainage basins	113
6.2 Alluvial fans	114
6.3 Axial fluvio-deltaic system	114
<b>References</b>	<b>117</b>
<b>Samenvatting</b>	<b>127</b>
<b>Dankwoord - Acknowledgements</b>	<b>133</b>
<b>Curriculum Vitae</b>	<b>135</b>



## Introduction

### 1.1 General introduction

A common approach in sedimentary basin analysis is to formulate concepts that explain stratigraphic patterns observed in outcrop and subsurface as the product of the historical interplay between four fundamental variables: tectonics, sea-level change, climate and sediment supply. The purpose of these concepts is to differentiate the relative importance of the variables, quantify their individual rates and understand how their interaction controls erosion, transport and deposition of sediment. Applications of these concepts range from unravelling the geologic history of a specific basin, to the assessment of stratigraphic trapping mechanisms and reservoir heterogeneity.

At present conceptual models are able to explain the evolution of sedimentary systems involving a limited number of controlling variables or a single dominant one. A well-known, successful concept is sequence stratigraphy, which improved our understanding of the effect sea-level change on passive margin stratigraphy (Posamentier and Vail, 1988; Galloway, 1989). However, in active-margin foreland basins, developing adjacent to an evolving mountain belt, the dominance of a single variable such as sea level is less evident and likely to vary in space and time (Butler and Grasso, 1993; Schwans, 1995; Dreyer *et al.*, 1999). Here, the geometries of the sedimentary sequences that fill the basin and the unconformities that partition them, are governed by the interaction between variables. The number of interacting variables and the three-dimensional complexity of the basin filling process and product in these settings is substantial, and conceptual models are insufficient to comprehend the complete basin-fill development, due to the wide range of poorly understood interactions, feedback mechanisms and non-linear effects.

The objective of this thesis is to gain insight into the effects of changes in both single and interacting variables creating foreland basin stratigraphy, by means of coupling them quantitatively in a numerical forward model, which produces a three-dimensional stratigraphic record. The focus is on two main variables, repeated tectonic activity and eustatic sea-level variation and their combined effects on stacking patterns of the depositional systems and the character of the sequence-bounding unconformities.



## 1.2 Foreland basins

### 1.2.1 Foreland basin definition

Foreland basins develop in response to advancing thrust and fold loads by flexural subsidence (Price, 1973; Dickinson, 1974). They are found in two tectonic settings: as peripheral basins in regions of continent/continent collision and as retro-arc basins in locations of ocean/continent collision. Examples of peripheral foreland basins are the Molasse Basin north of the Alps, the Ebro Basin formed in response to the Pyrenees, the Po Basin related to the Apennines (Figure 1.1), and the Indo-Ganges Basin associated with the topographic load of the Himalayas. Retro-arc foreland basins are found east of the Rocky-Mountain front in the Laramide Province, in the Andes orogenic belt, and in western Taiwan. The basement of both types of basins consists of continental lithosphere. Their basic geometry and large-scale evolution are controlled by the rheological properties of the underlying lithosphere and its temporal development in response to loading. As a result of lithospheric adjustment upon thrust loading the basin subsidence is maximum immediately adjacent to the mountain belt and gradually decreases onto the foreland until eventually uplift occurs in the form of a structure commonly referred to as the *foreland or peripheral bulge* (Turcotte and Schubert, 1982). This asymmetric geometry is reflected in the distribution of the sequences filling the foreland basin. They thicken towards the orogen and show feathered edge pinch outs towards the foreland bulge.

### 1.2.2 Underfilled versus overfilled foreland basins

The relief created by thrusting in the orogenic wedge is eroded and provides the detritus to fill the foreland basin. In response to the long-term changing balance between flexural subsidence and sediment supply delivered by the growing orogen, the basin first goes through an *underfilled* stage, followed by an *overfilled* stage of evolution (cf. Covey, 1986). Underfilled foreland basins take the form of turbidite or *flysch*-filled troughs, reflecting low sediment supply due to limited subaerial orogenic relief versus high subsidence rates. High subsidence rates are caused by initial thrust loading upon previously rifted lithosphere, which is thinned and therefore weaker (Stockmal *et al.*, 1986; Desegaulx *et al.*, 1991). During the subsequent stage of overfill, the basin is characterised by *molasse*, shallow-marine and alluvial depositional facies, as the result of increased orogenic relief, enhanced erosion and, consequently higher sediment supply. The transition from the underfilled to overfilled foreland basin stage is often envisaged as a simple process, which takes place in a section perpendicular to the orogenic wedge on a time scale of  $n \times 10$  Myr (Figure 1.2). However, the transition also follows the sediment dispersal pattern parallel to the orogen, due to along-strike differences in orogenic convergence rate (Matter *et al.*, 1980; Puigdefabregas and Souquet, 1986; Ricci-Lucchi, 1986).

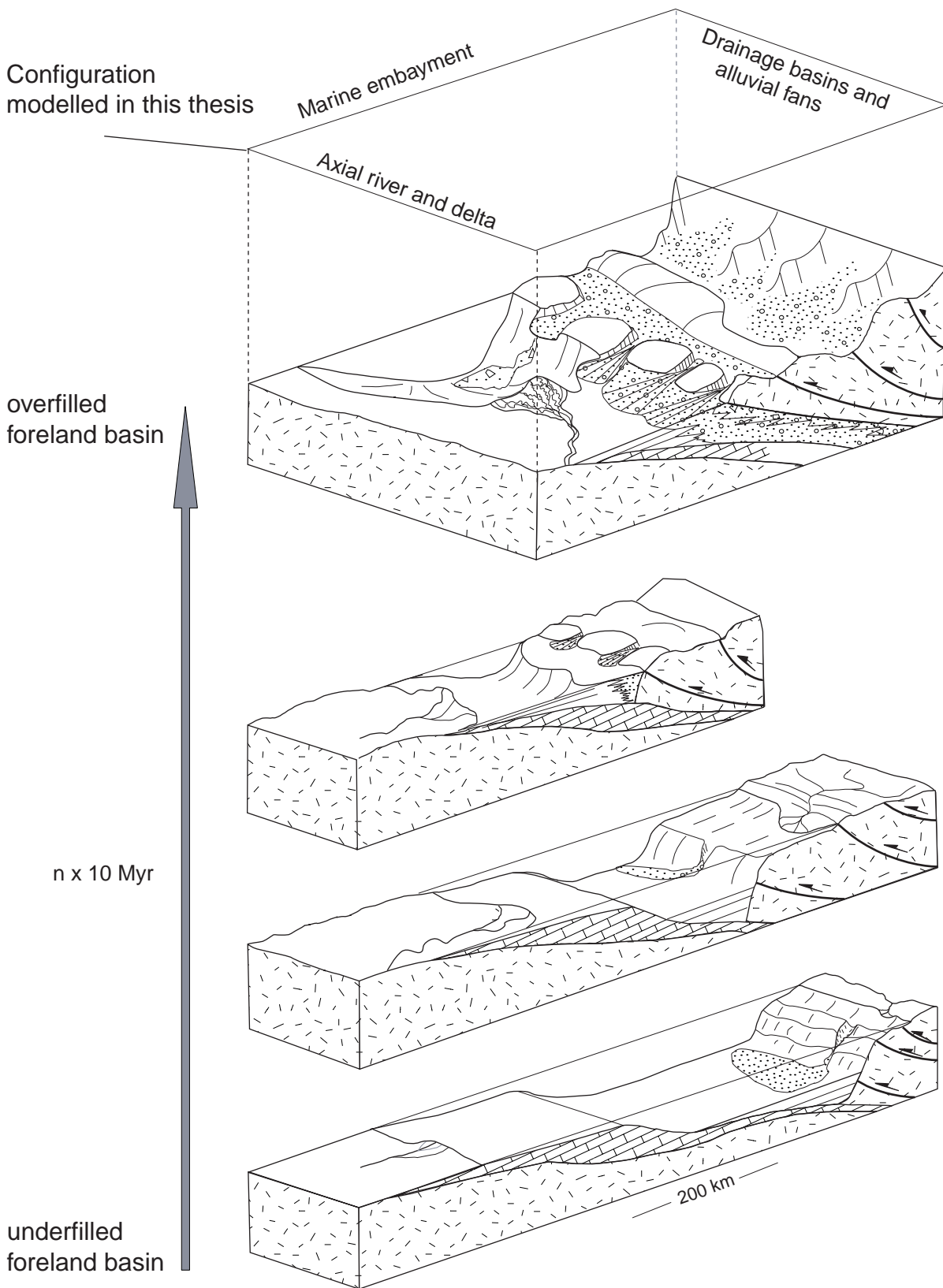


Figure 1.2 Block diagrams showing the schematic development of a foreland basin from underfill to overfill. The top block diagram illustrates the tectono-sedimentary configuration investigated in this thesis using numerical modelling experiments.

### 1.2.3 Two-phase foreland basin concept

A commonly applied concept in the molasse stage of a foreland basin is that of the ‘two-phase’ foreland basin system, controlled by the interplay between episodic thrusting and erosional unloading (Heller *et al.*, 1988; Jordan and Flemings, 1991). In this concept (Figure 1.3) periods of tectonic activity (phase 1) lead to thrust wedge loading and enhanced flexural subsidence at the rear of the basin, whereas the frontal forebulge experiences uplift and migrates towards the thrust front. The associated fluvial pattern in the foreland is that of a longitudinal river interlocked between the basin margin alluvial fans and the forebulge high. During a period of tectonic quiescence (phase 2), the thrust wedge is eroded and the amplitude of the forebulge diminishes while migrating outward. As a result of the erosion of the thrust wedge, the lithosphere is unloaded and the sediment accommodation space in the foreland basin is reduced. This is partly a self-sustaining process, as new material is continuously added from below and removed in efficient high-relief drainage basins. The reduction of basin accommodation space, combined with a high rate of sediment supply leads to widespread progradation of the alluvial fans, which now establish a dominant transversal drainage system (Burbank, 1992). Renewed tectonic activity results in a retreat of the alluvial fans by the increase of flexural accommodation space created close to the tectonic front. In addition, the flexural response again results in forebulge uplift, temporal erosion of distal foreland basin sediments and the creation of unconformities. Accordingly a repetitive tectonic activity/quiescence pattern is reflected as multiple cycles of gravel progradation into the foreland basin alternating with well-sorted axial sediments and forebulge unconformities.

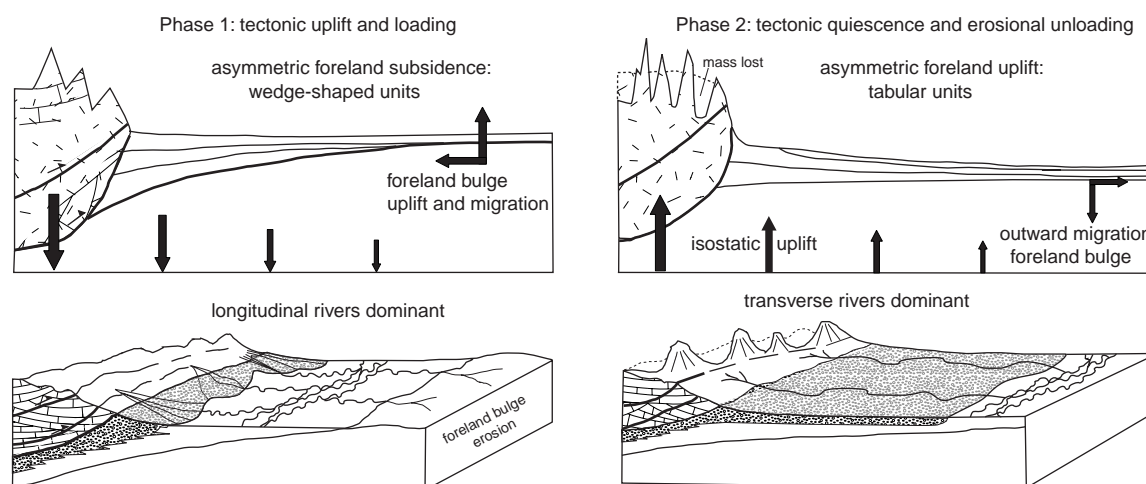


Figure 1.3 Two-phase foreland basin concept. Thrust wedge loading (phase 1) leads to flexural subsidence, whereas the frontal forebulge experiences uplift and migrates towards the thrust front. The fluvial pattern in the foreland is that of a longitudinal river interlocked between the basin margin alluvial fans and the forebulge high. During a period of tectonic quiescence (phase 2), the thrust wedge is eroded and the drainage is dominated by transverse alluvial fans (modified after Burbank, 1992).

A relatively instantaneous, elastic response of the lithosphere upon thrust loading and erosional unloading is assumed in the ‘two-phase’ foreland basin concept. Yet, another style of lithospheric behaviour, the visco-elastic response, is frequently advocated in literature and applied in model studies of foreland basins (Quinlan and Beaumont, 1984; Tankard, 1986). Visco-elastic models take into account time-dependent lithospheric processes such as thermo-mechanical weakening. These models are used to explain changes in basin geometry without changes in surface load. Inherently, visco-elastic models involve a relaxation time between loading of the orogenic wedge and lithospheric response. As yet, no well-documented case study exists that adequately assesses the value of the relaxation time in these settings from the stratigraphic record, and discrepancies exist between observed and modelled gravity anomalies (Watts, 2001).

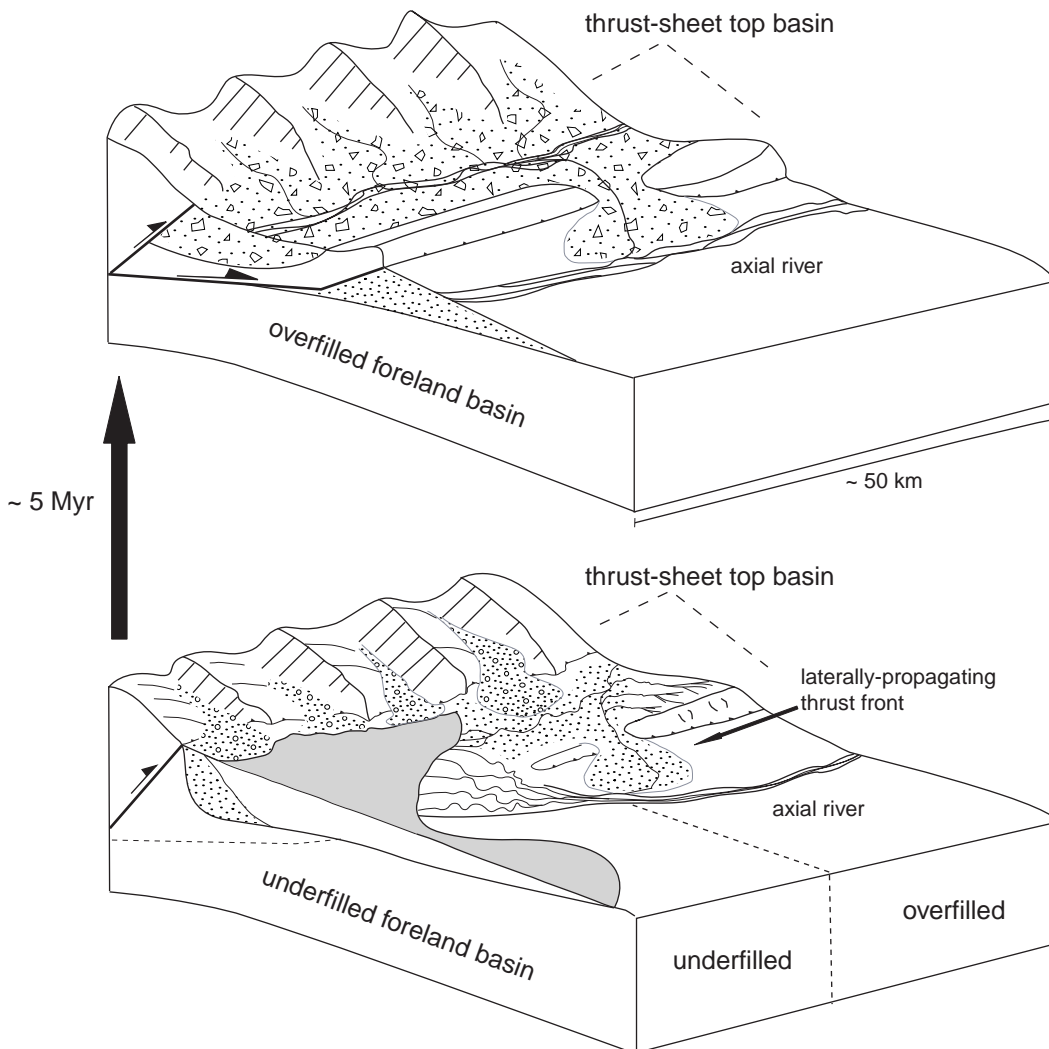


Figure 1.4 Segmentation of the foreland basin by a laterally propagating thrust front and the creation of a thrust-sheet top basin. Configurations such as this one are inferred from the thrust-sheet top basins of the Apennines (Ricci-Lucchi, 1986) and Pyrenees (Hirst and Nichols, 1986; Bentham et al., 1992; Ardevol et al., 2000). These basins show complex stratigraphic transitions from flysch (underfill) to molasse (overfill), parallel to the strike of the orogen.



#### ***1.2.4 Structural segmentation of the foreland and creation of thrust-sheet top basins.***

During both underfilled and overfilled phases the foreland basin sediments are progressively incorporated into the deformation of the advancing orogenic wedge (Figures 1.1 and 1.4). While sediment is being accumulated, the foreland basin sediments can be dissected by thrust structures or decoupled by shallow-dipping detachment faults in the subsurface. Consequently, the foreland basin is separated into sub-basins called piggyback basins or thrust-sheet top basins (Ori and Friend, 1984). The process of structural segmentation of the foreland basin during sedimentation results in complex sediment routing patterns where thrust-top basins spill over excess sediment into deeper, underfilled parts of the foreland basin (Ricci-Lucchi, 1986; Bentham *et al.*, 1992; Ardevol *et al.*, 2000). Again, the routing trend is parallel to the orogen during this process, but as finally all subbasins fill up, sediment transport patterns change from axial to transverse while cutting through the most frontal thrust structures at localized positions (Hirst and Nichols, 1986; Gupta, 1997).

### **1.3 Stratigraphic simulation models**

#### ***1.3.1 Why stratigraphic modelling?***

Stratigraphic simulation models are widely used in the academic and applied geological communities because of several reasons (cf. Waltham, 1992). Firstly, they are ideal teaching tools due to their interactive nature (Flemings and Grotzinger, 1996). The user gains insight into the long-term basin filling process and stratigraphy just by repeating a simulation while varying the intensity of tectonic, eustatic and climatic controls and comparing the stratigraphic results. Secondly, models are used to estimate unknown parameters (Helland-Hansen *et al.*, 1988). Observed geometries in a seismic section for example are the result of the complex interaction of these controls, most of the quantities such as sediment supply, subsidence rate, amplitude of sea-level change are partly unknown. The responsible set of controlling variables can be estimated within the limits of uniqueness by trying to match the stratigraphic simulation with the observed geometries. Existing field interpretations can, when quantified, be compared to each other in order to select the most likely of these ‘conceptual scenarios’. This approach may result in the recognition of unanticipated scenarios (Cross and Harbaugh, 1990; Watney *et al.*, 1999; Tipper, pers. com.). Thirdly, stratigraphic simulation is applied as a clever form of subsurface prediction (Wendebourg and Harbaugh, 1996), sometimes in combination with stochastic algorithms (Doligez *et al.*, 1999), or by conditional simulation constraint to well data (Karssenbergh *et al.*, 2001). Combined with hydrocarbon-maturation and migration modelling it allows an integrated assessment of sedimentary basin exploration potential (Wendebourg, 1997; Bagirov and Lerche, 1999).

Another important reason is that solely the construction and coding of a forward model forces the sedimentologists to recognise and quantify the main processes and variables involved, and to proceed

beyond the historical descriptive nature of their scientific discipline. Nevertheless, quantification of model input and model construction is not a straightforward task, as both are limited in their verification and validation (Oreskes *et al.*, 1994).

### **1.3.2 Overview of modelling methods**

Stratigraphic models are either static or dynamic. **Static stratigraphic models** are the result of the application of geostatistical methods in order to quantify and visualize subsurface natural resources. They are based on interpolation techniques (Deutsch and Journel, 1997), Markov statistics (Lin and Harbaugh, 1984; Carle *et al.*, 1998), fractals (North and Halliwell, 1994) or combinations of these stochastic algorithms (Tyler *et al.*, 1992). They have been successful in describing reservoir heterogeneity (Dubrule, 1989), but lack geological process-response relationships and temporal evolution.

**Dynamic stratigraphic models** in contrast focus on the suite of deterministic time-dependent processes that progressively fill a basin with sediment, as a function of geologically relevant external processes such as eustasy, tectonic activity and climate change. Dynamic models incorporate geological time either in a forward or in a backward sense. Forward models predict a stratigraphic response as function of a collection of interacting processes with a strong dependence on previous variables and configuration. Backward, or inverse models try to distil these variables or the evolutionary process from a known stratigraphic architecture in an automated fashion (Lessenger and Lerche, 1999). This has proven to be a difficult task, and many inverse models presented are actually pseudo-inverse models, by incorporating a forward model (Bornholdt *et al.*, 1999; Cross and Lessenger, 1999). Pseudo-inverse models try to approximate the suite of controlling variables within the limits of uniqueness (Heller *et al.*, 1993) by iteratively running and progressively adjusting a forward model until the model result matches the observation.

**Forward stratigraphic simulation models** are divided into two categories, geometric and dynamic, a distinction based on the detail and complexity of the method applied to simulate erosion and deposition of sediment. **Geometric models** approximate the net result of many erosion-deposition events on the basin fill patterns by using empirically determined large-scale geometries of depositional surfaces. These equilibrium profile-like geometries are translated and stacked as function of the bulk sediment supply and accommodation space. Examples of the geometric approach are found in two-dimensional models for general basin filling such as SEDPAK (Helland-Hansen *et al.*, 1988; Strobel *et al.*, 1989) and STRATAGEM (Aigner *et al.*, 1989; Lawrence *et al.*, 1990), and models for long-term coastal evolution (Cant, 1991; Cowell *et al.*, 1995). In particular, coastal geometric models are computationally fast, which makes them suitable for running multiple simulations. They allow extensive sensitivity analysis and quantitative comparison of model results to geological hypotheses (Storms *et al.*, 2002).

A different type of geometric model used by several workers is the Bridge and Leeder fluvial architecture model (Bridge, 1979). The original two-dimensional version uses a combination of empirically determined avulsion frequency and fixed floodplain overbank geometries to model the channel belt interconnectedness in alluvial basins. This model has been utilised in exploring the stratigraphic effects of an asymmetrically subsiding half graben (Alexander and Leeder, 1987) or to constrain stochastic modelling (Clements *et al.*, 1990). In the three-dimensional follow-up (Mackey and Bridge, 1995), a cellular channel belt positioning routine was incorporated.

**Dynamic models** have more attention for the process of erosion and sedimentation, and operate at a scale smaller than the resulting stratigraphic pattern. Again, one can distinguish two approaches, the fluid-flow models and the dynamic slope models.

**Fluid-flow models** apply engineering time-scale, sediment transport formulae (Bitzer and Plug, 1989; Syvitski *et al.*, 1998; Haupt *et al.*, 1999). One of the best-known and fully three-dimensional stratigraphic models in this category is SEDSIM (Tetzlaff and Harbaugh, 1989), which has been modified for application in hydrocarbon exploration (Griffiths *et al.*, 2001; Tetzlaff and Priddy, 2001). In this model, fluid flow and sediment transport of multiple grainsizes is solved using a simplification of the Navier-Stokes equation and the marker-in-cell method (Hockney and Eastwood, 1981). It is capable of dynamically adapting to a changing surface morphology and is currently extended with geostatistical procedures to assess the subsurface hydraulic conductivity of the generated stratigraphy (Tuttle and Wendebourg, 1999). Yet, this model approach demands very detailed spatial and temporal discretisation, and consequently the computational power needed to accumulate a stratigraphy over geologic time spans is substantial, just as the number of transport-related input variables. Hence, the computationally less demanding **dynamic-slope models** were more popular during the last two decades (Kenyon and Turcotte, 1985; Syvitski and Daughney, 1992; Flemings and Grotzinger, 1996). These models use diffusion as an approximation for sediment transport because of the method's ability to produce realistically looking delta clinoform profiles (Jervey, 1988; Kaufman *et al.*, 1991; Steckler *et al.*, 1993) and flexibility to work at a wide range of spatial and temporal scales. As a result of this flexibility, the published estimates for the apparent sediment diffusion coefficient vary from  $1 \times 10^{-4} \text{ m}^2/\text{yr}$  for degrading fault scarps (Colman and Watson, 1983) to  $5.6 \times 10^5 \text{ m}^2/\text{yr}$  for prograding deltas (Kenyon and Turcotte, 1985). Rivenas (1992) fundamentally extended the approach by incorporating two grainsizes with different diffusion coefficients. Multi-lithological diffusion models and empirical, rule-based models have evolved to the present generation of commercial simulation packages such as PHIL (2D) (Bowman and Vail, 1999) and DIONISOS (3D) (Granjeon and Joseph, 1999), by adding tectonic and user-friendly visualization routines.

With the recent progress from two- to three-dimensional stratigraphic modelling, it is recognized that complex fluid-flow models and diffusion-based dynamic slope models are inadequate to simulate

Reference and model name	Setting	Tectonic uplift / subsidence style	Flexure	Erosion and sedimentation	Stratigraphic attributes	Scale
Flinnings and Jordan, 1990	foreland	self-adapting critical wedge	elastic	diffusion	timelines and slope facies	200 km
Coakley and Wats, 1991	foreland	self-adapting critical wedge	elastic	diffusion	timelines	200 km
Sinclair <i>et al.</i> , 1991	foreland	self-adapting critical wedge	elastic	diffusion	timelines	200 km
Zoetemeijer, 1993	foreland	multiple fault-bend folds	elastic	geometric, flat fill to top	timelines	100 km
Paola <i>et al.</i> , 1992	-	single half graben	-	diffusion	timelines and perfect sorting	25 km
Waltham, 1992	rift basin	multiple half grabens	-	diffusion	timelines and slope facies	20 km
Peper, 1993	foreland	self-adapting critical wedge	elastic, intraplate stress	diffusion, facies dependent coefficient	timelines, and slope facies	200 km
Tucker and Slingerland, 1994, 1996 (GOLEM)	foreland, rift margin	sinuous fold pattern, block uplift	elastic	fluvial streampower following steepest descent path, diffusion on hillslopes, bedrock collapse	2D cross section with timelines	100 x 50 km, Δx 1 km
Hardy and Poblet, 1995	foreland	fault-bend fold	-	diffusion	timelines	10 km
Johnson and Beaumont, 1995 (DRAINAL)	foreland	self-adapting critical wedge	2D elastic, evaluated in multiple sections	fluvial streampower following steepest descent path, diffusion in marine realm	timelines, 3D fence diagrams showing streampower during deposition as facies	1500x750 km, Δx 15km
Chaleron, 1995	foreland	multiple fault-bend folds, thrust-sheet top basins	-	diffusion	timelines	50 x 50 km, Δx 500 m
Garcia-Castallanos, 1997, 2002 (DRAINAL)	foreland	fault-bend fold	3D elastic, visco-elastic	fluvial streampower transport following steepest descent path	timelines	500 x 500 km, Δx 10 km
Den Bezemer, 1998	foreland,	several fault-bend fold types	elastic	dual-lithology diffusion (Rivenetas, 1992)	timelines, grainsize distributions	10 km, Δx 100 m
Densmore <i>et al.</i> , 1998, 1999 (ZSCAPE)	-	half-graben	-	fluvial streampower transport following steepest descent path, bedrock collapse	no stratigraphy	10 x 10 km, Δx 100 m
van der Beek, 2002 (CASCADE)	foreland	fault-bend fold	-	fluvial streampower transport following steepest descent path, bedrock collapse	no stratigraphy	triangular, 40 x 40 km, Δx 500 m
Bernal and Hardy, 2002	foreland	fault-bend fold	-	diffusion	2D section timelines	10 km
Tucker <i>et al.</i> , 2002 (CHILD)	-	block uplift	-	fluvial streampower/shear stress transport following steepest descent path, two-fraction grainsize sorting (Wilcock, 1998), active meandering and overbank deposition	grainsize distributions in 2D section	triangular, 5 x 5 km, Δx 40 m
Clevis, <i>this thesis</i>	foreland	fault-bend fold, thrust-sheet top basins	2D elastic 'broken-plate', evaluated in multiple sections and 3D elastic flexure	fluvial streampower following steepest descent and bifurcating paths, diffusion in marine realm, collapse of oversteepened bedrock and delta clinoforms, distinction between axial deltas and alluvial fans, perfect grainsize sorting	3D fence diagrams in normal or time-space, user-defined timeline spacing in sections showing grainsize facies or relative sea-level change during deposition, voxel representation of channel belts or other sandstone bodies	75 x 75 km, Δx 100-500 m

Table 1.1 Chronological overview of coupled models and their basic functionality.

the details of channelized sediment transport on a topographic surface. New methods are required that are, on the one hand, capable of imitating fluvial patterns and sediment transport, and on the other hand are computationally more efficient than the fluid-flow models.

The transition to three-dimensional stratigraphic modelling is currently taking place by applying methods developed in the geomorphologic and GIS community, such as cellular flow algorithms (Freeman, 1991; Burrough and McDonnell, 1998) and streampower-based sediment transport, commonly used in models for long-term landscape evolution (Willgoose *et al.*, 1991; Chase, 1992; Howard, 1994; Tucker, 1996b) and soil erosion (Kirkby, 1992). Examples are the foreland basin model of Johnson (Johnson and Beaumont, 1995), delta simulators (Ritchie *et al.*, 1999; Meijer, 2002) and carbonate models (Burgess *et al.*, 2001; Warrlich *et al.*, 2002).

## 1.4 Model scope and description

### 1.4.1 Model scope

Only few models couple sediment transport and deposition in basins directly with erosion in domains of tectonic uplift (Johnson and Beaumont, 1995; Coulthard *et al.*, 2002; Tucker *et al.*, 2002). Most of these coupled models that study foreland basin systems operate on a geodynamic scale (100-500 km, Table 1.1), focussing on the relationships between flexural response upon thrust loading and large-scale stratigraphic patterns recorded in the basin. (Flemings and Jordan, 1990; Sinclair *et al.*, 1991; Peper *et al.*, 1992; Johnson and Beaumont, 1995). In addition, there is an increasing number of small-scale models that investigate the potential of growth strata to record thrust-related process in foreland basins (~10 km) (Zoetemeijer *et al.*, 1993; Hardy *et al.*, 1996; Den Bezemer *et al.*, 1998; Bernal and Hardy, 2002). Currently, there is a need for coupled models with a resolution detailed enough to visualize sedimentary architectural elements, which at the same time address recurring questions at basin scale. Examples of such outstanding questions, which will be addressed in this thesis, are:

- The response time between the onset of tectonic activity and the deposition of alluvial fan gravels in the basin (Burbank and Reynolds, 1988; DeCelles *et al.*, 1991a; Fraser and DeCelles, 1992; Dreyer, 1993; Burbank *et al.*, 1996; Whipple and Trayler, 1996).
- Tectonic significance of shifts and architectural styles of axial fluvial systems (ribbons vs. sheets, Kraus and Middleton, 1987; Warwick and Flores, 1987; Marzo *et al.*, 1988; Bentham *et al.*, 1992; Nijman, 1998; Anderson and Cross, 2001; Ramos *et al.*, 2002).
- The origin of composite sequences and the hierarchical organisation of shallow marine delta deposits in foreland basins. Examples of composite sequences are found in the Cenomanian Dunvegan Formation of the Alberta Foreland Basin, Canada (Bhattacharya, 1991; Plint *et al.*, 2001), the Upper Cretaceous Castlegate Sandstone, Utah (Schwans, 1995; Yoshida *et al.*, 1996), and the Eocene Montanyana Group (Nijman, 1998) and Sobrarbe Formation in the Spanish Pyrenees (Dreyer *et al.*, 1999). Commonly, these composite sequences are interpreted to reflect tectonic-controlled increases in accommodation space

because of their duration (0.2-2.0 Myr), whereas smaller-scale cycles within the sequences (< 0.2 Myr) are seen as the effect of sea-level or climate fluctuations. The interplay between subsidence and eustasy may appear simple (e.g. Posamentier, 1999), but prudence is called for because subsidence rates are not spatially invariant at both timescales (Olsen *et al.*, 1995; Yoshida *et al.*, 1996; Plint *et al.*, 2001).

- Difference between regional flexure-related and thrust-induced reduction of the accommodation space in deforming foreland basins. Both are known to create unconformities, amalgamating sheet sandstones and forced regressions but are difficult to distinguish as thrust deformation increases in size (Butler and Grasso, 1993; Peper and de Boer, 1995; Dreyer *et al.*, 1999; Gawthorpe *et al.*, 2000).

#### **1.4.2 Model description and flow chart**

The model presented in this thesis is operational at intermediate scales (~75 km, ~3 Myr, Table 1.1), and its capabilities represent a compromise between computational efficiency and stratigraphic detail. The model differs from existing coupled models by the addition of several new tectonic, geomorphic and stratigraphic features:

- Application of the cellular braiding principle (Webb, 1994; Murray and Paola, 1997) besides the commonly used steepest descent flow algorithm, facilitating the simulation of sediment dispersal on alluvial fans and deltas.
- Flow-tracer-based distinction between erosion and depositional domains and individual depositional systems (bedrock drainage basin vs. alluvial fans, axial rivers, etc.), in order to track facies-specific sediment budgets as a function of the external forcings.
- Increased realism of the stratigraphy by active grainsize sorting through the cellular flow networks and a three-dimensional, high-resolution discretisation of the subsurface. Grainsize, a fundamental feature in sedimentary sequences, is chosen as main characteristic visualized in fence-diagrams.
- Visualization of the stratigraphy according to the status of tectonic, eustatic or combined forcing, such as rate of relative sea-level change at the time of deposition of each individual layer. This facilitates the recognition of causal relationships between the external forcings and the stratigraphic patterns recorded in the basin.
- Sub-horizontal translation of syn-tectonic sediment accumulated in a thrust-sheet top basin.
- Low-cost, automated three-dimensional visualization of the foreland basin landscape evolution and stratigraphy by coupling of the C/C++ source code to Surfer® and Matlab® scripts.
- Automated selection and three-dimensional visualization of geometrically complex subsurface features of economic interest such as incised valley fills and interconnected sandstones.

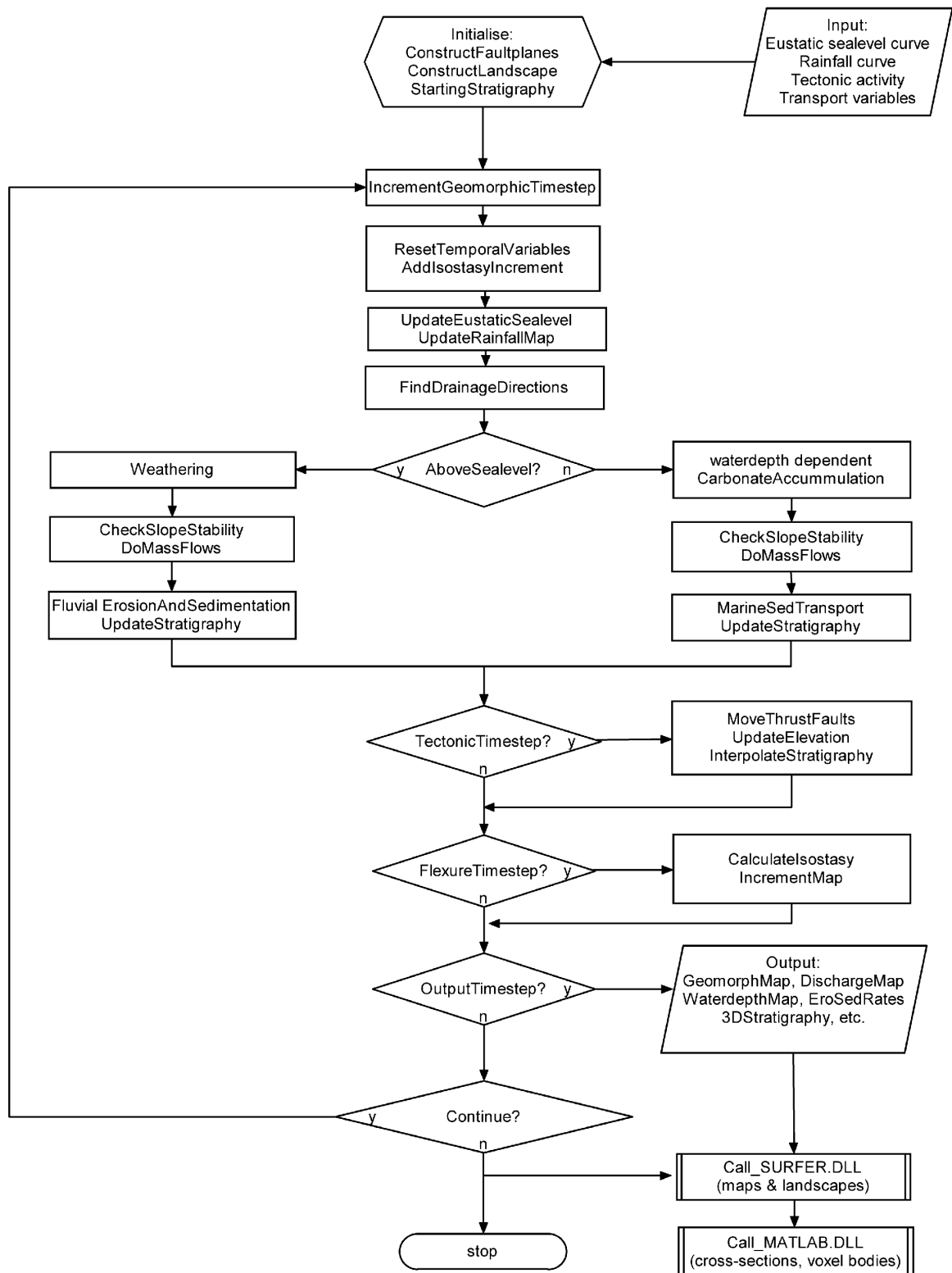


Figure 1.5 Simplified flow diagram of the procedure followed by the model presented in this thesis.

A simulation starts with initialisation of the basin topography, the subsurface geometry of the fault planes and reading of the input variables (Figure 1.5). The main input variables are the coefficients and exponents of the transport equations and the time-dependent values of the external variables such as eustasy, rainfall, and fault-specific tectonic activity curves. These curves are read from an MsExcel® spreadsheet or constructed during the initialisation process. Options are simple on/off step function, a sine wave, or more complex harmonics representing interference patterns of Milankovitch insolation signals. The simulation is performed in a sequence of timesteps representing 10 or 50 yrs, in which the main components of the creation of accommodation space, eustatic change and isostatic adjustment are applied incrementally to the landscape surface discretised on a rectangular grid. Subsequently, the potential water discharge and sediment distribution slopes are evaluated for every node in the eight surrounding directions. Water discharges are assumed to represent the effective surface runoff. Depending on the node positions with respect to sea level they are subjected to a set of marine or continental deterministic sediment transport equations. All transport equations conserve mass and are solved explicitly in order to facilitate the change of node elevation simultaneously with the updating of subsurface stratigraphy. At fixed time intervals this repeating tectonic-geomorphic sequence of events is interrupted by thrust-fault re-activation, an evaluation of the isostatic equilibrium and writing of the output files. The file contents are visualized as landscapes and stratigraphic fence diagrams, during run time or at the end of a simulation, by calls from the model code to Surfer (Golden Software, inc.) and Matlab (The Mathworks, inc.) scripts.

The geometry of the model and the rates of tectonic and sedimentation processes were tailored to the Eocene Tresp Basin in the Spanish Pyrenees (Nijman, 1998) in order to be able to compare model results to a natural basin fill. Geological research questions addressed in this thesis are based on this setting, and resemblances and differences between the modelled synthetic stratigraphy and the field observations are discussed. It has not been the intention to reproduce the stratigraphy of the Tresp Basin, because of the uncertainties involved in estimating the exact timing and rates of all variables in a natural setting due to poor dating constraints. Moreover, the problem of convergence or equifinality, whereby different processes and causes produce similar stratigraphic results may preclude a single and unique solution (Heller *et al.*, 1993; Schumm, 1998, p.58). Rather, the model results are used to offer insight into the effect of fundamental variables in a comparable setting.

### **1.5 Aim and outline of this thesis**

The aim of the numerical experiments presented in this thesis is to recognize stratigraphic features diagnostic for single or interacting variables in a three-dimensional foreland-basin record. Investigated variables include tectonic activity, eustatic sea level, intra-basinal detachment fault geometry, as well as the flexural rigidity of the underlying lithosphere. The quantitative numerical model was stepwise developed and extended during the research. Consequently, the complexity of



the experiments in terms of tectono-sedimentary setting and interacting variables increases throughout the successive chapters of this thesis.

**Chapter 2** is an introduction into the origin of the surface process equations applied, and their numerical implementation in the model. Techniques used to simulate thrusting and basin subsidence are illustrated. The model set-up consists of a basic orogen/foreland basin system represented by a linear, advancing thrust front and an asymmetrical subsiding basin being filled by alluvial fans. Two aspects of the system are explored. First, the effect of bedrock erodability versus thrust displacement rate on the morphology of the evolving orogenic drainage network. Secondly, the effect of episodic tectonic activity on the three-dimensional distribution of alluvial fan gravels in the basin.

In **Chapter 3** the model set-up is modified to a configuration of three depositional elements commonly observed in present-day and fossil foreland basins. Transverse alluvial fans, a longitudinal river flowing along strike of the orogen, and a shallow-marine domain. The foreland basin is subjected to simultaneously active episodic tectonism and eustatic sea-level variations to investigate how their interplay determines the geographic positions of the depositional elements and the corresponding three-dimensional stratigraphic architecture recorded in the foreland basin. In addition, the complex subsurface distribution of incised-valley fills, which are potential reservoir bodies, is visualized in three dimensions and related to the evolution of the accommodation space in the basin.

In **Chapter 4** the transformation of a foreland basin into a thrust-sheet top basin is modelled. The effect of the competition between two variables, the rate of regional flexural subsidence, and the uplift rate due to translation over the inclined detachment fault, is shown in the model stratigraphy. The interconnectedness of sheet sandstones and the sensitivity to fluvial entrenchment as a function of increasing detachment angle is systematically explored. This variable is commonly neglected in foreland basin analysis. The resulting experimental stratigraphy is used to explain the character of the Castissent Formation incised-valley sheet sandstones.

**Chapter 5** is a look forward towards a new modelling technique. The rectangular grid discretisation applied in the previous chapters is the most feasible method if one aims to model foreland basin drainage patterns and stratigraphy at long temporal and spatial scales. However, with the steady increase in cost-effective computer speed and memory it is to be expected that this approach will be replaced by an advanced generation of models based on a Triangular Irregular Network (TIN) that allow more refined representations of tectonic and fluvial patterns. Anticipating on such a development, examples are shown of stratigraphic simulation of alluvial fans, a meandering river and a normal fault-bounded basin fill, by using a modified version of the CHILD landscape evolution model (Tucker *et al.*, 2002).

*Chapter 1*

## Numerical modelling of drainage basin evolution and three-dimensional alluvial fan stratigraphy

### Abstract

A forward numerical model is presented to study the effects of bedrock erodability, thrust displacement rate, pulsating tectonic activity and sea-level fluctuations on drainage basin morphology and stratigraphy of large alluvial fan systems. A low value of the bedrock erodability coefficient ( $K_b = 0.5 \times 10^{-4} \text{ yr}^{-2/3}$ ) versus thrust rate ( $R_{\text{thrust}} = 2.0 \text{ m/kyr}$ ) is associated with a time lag between cessation of tectonic activity and maximum sedimentation rates observed on the alluvial fans. Applying higher  $K_b$  values, ranging between 1.0 and  $8.0 \times 10^{-4} \text{ yr}^{-2/3}$ , results in higher sediment yields due to more rapid headward catchment erosion and elaborate sideways branching of drainage networks. Pulsating tectonic activity is reflected in a stratigraphic alternation of prograding and retrograding alluvial fan gravels. During tectonic activity fan gravel fronts and coastlines retreat because catchment yields are insufficient to fill the accommodation space created by the flexural response due to thrust loading. Phases of tectonic quiescence and cessation of flexural subsidence are indicated by progradation of the gravel front. Depending on the position in the basin, the lag time for arrival of the gravel associated with tectonic cessation is several tens to hundred kyrs. A combination of pulsed tectonic activity with sinuous sea-level fluctuation leads to a more complex stratigraphic pattern. In that case stratigraphic response to tectonic pulses is masked by a similar but higher-order frequency-stacking pattern, especially in the more distal parts.

### 2.1 Introduction

Alluvial fans are sedimentary landforms that develop at the base of mountain fronts where confined feeder streams emerge from catchments and release their sediment load into unconfined zones of reduced streampower (Figure 2.1) (Bull, 1977; Blair and McPherson, 1994a; Harvey, 1997). Spreading their loads in a radiating pattern from a single apex, they form conical bodies with slightly concave length profiles and convex cross-profiles (De Chant *et al.*, 1999). In regions with multiple sources, the fans tend to obstruct each other and coalesce into a continuous belt of deposition,



Figure 2.1 Panamint Range alluvial fans, Death Valley, California, USA (source USGS).

or *bajada* (Davis, 1912). Basinward fan systems may join with axial fluvial systems, aeolian deposits, lakes or a marine embayment (Hooke, 1968; Baltzer and Purser, 1990; Nijman, 1998). Typical longitudinal fan lengths are in the order of 5 to 15 km and fan slopes range between  $0.5^\circ$  and  $10^\circ$ , depending on the position on the fan, its size and the dominant depositional process (Rust and Koster, 1984). Debris-flow-dominated fans reach slopes up to  $10^\circ$ , while the slopes of stream-flow-dominated fans decrease rapidly with increasing drainage basin size and river stream power (Blair and McPherson, 1994b; Milana and Ruzycki, 1999). Examples of large-sized end-members are the fluvial *megafans* of the present-day Himalayas (Wells and Dorr, 1987), Andes (Horton and DeCelles, 2001) and stratigraphic records of the Pyrenees (Hirst and Nichols, 1986) and Alps (Pfiffner, 1986; Schlunegger *et al.*, 1997). Stratigraphic patterns of ancient alluvial fans of various sizes show repetitive phases of gravel front progradation and retrogradation (Steel *et al.*, 1977; Blair and Bildeau, 1988; Whipple and Trayler, 1996). A recurring issue in the sedimentological literature is the significance of these progradation/retrogradation patterns and their relation to tectonic activity (Burbank and Reynolds, 1988; Nijman, 1998; Anderson and Cross, 2001). Traditionally, progradation of coarse sediment is explained as the result of synchronous tectonic uplift of source areas. This relationship is intuitively very appealing and was already postulated by early geologists such as Playfair (1802) and Barrel (1917). Active uplift of the source area would in their view result in a rise of the slopes and a general increase in the capacity of the streams to detach and transport larger-sized clastic material to adjacent depositional basins.

Throughout the mid-eighties it was realized that gravel progradation is not exclusively a syn-tectonic phenomenon (Beck and Vondra, 1985; Blair and Bildeau, 1988; Heller *et al.*, 1988; Paola *et al.*, 1992). Bedrock erosion and gravel production do increase with created relief, but because these geomorphic processes generally operate at a slower rate than tectonic uplift, they respond with a significant time lag (Schumm, 1963). In addition, the potential of alluvial fan progradation is a function of the ratio between the supply rate and the rate of accommodation space creation (Schlager, 1993). Tectonic activity is generally associated with an increasing rate of subsidence near the active fault, inhibiting the progradation of the gravel front into the depositional basin (Heller *et al.*, 1993). Instead, most sediment is accumulated in this subsiding zone close to the fault.

In the past the gravel-front progradation issue was dealt with using forward models of basin filling (Jordan and Flemings, 1991; Sinclair *et al.*, 1991; Paola *et al.*, 1992; Bezemer, 1998; Marr *et al.*, 2000). These models use diffusion as a metaphor for sediment transport and are capable of producing realistic stratigraphic cross sections. However, these models are two-dimensional and lack drainage basin excavation and fluvial stream networks.

Fluvial patterns are produced by drainage basin models developed in geomorphology, but usually ignore sediment transport and deposition in adjacent sedimentary basins. The few models that combine drainage basin excavation and synchronous deposition of sediment in three dimensions do not actively sort gravel from sand. Consequently a high-resolution stratigraphic record is not accumulated (Johnson and Beaumont, 1995; Ellis *et al.*, 1999; Gawthorpe and Hardy, 2002). Two notable exceptions are the CHILD (Tucker *et al.*, 2002) and CAESAR model (Coulthard *et al.*, 1999). The first performs coupled erosion and deposition of two grainsize fractions on an irregular triangular mesh. The second produces very realistic alluvial fan morphologies (Coulthard *et al.*, 2002), but they operate at time-scales too small to study the effect of tectonic perturbations.

The landscape evolution model presented here (Figure 2.2) accumulates a 3D, alluvial stratigraphic record of the long-term tectonic evolution of a catchment–fan system at a vertical resolution of approximately 1 m. Based on a surface process model (GOLEM, Tucker, 1996b), it produces dendritic catchment networks. New features are sediment redistribution on alluvial fan surfaces using divergent channel networks, grainsize sorting and deposition of gravel-sand sediment mixtures. In addition, subsurface stratigraphy is visualized as synthetic wells and fence-diagrams. Using thrusting as a tectonic process to create topography, the model smoothly translates the drainage networks and surface sediment properties horizontally on a rectangular grid without disrupting the surface processes.

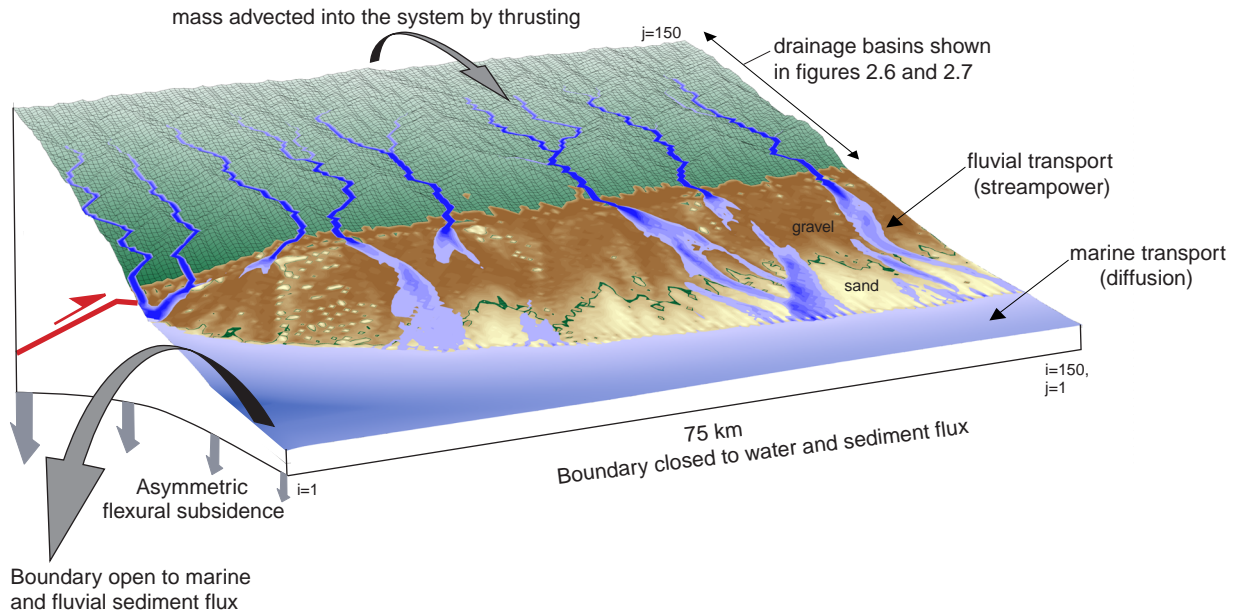


Figure 2.2 The model set up consists of a 150 x 150 rectangular grid of 500 m cells. The grid is divided into a linear uplifting thrust block and an asymmetric sedimentary basin created by flexural subsidence. Mass enters the system as bedrock advected over a thrust ramp of 20°. Bedrock is eroded in drainage basins, transported by streampower-type transport rules and deposited as alluvial fans. Sediment bypassing the alluvial fans is transported further by diffusion in a marine embayment with a constant sea level of 0 m. Sediment carried by fluvial and marine transport rules is allowed to leave the system at the left-hand side, whereas all other boundaries are closed to sediment and water.

## 2.2 Methodology

### 2.2.1 Geomorphic and stratigraphic model

Using landscape evolution models has become common practice in geomorphology nowadays. The focus has remained on erosional processes. Many studies investigate the relationships between uplift rates, drainage patterns, erosional fluxes and parameter sensitivity (Chase, 1992; Kooi and Beaumont, 1994; Tucker, 1996b). The evolution of the drainage basin is a first-order control on the development of the stratigraphic patterns stored in adjacent depositional basins. The importance of this link is increasingly being recognized, and the number of model-related publications dealing with the interactions between both systems on geological timescales, is growing steadily (e.g. Humphrey and Heller, 1995; Johnson and Beaumont, 1995; Ellis *et al.*, 1999; Allen and Densmore, 2000). Landscape evolution models designed for large spatial and long geological time-scale simulations are forced to step away from describing transport processes at a small scale due to poor information on detailed paleohydraulics and limited computation power. Instead they use a mix of empirical relationships and simplifications of engineering time-scale transport laws (Howard and Kerby, 1983; Willgoose *et al.*, 1991; Howard *et al.*, 1994; Tucker, 1996b; Whipple and Tucker, 1999). Many engineering bedload transport formulae take the form (Knighton, 1998)

$$q_s = k_1 (\tau - \tau_c)^p \quad (2.1)$$

where  $q_s$  is the volumetric transport rate per unit channel width ( $m^2/s$ ),  $k_1$  a sediment coefficient,  $\tau$  is the channel-averaged fluid shear stress ( $N/m^2$ ) performed by the flow,  $\tau_c$  the critical threshold stress to initiate motion, and  $p$  is an empirically determined power (for gravel  $p \sim 3/2$ , (Bagnold, 1980; Yang, 1996), for fine sediment  $p \sim 5/2$  (Whipple *et al.*, 1998)). In order to go from these physically-based transport equations to a more suitable, long-term description of sediment transport, shear stress needs to be expressed in accessible quantities such as water discharge and slope. The following derivation illustrates stepwise the assumptions involved to achieve this (Tucker, 2000). In steady uniform flow the shear stress is defined as

$$\tau = \rho g R S \quad (2.2)$$

where  $\rho$  is the density of water,  $g$  the gravity constant,  $R$  the hydraulic radius of the channel and  $S$  the slope. For wide channels  $R$  is equal to the water depth  $h$ . The volumetric water transport rate per channel width is

$$q_w = V h \quad (2.3)$$

where the velocity  $V$  of the water is given by an empirical bed friction relationship such as the Manning-Strickler or Darcy-Weisbach equation (Knighton, 1998).

$$V = C_f R^{\frac{\varepsilon}{2}} S^{\frac{1}{2}} \quad (2.4)$$

where the values of the coefficient  $C_f$  and exponent  $\varepsilon$  depend on the resistance equation chosen. Using the Manning-Strickler  $C_f = 1/n$  ( $n \sim 0.02$ , is 'Manning's  $n$ ') and  $\varepsilon = 4/3$ , while for the Darcy-Weisbach equation  $C_f = \sqrt{(8g)/f}$  and  $\varepsilon = 1$  ( $f$  is friction factor). After combining equation 2.3 and 2.4 shear stress is

$$\tau = (\rho g C_f^\alpha) q_w^\alpha S^\beta \quad (2.5)$$

where  $\alpha = 0.6$  and  $\beta = 7/10$  if Manning-Strickler is used, or  $\alpha = \beta = 2/3$  if Darcy-Weisbach is used. Shear stress and total sediment transport rate  $Q_s$  ( $m^3/s$ ) can be written in terms of total water discharge  $Q$  by inclusion of the channel width  $W$ .

$$\tau = (\rho g C_f^\alpha) \left( \frac{Q}{W} \right)^\alpha S^\beta \quad (2.6)$$

$$Q_s = k_f W (\tau - \tau_c)^p \quad (2.7)$$

where the channel width  $W$  (m) is approximated by a well-known empirical relationship, stating that the channel width is proportional to the square root of the bankful discharge (Leopold and Maddock, 1953)

$$W = k_w Q^\omega \quad (2.8)$$

The value of the exponent  $\omega$  is 0.5 for most data, while  $k_w$  ranges between 2 and 5  $m^{-1/2}s^{1/2}$  (Knighton, 1998). Substituting this width-discharge relationship into equations 2.6 and 2.7, these equations can be rewritten as

(2.9)

$$Q_s = k_f k_w Q^\omega (k_2 Q^{m_f} S^{n_f} - \tau_c)^p \quad (2.10)$$

where  $k_2 = \rho g C_f^\alpha k_w^{-\alpha}$ ,  $m_f = \alpha(1-\omega)$  and  $n_f = \beta$ . Equation 2.10 needs to be simplified further in order to make it applicable on the large grid size computational mesh used in the model (500 m grid cells). Coefficient  $k_2$  and the threshold term  $\tau_c$  are omitted,  $k_w$  folded into  $K_f$ , and exponent  $p$  is multiplied with the discharge and slope exponents. The resulting equation for the sediment transport capacity becomes

$$Q_s = K_f Q^\omega (Q^{m_f} S^{n_f}) \quad (2.11)$$

The fluvial transport efficiency coefficient  $K_f$  is dependent on climate, bed roughness and material properties such as sediment grain size and porosity. It can be approximated by substitution (Tucker, 1997 their equation 10 and 11), giving a value between 0.001 and 1.0. In the model  $K_f = 0.01$  is chosen because it gives realistic long-term rates of deposition and equilibrium slopes for the alluvial fans on the coarse computational grid. The values of the discharge and slope exponents chosen are  $m_f \sim 0.5$  and  $n_f \sim 1.0$  using  $p=3/2$ , which is appropriate for gravel-dominated systems (Gomez, 1989), such as the fans modelled here. From sensitivity analysis it can be said that any other choice of the exponents, not directly dictated by the sediment transport relations, has implications for the stability and morphology of the channel networks on the modelled alluvial fans. Values for  $n_f$  higher or lower than 1.0 may lead to undesired amplifications of channel slope and numerical instabilities, while  $m_f$  values higher or lower than 1.0 stimulate bifurcating of channel networks (Murray and Paola, 1997; Crave and Davy, 2001). The water discharge  $Q$  at a cell location is found by multiplying the contributing drainage area  $A$  with effective runoff rate  $R$ .

$$Q = AR_{rain} \quad (2.12)$$

This approach is justified because over large time scales, water discharge is dominated by annual bankful discharges or decadal peak floods and not by short-time variations in rainfall (Slingerland *et al.*, 1993). It is possible to substitute equation 2.12 into 2.11 and reformulate the transport law into verifiable topographic quantities as slope ( $S$ ) and cumulative drainage area ( $A$ ) (Howard, 1994; Tucker, 1996b).

The potential sediment transport capacity  $Q_s$  is partly used to transport the sediment flux contributed by upstream cells ( $\Psi$ ), leaving a smaller net carrying capacity  $Q_s^*$  to mobilise the local river bed and add it to the sediment load of the flow.

$$Q_s^* = Q_s - \Psi \quad (2.13)$$

Based on evaluation of the local balance between carrying capacity  $Q_s^*$  and sediment load  $\psi$ , three types of fluvial transport behaviour emerge in various parts of the model grid:

1. Detachment-limited bedrock channels
2. Transport-limited alluvial channels
3. Hybrid, alluvial covered bedrock channels



### 2.2.1.1 Detachment-limited bedrock channels

If the volume of sediment supplied from upstream cells is small or the thickness of the movable sediment cover on the channel bed is negligible, the flow at this location may be below its capacity to transport sediment. The rate of channel lowering by bedrock erosion is then determined by the rate of bedrock detachment.

$$\frac{dh}{dt} = -K_b Q^{m_b} S^{n_b} \quad (2.14)$$

where the variable  $K_b$  ( $\text{yr}^{-2/3}$ ) is the intrinsic bedrock erosion coefficient, which determines the time-averaged incision rate of bedrock lithology. Several studies have attempted to predict parameters  $m_b, n_b$  and  $K_b$  using inverse modelling, empirical relationships and measurements of erosion rates in badlands.  $K_b$  ranges between  $7 \times 10^{-3}$  (mudstones) and  $6 \times 10^{-6} \text{ yr}^{-2/3}$  (granite and basalt) (Stock and Montgomery, 1999). Theoretically the value of  $n_b$  is between 0.7 and 1.7, but the range is narrowed by field data (0.6-1.0) (Howard and Kerby, 1983; Stock and Montgomery, 1999; Whipple and Tucker, 1999; Kirkby and Whipple, 2001). Despite the range in  $n_b$ , the ratio between the two exponents is restricted between 0.4 and 0.6 by theory and empirical data (Snyder *et al.*, 2000). The values used are 1/3 and 2/3 for  $m_b$  and  $n_b$  respectively, where detachment rate is proportional to bed shear stress (Howard, 1994). Detachment-limited grid cells are found in regions dominated by uplift. Under these incisive transport conditions, the cells eventually route the sediment to the lowest neighbouring cell (Figure 2.3a). The flow networks excavated in the uplifted domains are dendritic, similar to the flow paths in drainage basins (Goodchild and Mark, 1987; Chase, 1992).

### 2.2.1.2 Transport-limited alluvial channels

Cells that receive sufficient sediment from upstream sources to equal their potential carrying capacity are filled to capacity. The rate of change of the local cell elevation is *limited* by the rate of *transport* away from this location. Most of the time this rate is minimal and cells aggrade due to oversupply of sediment. Locally, conditions of increased net transport potential, resulting in alluvial channel erosion may occur, but are not dominant. An external trigger is required here, such as substrate steepening, baselevel fall, and water discharge increase versus sediment flux decrease. Erosion and deposition (eq. 2.11 and 2.15) are caused by small divergences around the local balance between supply and flow capacity.

$$\frac{\partial h_{all}}{\partial t} = -\frac{K_f}{W} \left( \frac{\partial Q^{m_f} S^{n_f}}{\partial x} + \frac{\partial Q^{m_f} S^{n_f}}{\partial y} \right) \quad (2.15)$$

If possible, water fluxes are spread proportional to slope to downward situated neighbour cells (Figure 2.3b) (Freeman, 1991). This style of bifurcation routing produces flows with braided or deltaic patterns (Webb, 1994; Murray and Paola, 1997; Coulthard *et al.*, 2002). Evaluation of the

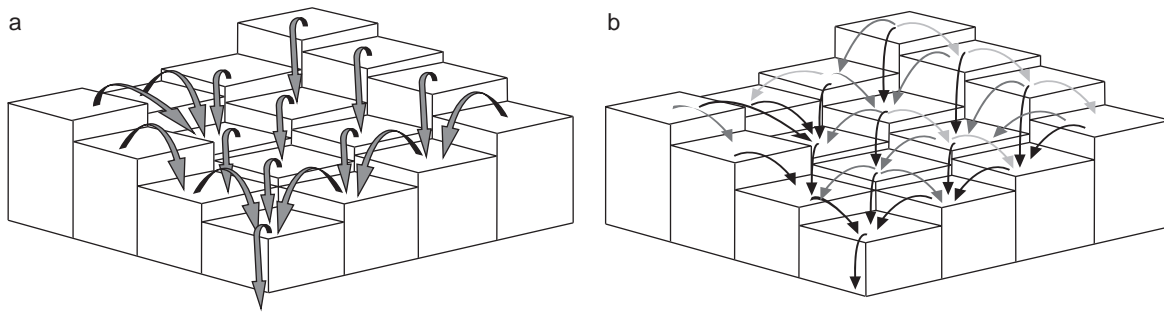


Figure 2.3 Water and sediment routing schemes used in the drainage basin-fan model. (a) Steepest descent routing, where material is passed on to the neighbour cell holding the steepest slope (b) Disperse or bifurcation routing, where material is distributed proportionally to slope in all down-going directions.

transport capacity  $Q_s$ , is in these cases done by taking the average of all increments of capacity generated by the flows of water to the different downward directions (eq. 2.11).

Bifurcation routing is also applied to the sediment load leaving a cell where possible. However, if the cell is eroding long enough, the transit material and the load produced is eventually routed to the lowest neighbour only, because the cell's elevation drops below the elevation of its neighbours. The decision between disperse and steepest descent transport in alluvial areas can also be made a function of local slope and drainage threshold values in the model (Lewin and Brewer, 2001) in order to study the stratigraphic signature of braided/ meander transitions, but this is not done here. Calculating the erosion/deposition response of a cell with multiple upstream contributing and distributive cells is a relatively simple procedure if done explicitly. However, straightforward evaluating the mass balance by simple bookkeeping can lead to numerical instabilities on the coarse computational grid in the form of closed depressions of which the differential elevation with the neighbours is amplified in successive time steps. This is avoided by choosing small timesteps of 10 yr for calculating geomorphic processes and solving the multidirectional mass-balance using a root finding procedure (Press *et al.*, 1992). The root finding procedure fine-tunes the balance between transport capacity with the upstream sediment supply while ensuring that the resulting slope is not reversed.

### 2.2.1.3 Hybrid, alluvial-covered bedrock channels

If a combination of the above transport conditions is encountered during a geomorphic time step, the channel cells are called 'hybrid' (or mixed-channel systems, Howard, 1994). These are cells with sufficient net carrying capacity to remove the small veneer of alluvial strata and to incise bedrock. The local change of elevation is a combination of the ability to remove the alluvial sediment cover and to erode bedrock. Channel cells of this category are found in domains of transition from drainage basin to depositional basin and alluvium-veneered mountainous streams such as the feeder channels of the alluvial fans.

### **2.2.2 Perfect sorting**

Bimodal sediment mixtures liberated by bedrock erosion are sorted along the fluvial paths with the perfect-sorting method (Paola *et al.*, 1992), using two grainsize fractions. The gravel fraction carried by the streams is selectively deposited in the alluvial bed until it is depleted from the flow. Starting from this location on the stream's route, the sand fraction is deposited downstream. The flux of gravel supplied to the depositional basin is a fraction of the total sediment volume supplied by the drainage basins. Active bedrock erosion in the drainage basins is set to release a volume fraction of 50% gravel and 50 % sand.

The diffusivity coefficient used in the original perfect-sorting model (Paola *et al.*, 1992) applies to the entire sediment composition, implying that both grainsize fractions are detached from alluvial beds and moved at equal rates. The rates of down-slope sorting and stratigraphic patterns observed are therefore controlled only by the rate of deposition through *selective deposition*. Segregation by *size-selective entrainment* or related phenomena such as channel-bed armouring (Gomez and Sims, 1981) and winnowing are not modelled with this technique. The perfect sorting approach used in our model is complemented with a simple selective entrainment rule. Bimodal sediment mixtures stored in natural alluvial beds are organized in a framework of the larger clasts and smaller sediment is hidden in it. This protective framework of large clasts collapses if the fine-grained fraction constitutes more than 40 % of the bed volume (Leeder, 1999). In the model, the finer grained fraction is therefore preferentially taken up during erosion of an alluvial bed and transported if the finer fraction constitutes more than 40 % of the alluvial bed because no protective framework is expected. No distinction in relative mobility is made for beds with less than 40% fine sediment. If a flow is able to erode the large framework clasts, all smaller grains will be mobilized at the same rate. This segregation rule is suited for our coarse grid because it is independent of cell size. Finer-sized grids should make use of more physically based methods to model armouring and winnowing (Robinson and Slingerland, 1998; Gasparini *et al.*, 1999).

### **2.2.3 Handling depressions in the grid**

Instabilities in the morphology of the fluvial network are avoided by solving local erosion and deposition using a root-finding procedure. However, small depressions hindering the flow of water on the grid may occur. Dealing with this type of topographic depressions is a classic problem in drainage-modelling literature (Hutchinson, 1989). Extraction of drainage networks from digital elevation models often involves smoothing or finding outlets for pits. Many solutions search around a recognized depression for outlets, by incrementing the size of the depressions until a suitable drainage is found for continuation of the flow. These are computationally slow procedures and are not suited for modelling landscape evolution over geologic time. Our method is fast by making use of sediment carried by the flow to fill the depressions encountered and continue the stream paths (Figure 2.4).

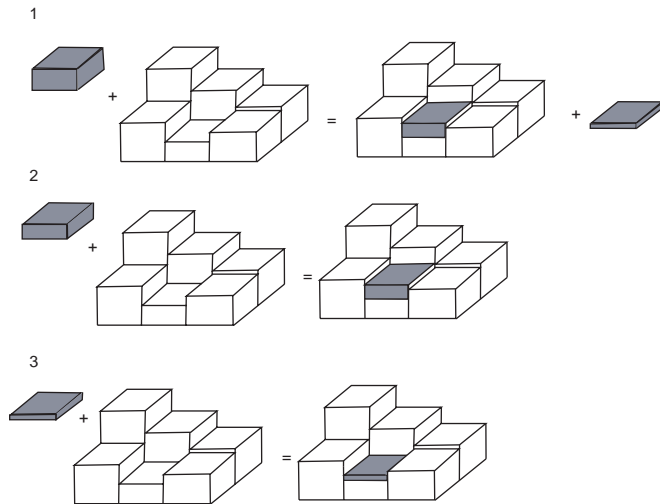


*Figure 2.4 Depressions hindering the continuation of flow are dealt with by filling them with the sediment transported by the streams. After identification of a depression three options arise. (1) A stream carrying sufficient sediment fills the depression till the level of the second lowest cell surrounding the depression. Water and excess sediment continue downstream. (2) A stream carrying too little to fill up to this level drops all load, and only the water flux continues. (3) If the load carried is not sufficient to fill up the depression, the load is dropped and the stream stops.*

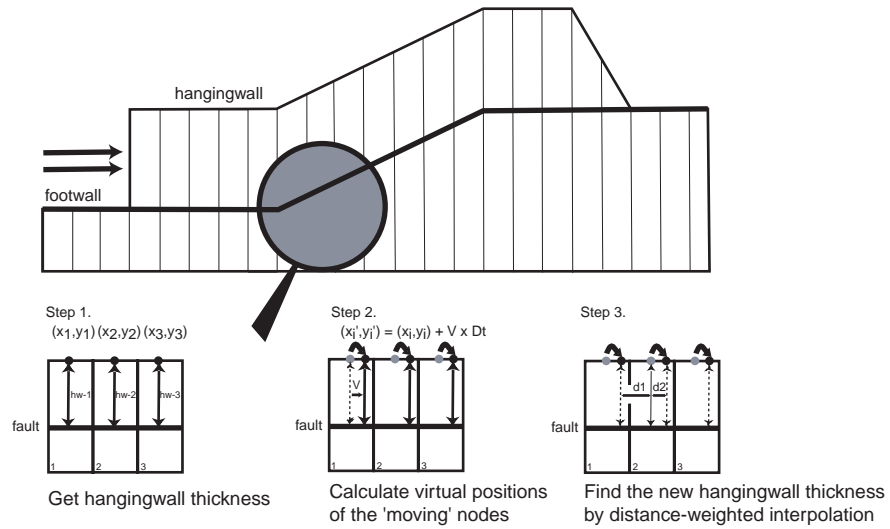
### 2.2.4 Tectonic mass translation

On the rectangular grid the surface development above a single thrust ramp is modelled as fault-bend folding in the simplest possible way. Other geometrically correct methods were tested (Suppe, 1983; Zoetemeijer, 1991), but led to instabilities in combination with the sensitive surface process algorithms on the relatively coarse computational grid. In our model the mass translation during fault-bend folding is simulated by moving grid positions according to the tectonic deformation field, and subsequently interpolating new hanging-wall thicknesses for the stationary grid cells (Figures 2.5a and b). This fault-bend folding technique is comparable to methods used by others (Jones and Linsser, 1986; Chaleron and Mugnier, 1993; Hardy and Poblet, 1995; Bezemer, 1998). The advantage is that mass is explicitly conserved, a requisite not always met by more complex thrusting methods which consider the hanging wall as a compressible entity (Erslev, 1991; Zoetemeijer, 1991). Conservation of mass is more important than mechanical realism when erosion and sedimentation are to be calculated during thrusting. The hanging-wall translation routine in the model is called in time intervals of 5 kyr, which are larger than the geomorphic time steps. This is done out of computational considerations because the hanging-wall displacement is a time-consuming procedure in the model. A more complex variant of thrusting involving the overthrusting of basin margin sediment is shown in Chapter 3 (Figures 3.10 and 3.11).

### 2.2.5 Flexure and basin subsidence

The model presented in this study incorporates two-dimensional elastic flexure response of a broken plate typically used for foreland basins, in spite of the limited size of the simulated area with respect to flexural wavelength. Possible boundary effects are avoided by temporarily extending the spatial dimensions of the grid during computation of the flexural isostatic adjustments. Uplift of the flexural bulge takes place outside the model boundaries and is not visible in the simulated

a



b

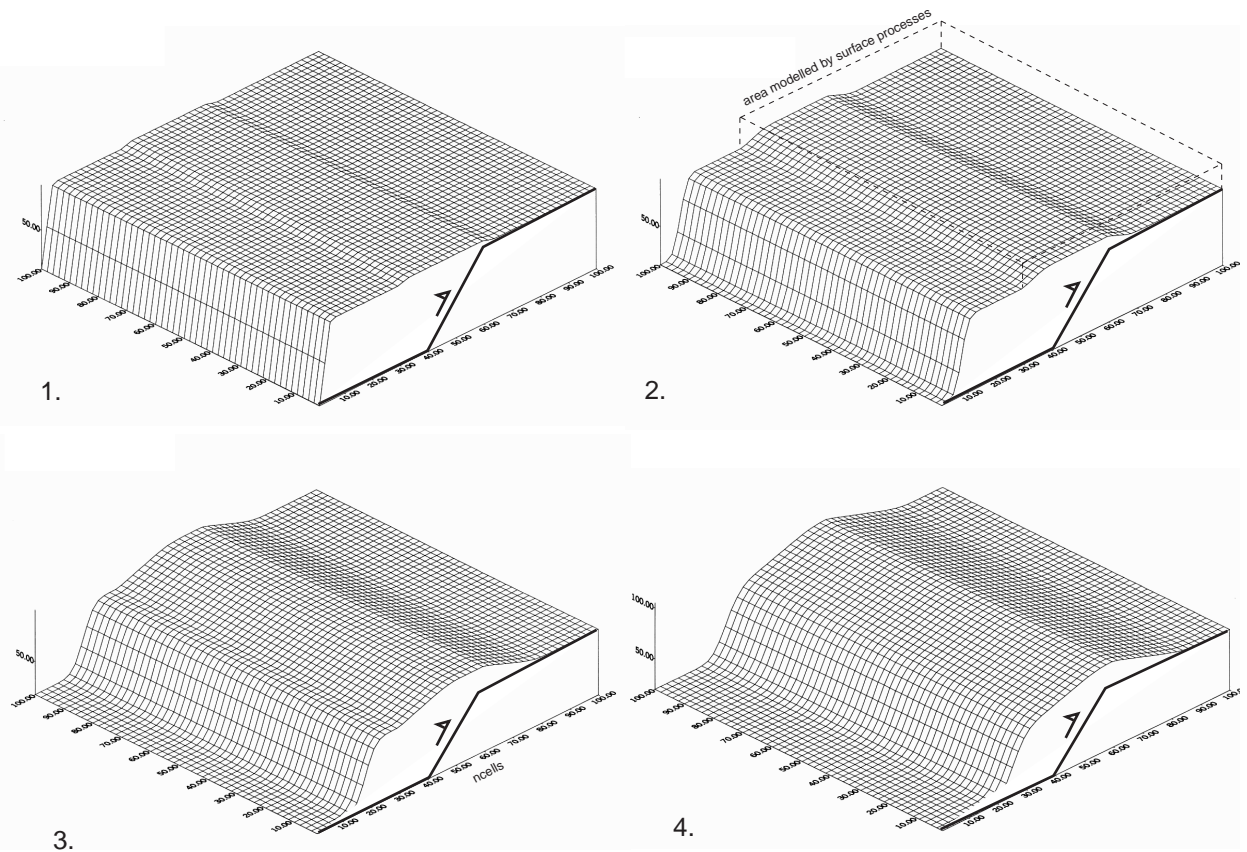


Figure 2.5 (a) Technique used to model the topographical development of a fault-bend fold above a thrust ramp. Hangingwall positions are displaced virtually and the new thicknesses for the static grid positions are determined by linear interpolation of the displaced values. (b) Example of successive steps in the development of the topography above a thrust ramp. In the following experiments the grid boundary for the surface processes is taken at the beginning of the ramp.

landscape surface. The noticeable response is that of an asymmetric subsiding basin. Subsidence rates decrease with increasing distance from the thrust fault. The two dimensional flexural isostatic response to a load in a two dimensional model is defined by (Turcotte and Schubert, 1982):

$$\frac{d}{dx^2} \left( D \frac{d^2 w(x)}{dx^2} \right) + (\rho_m - \rho_f) g w(x) = L(x) \quad (2.16)$$

where  $D$  is the flexural rigidity,  $\rho_m$  and  $\rho_f$  the density of mantle and the material filling in the depression,  $L$  the load as a function of the position  $x$  along the plate and  $w$  the resulting lithosphere deflection. The flexural rigidity used is low and corresponds with an effective elastic thickness (EET) of 10 km. A simple 2-D analytical Green Function solution for broken-plate flexure is incorporated in the model (Slingerland *et al.*, 1993) to limit computational effort. The state of bending due to thrust and sediment load is calculated in two N-S sections every 5 kyrs. Next, the predicted deflection is averaged and applied to the entire model space incrementally during the smaller geomorphic time-steps. Flexure is a three-dimensional problem and should be calculated as such (Wees and Cloetingh, 1994; Hodgetts *et al.*, 1998). However, the moving thrust load in the model is linear, and a full 3D solution would result in a similar linear depression as the one generated by the current method.

### 2.3 Numerical Experiments

A set of experiments was carried out to study the development of drainage basins and the synchronous deposition of alluvial fans associated with an uplifting thrust block (see Table 2.1 for parameter values). Vertical uplift rates corresponding to lateral movement over a 20° thrust-ramp ranged between 0.65 and 2.6 m/kyr (Figure 2.5). The alluvial fans are deposited in an asymmetrical basin created by flexural subsidence. Basin subsidence rate is highest near the faulted margin and has an average of 0.2 m/kyr during tectonic activity. Created accommodation space is filled by the alluvial fans and a shallow marine embayment. Geologic simulation times cover 0.5 to 1.5 Myr, depending on the type of external forcing used in the experiment. In the next section the effects of the following factors are discussed:

1. Bedrock erodability and tectonic displacement rate (experiments 1-7)
2. Pulsating tectonic activity (experiment 8)
3. Sea-level fluctuation superimposed on pulsating tectonic activity (experiment 9)

#### 2.3.1 The effect of variable bedrock erodability and tectonic displacement rate

The erodability of bedrock has been derived by inverse modelling of fluvial profiles (Stock and Montgomery, 1999) and approximates time-averaged denudation rates found in fission-track field studies (Morris and Sinclair, 1997; Meigs *et al.*, 1999; Kirky *et al.*, 2002). Bedrock erodability is represented in the model equations by the bedrock erodability coefficient  $K_b$  (eq. 2.14). The effect of different  $K_b$  values on drainage development in the catchment-fan system was studied (from 0.5

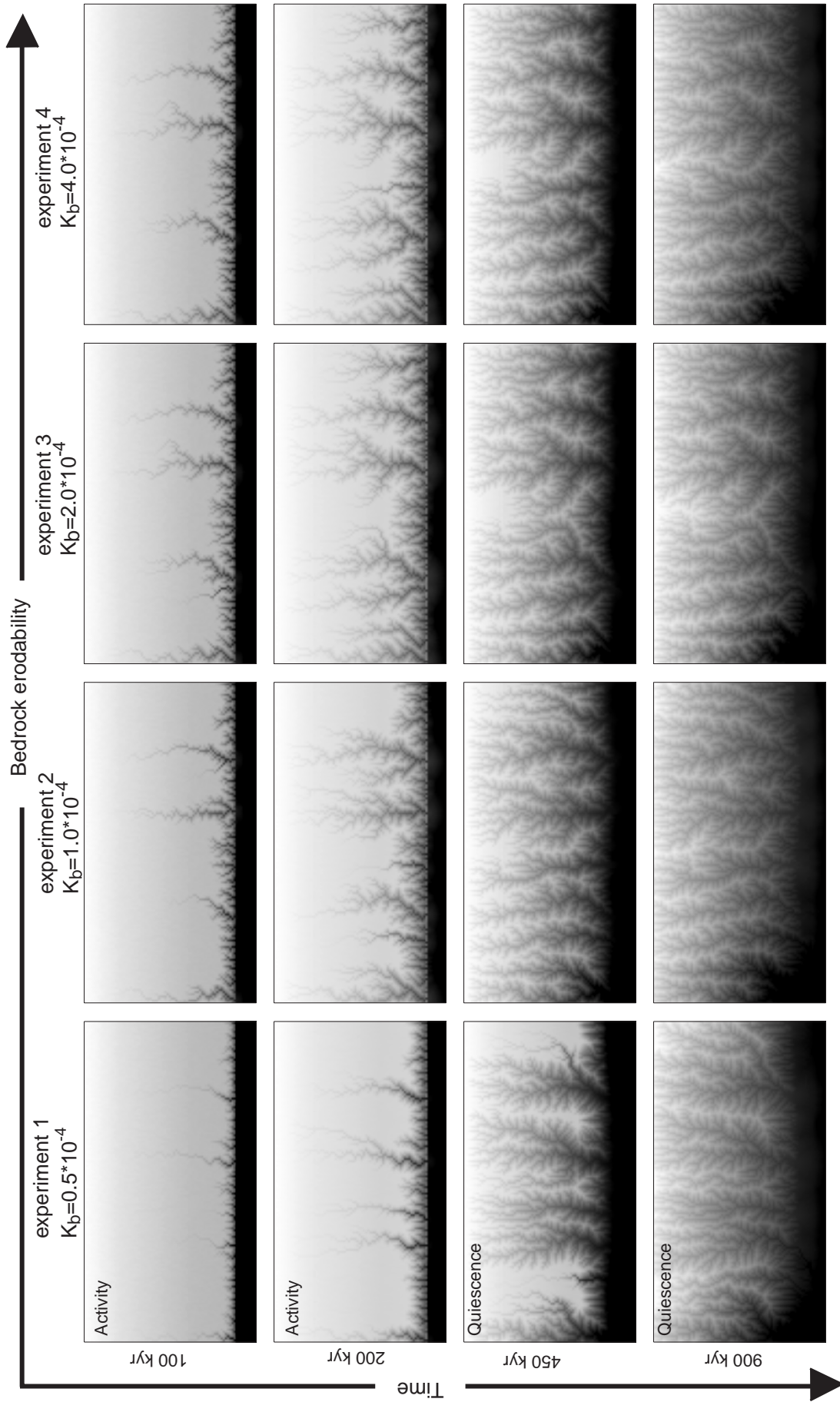
parameter	unit	1	2	3	4	5	6	7	8	9
final time	kyr	900	900	900	900	900	900	900	1800	1800
tectonic history	kyr	0-200	0-200	0-200	0-200	0-200	0-200	0-200	pulses 200 kyr	pulses 200kyr
baselevel	m	0	0	0	0	0	0	0	0	sine, 100 kyr/ 20m
displacement rate	m/kyr	2.0	2.0	2.0	2.0	2.0	4.0	8.0	2.0	2.0
erodability $K_b$	$\times 10^{-4} \text{ yr}^{-2/3}$	0.5	1.0	2.0	4.0	8.0	8.0	8.0	4.0	4.0
timestep size	yr	10	10	10	10	10	10	10	10	10
tectonic timestep	kyr	5	5	5	5	5	5	5	5	5
rainfall rate	$\text{myr}^{-1}$	1	1	1	1	1	1	1	1	1
thrust ramp angle	degrees	20	20	20	20	20	20	20	20	20

Table 2.1 Parameters used in the experiments. Shaded columns represent experiments with pulsating tectonic activity.

$\times 10^{-4} \text{ yr}^{-2/3}$  to  $8.0 \times 10^{-4} \text{ yr}^{-2/3}$ , Figures 2.6 and 2.7, exp.1-5). The catchment-fan system was subjected to a single tectonic uplift pulse of 2.0 m/kyr horizontal thrust displacement during a period of 200 kyr. The corresponding vertical uplift rate was 0.65 m/kyr and flexural subsidence response had a maximum rate of 0.2 m/kyr at the basin margin. The tectonic pulse was followed by a long period of tectonic quiescence (200 to 900 kyr) and consequent cessation of basin subsidence. In order to study the effect of displacement rate, the experiment with  $K_b = 8.0 \times 10^{-4} \text{ yr}^{-2/3}$  was repeated with  $R_{\text{thrust}}$  of 4.0 m/kyr and 8.0 m/kyr (Figure 2.7, exp. 6 and 7).

In all experiments the main drainage channels initiate at the same locations along the fault front (Figures 2.6 and 2.7, upper row of illustrations). This is because all experiments had the same topographic surface as a starting condition. The flat surface is complemented with 1.0 m amplitude, randomly distributed noise in order to stimulate the initial development of drainage channels. Once these drainage channels are established by incision, they are hardly ever abandoned during further evolution of the networks. The initial surface noise is etched out by continuous incision during progressive network evolution. Changes in the drainage networks are accomplished by stream capture (= piracy by neighbouring channels).

After 100 kyr of simulation, a difference in drainage-pattern development is found between experiment 1 with the lowest  $K_b$  value ( $0.5 \times 10^{-4} \text{ yr}^{-2/3}$ ) and experiments 2 to 5 with  $K_b = 1.0 \times 10^{-4} \text{ yr}^{-2/3}$  or higher (Figures 2.6 and 2.7). For the low  $K_b$  value, the landscape shows only small incisions, whereas the higher  $K_b$  experiments show four juvenile catchments. In these catchments headward erosion migrate into the bedrock as linear valleys with minor side branches. In addition, there is an increasing tendency for sideways branching from the main valleys with increasing  $K_b$  value. These branches continue to expand farther at the end of the tectonic pulse (time = 200 kyr, Figures 2.6 and 2.7) at  $K_b$  values 2.0, 4.0 and  $8.0 \times 10^{-4} \text{ yr}^{-2/3}$ . It is remarkable that these three landscapes do not show much difference in the geometry of the catchments at this time-interval. The low  $K_b$  value landscape is very different from the others; it shows limited branching and headward erosion, less far into the hangingwall block. As time progresses the drainage patterns in the different catchments





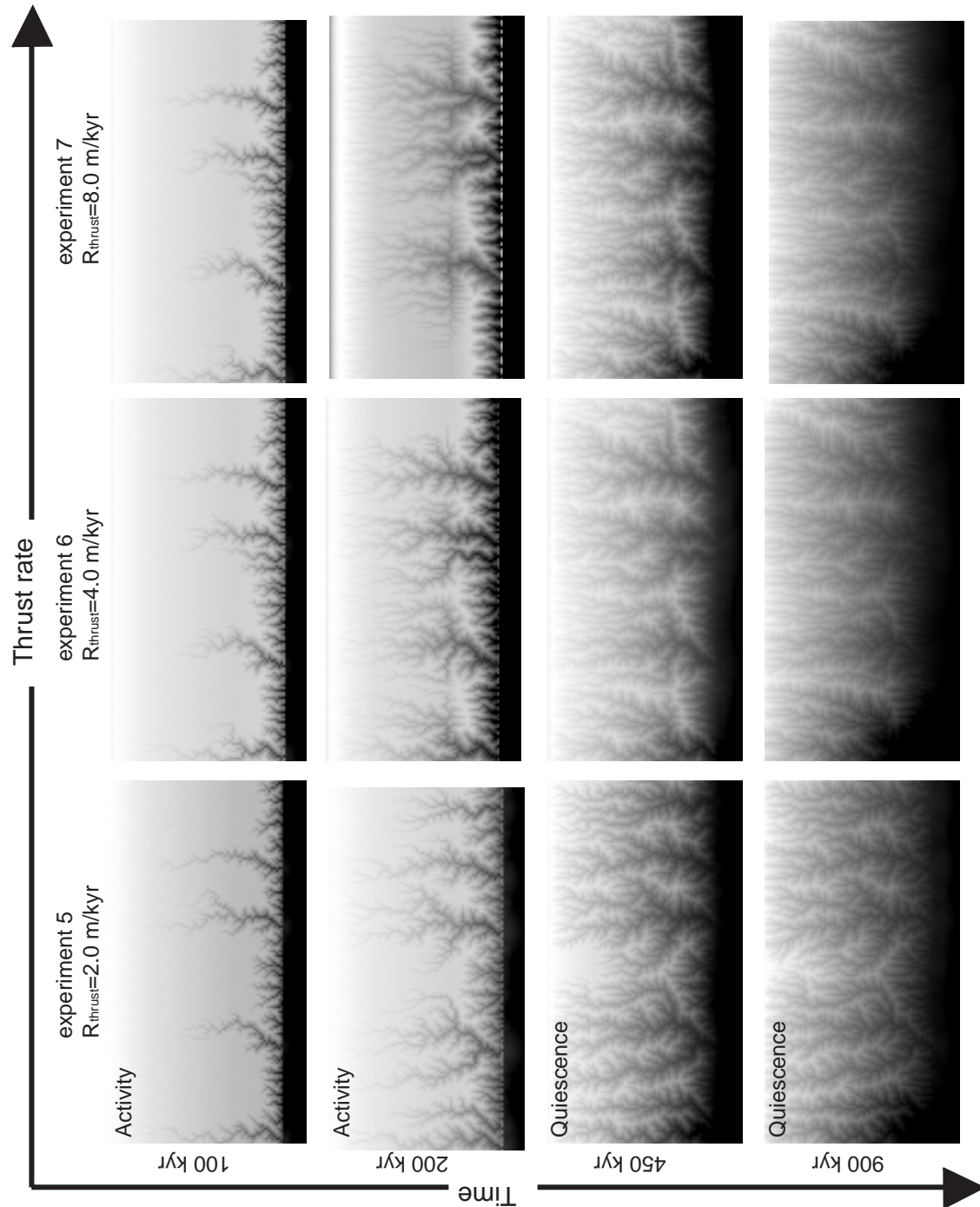
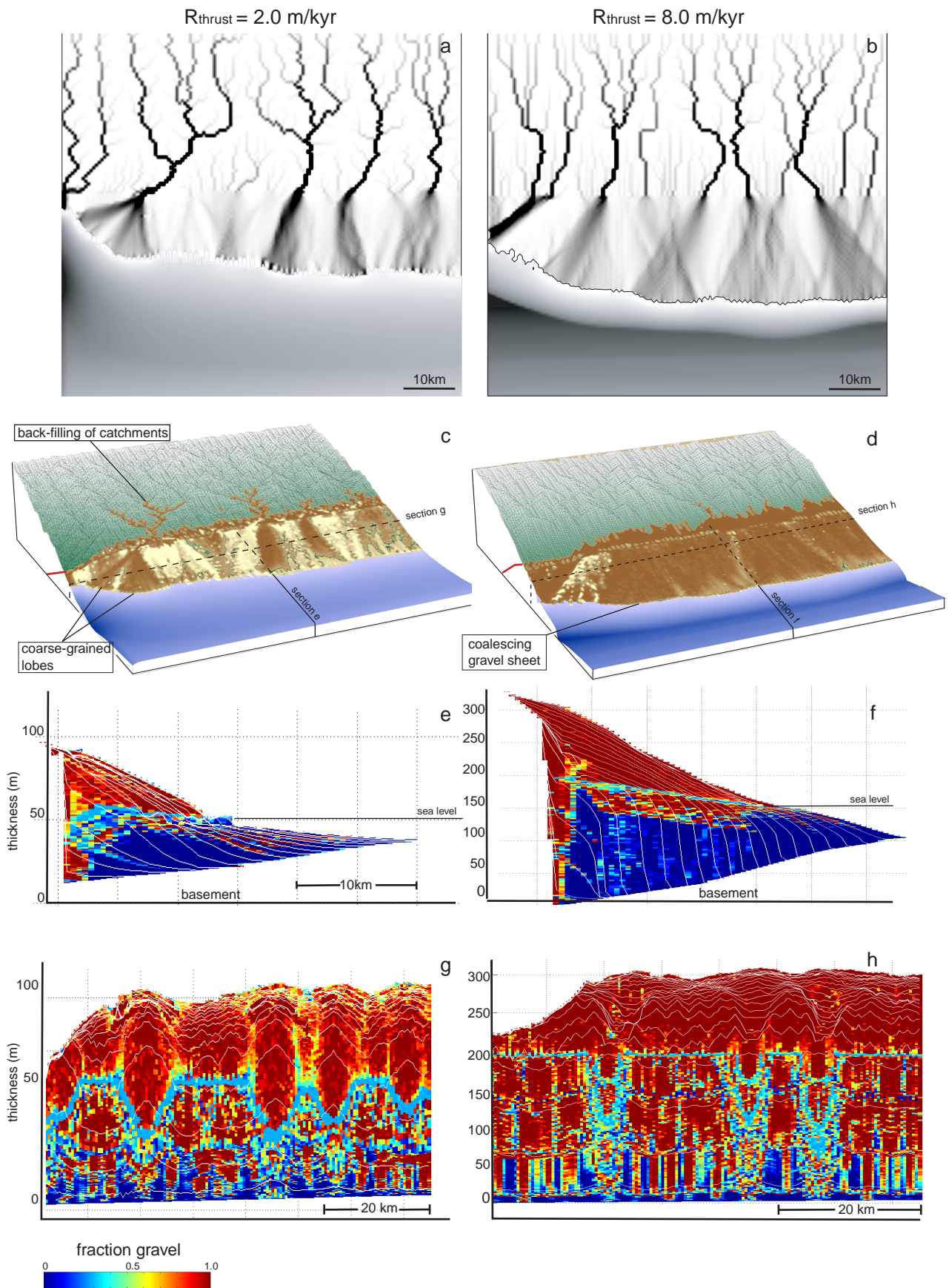


Figure 2.7 Results of experiments 5-7, showing successive steps in drainage network development under different values of  $R_{thrust}$  (2.0, 4.0 and 8.0 m/kyr) and a constant erodability coefficient  $K_b$  ( $8.0 \times 10^{-4} \text{ yr}^{-2/3}$ ). Tectonic activity lasted 200 kyrs, followed by 700 kyrs of quiescence.

Figure 2.6 (previous page) Results of experiments 1-4, showing successive steps in drainage network development under different values of the bedrock erodability coefficient  $K_b$  ( $0.5 - 4.0 \times 10^{-4} \text{ yr}^{-2/3}$ ) and constant thrust rate ( $R_{thrust} = 2.0$  m/kyr). Tectonic activity lasted 200 kyrs, followed by 700 kyrs of quiescence.



converge to a similar configuration at 900 kyr (Figures 2.6 and 2.7). A four-fold increase in the  $K_b$  value has no significant effect on the long-term channel pattern of the model catchments. The same applies for the grain-size trends in the alluvial fan subsurfaces. Therefore only the stratigraphy of  $K_b = 8.0 \times 10^{-4} \text{ yr}^{-2/3}$  is shown (Figure 2.8, left column). The section shows vertical stacking of fine and coarse sediment followed by an expansion of the coarse sediment into the basin. The vertical stacking is correlated to tectonic activity, whereas the gravel progradation correlates to the phase of quiescence. Viewed in a section parallel to the fault front, the fan deposits are represented by sideward fining, coarse-grained bodies (Figure 2.8c). The velocity of the prograding gravel front during tectonic quiescence is approximately 0.30 m/kyr.

Juvenile fans (time = 200 kyr) are completely covered by coarse-grained sediment. As the fans prograde into the basin the coarse veneer becomes interrupted and coarse-grained lobes spatially alternate with finer-grained inter-fan deposits (Figure 2.8). This situation is achieved earlier in case of the high  $K_b$  landscapes. The coarse-grained lobes change their position on the fan surfaces every 20 to 60 kyr. Animations of the landscape development reveal that this lobe switching is a non-periodic, semi-regular process. Transitions of the depositional lobes over the fan surfaces are both gradual and abrupt, depending on the location of the upstream avulsion.

Experiment 5 with  $K_b = 8.0 \times 10^{-4} \text{ yr}^{-2/3}$  was repeated with higher tectonic displacement rates of 4.0 and 8.0 m/kyr, corresponding to a vertical uplift rate of 1.3 m/kyr and 2.6 m/kyr (Figure 2.7, exp. 6 and 7). Subsidence rate and sediment accommodation space are larger due to increased flexural response (0.4 to 0.8 m/kyr). Interaction between the configuration of the thrust fault, kink axes and flexure on the rectangular grid results in a linear bulge behind the fault (Figure 2.7, exp. 7). This bulge captures drainages and results in trident-shaped drainage network, feeding three outlets. The exact nature of this tectonic interaction is not understood, but the geomorphic response shows that the fan feeder channels are capable of forming antecedent drainages. Small incisions at the fault front are more pronounced in comparison to the lower displacement rate experiments (Figures 2.6 and 2.8). This is due to the larger offsets created at the fault front, which gives the incisions more

*Figure 2.8 (previous page) Discharge patterns, landscapes and stratigraphic sections for two of the modelled catchment-fan systems (exp. 5 and 7) at final time = 900 kyr. Dark brown and red represent coarse-grained surface sediments, light brown and blue are fine-grained. Final discharge patterns in both experiments are characterised by dendritic catchment drainages and braided streams on the alluvial fan surfaces (a,b). The right-hand system was subjected to a higher thrust rate (8.0 vs. 2.0 m/kyr) resulting in more closely spaced linear catchment channels and a coalescing sheet of gravel on the fans (d) instead of individual coarse lobes (c). Stratigraphic sections (e,f) reveal fault-perpendicular progradation of coarse-grained facies during quiescence (200-900 kyr). The difference in stratigraphic thickness between sections e and f is due to the increased flexural accommodation space created by the higher thrust load of exp. 7. Fault-parallel sections g and h illustrate the coarse-grained subsurface alluvial fan bodies, which are more pronounced on the low tectonic rate experiment. Timelines in the sections (white) are drawn every 50 kyr.*

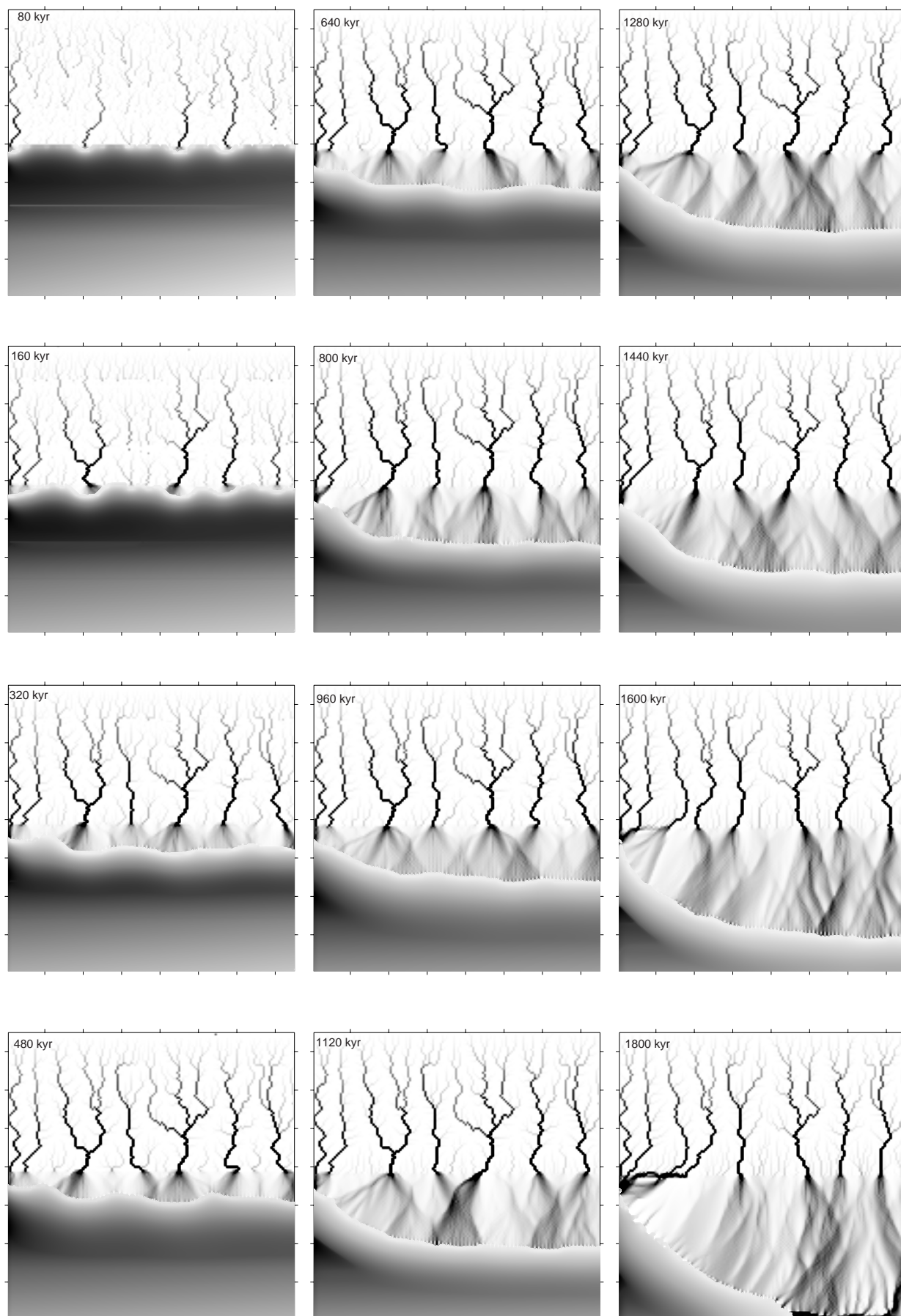
potential to grow. Incisions continue to grow during the quiescent phase, and migrated as a linear front through the hanging wall. Eventually this migrating front captures the drainages of the more complex upstream networks. As a consequence, the few large outlets delivering sediment to the basin decrease in sediment yield and are replaced by a row of smaller, closely spaced outlets feeding a bajada (Figure 2.8). This has implications for the subsurface sediment grain-size distribution near the fault front. Instead of discrete bodies of sideways fining gravel, a thick laterally connected sheet of the gravel bajada is formed (Figure 2.8f).

### ***2.3.2 The effect of pulsating tectonic activity on alluvial fan stratigraphy***

In experiment 8 the catchment-fan system was subjected to a succession of tectonic pulses of 200 kyr duration alternating with quiescent intervals of the same duration throughout a period of 1.4 Myr. The experiment was ended with a longer quiescent interval of 400 kyr (1.4 -1.8 Myr). The general evolution of the catchment-fan system is illustrated by two figures of fluvial discharge patterns and the general landscape evolution coloured according to the surface layer grainsize distributions (Figures 2.9 and 2.10). As basin filling is in progress, the surface area occupied by the shallow marine embayment diminishes and the fans change from small fan-deltas to major alluvial fans. Fan surfaces develop rapid switching of braided networks, while the catchments show clear dendritic, converging channels (Figure 2.9). Transgression of the coastline and the retrogradation of the gravel front towards the fault correspond to the periods of tectonic activity, whereas progradations correspond to periods of tectonic quiescence (Figure 2.10). This behaviour is stored as a three-dimensional, alternating grainsize pattern in the final basin fill (Figures 2.11 b,c,d). In the section perpendicular to the fault, the general vertical trend at every location along the section is coarsening-up (Figures 2.11c and d). Superimposed on this general trend are at least four intervals of gravel progradation. Progradation is associated with closely spaced timelines at the left-hand side of the section, indicating reduced sedimentation rates in the fan apices. Identical to the single-pulse experiments, the gravel progradation intervals correspond with periods of tectonic quiescence. Laterally, the quiescence gravel progradations are distributed as coarse sheets (Figure 2.11b). These sheets become coarser and more pronounced as time progresses. During every following quiescence interval the associated sheet progrades farther into the basin and its lateral connectivity and thickness increase. Tectonic activity intervals are reflected in the section (Figures 2.11b, c and d) by gravel front retrogradation and vertical stacking of dominantly fine-grained strata. The transition from activity to quiescence is characterised by gentle progradation of the coarse sediment. The stratigraphic

*Figure 2.9 (next page) Development of the water discharge patterns in the drainage basins and on the alluvial fan surfaces during experiment 8. Drainage basin networks are dendritic and rigid features whereas the braided channels on the alluvial fans frequently split, avulse and merge. The fan sediment progressively fills the shallow marine embayment, of which the intensity of grey indicates water depth. Final confluences of the stream patterns at the grid edges are boundary effects.*

*Modelling drainage basins and alluvial fan stratigraphy*



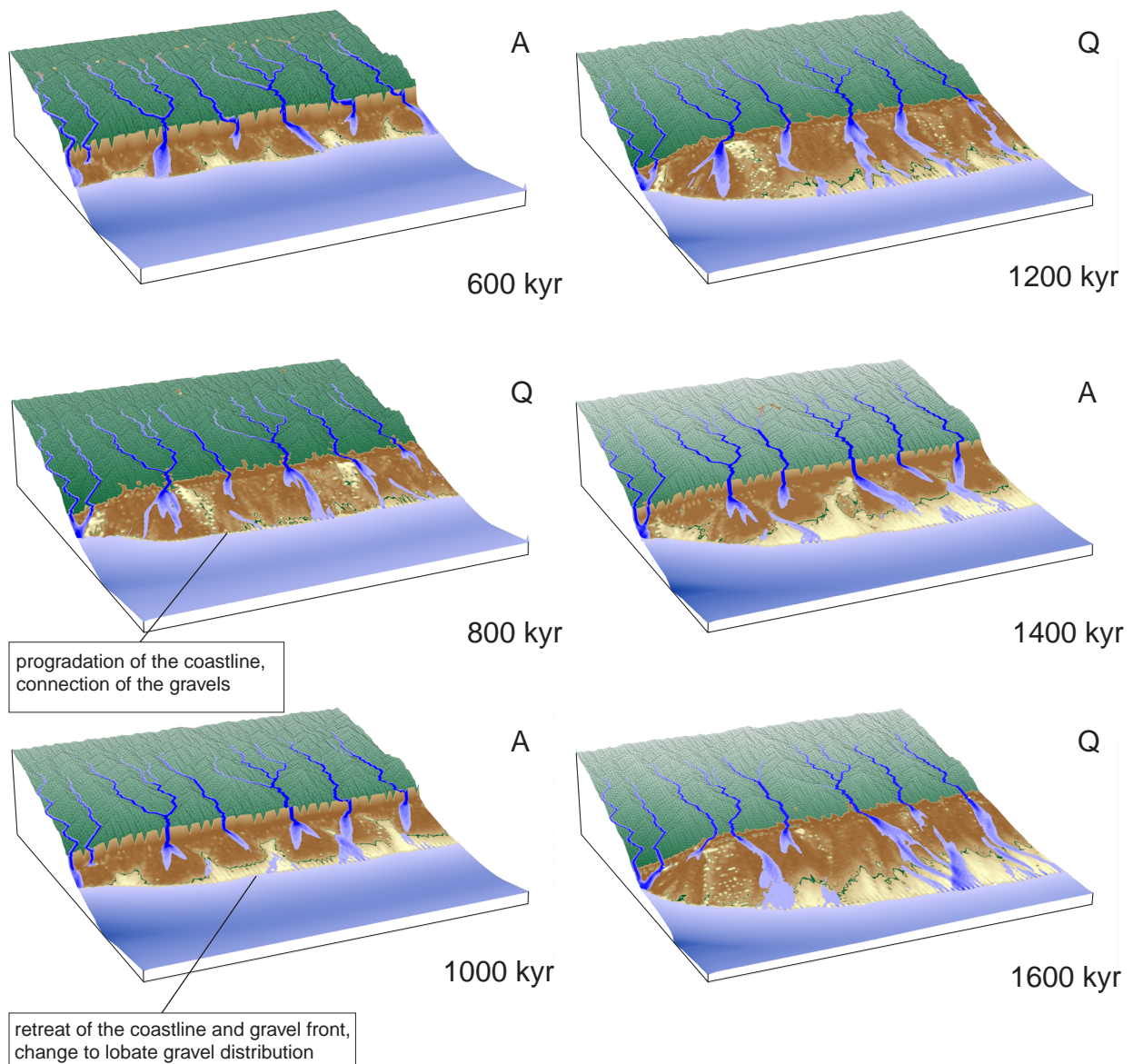
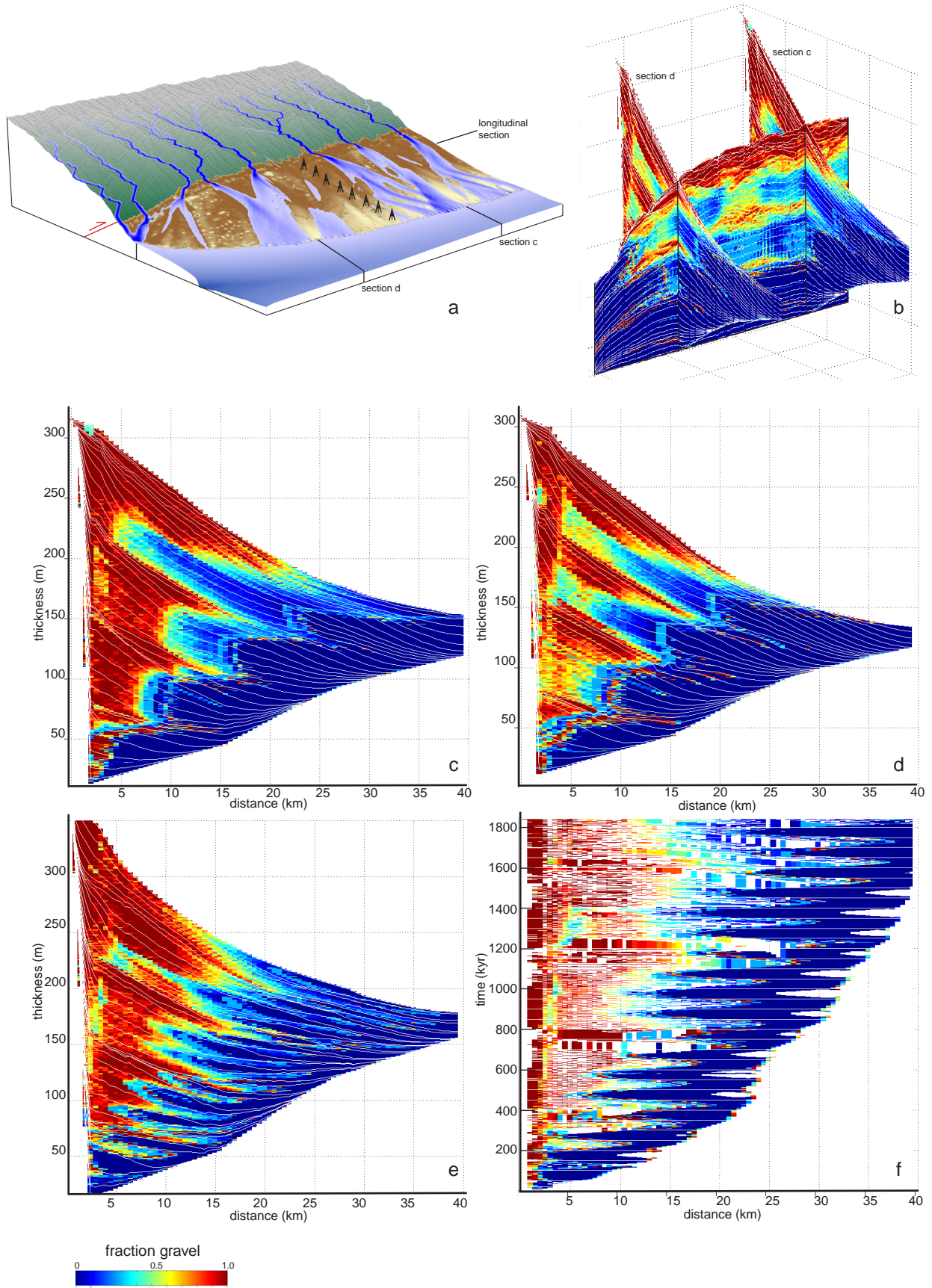


Figure 2.10 Perspective views of successive stages of the landscape subjected to tectonic pulsations (exp. 8). Phases of tectonic activity (A) are reflected by faultward retreat of the coastline and the gravel front and by changes to lobate gravel patches. Quiescence (Q) is associated with their progradation and lateral connection of the gravels.

Figure 2.11(next page) Sections visualizing the gravel distribution resulting from experiment 8 with a history of tectonic pulsation (exp. 8, 200 kyr on/off). Progradations of gravel are synchronous with phases of tectonic quiescence and are reflected in the subsurface as three-dimensional continuous sheets (b). Some differences in the basinward reach of the syntectonic gravel front (c,d) are the result of the local development of fan topography. Sinusoidal sea-level fluctuation (exp. 9, period 100 kyr, amplitude 20 m) superposed on tectonic pulsation complicates the progradation-retrogradation pattern (e). In time-space (f) the quiescence gravel progradation is distinguished more clearly from the higher frequency sea-level fluctuation. Timelines are drawn every 50 kyr.

*Modelling drainage basins and alluvial fan stratigraphy*



response to a transition from quiescence to activity is more abrupt. Within a period of 100 kyr, finer-grained sediments, deposited by the retrograding fans, cover the coarse quiescence sediments.

### ***2.3.3 The effect of pulsating tectonic activity and sinuous sea-level variation***

In experiment 9, the alluvial fan setting was again subjected to a pulsating tectonic signal. In addition, a sinusoidal sea-level signal was superimposed on the tectonic pulses. This sea-level variation had a Milankovitch period of 100 kyr and amplitude of 20 m. Landscape evolution is characterised by dendritic excavation of the catchments and progradation of the fan deltas. The stratigraphic response to tectonic pulses in the section is obscured by the smaller scale sealevel cycles, although 3 major progradations can be recognised (Figure 2.11e). Plotting the section in a time-space (Wheeler, 1958, 1964) makes it is easier to distinguish the forcing signals in the stratigraphic record (Figure 2.11f). Progradations associated with tectonic quiescence consist of thicker sequences with gravel fronts reaching farther into the basin. These sequences also show layer stretching in time-space, indicating a long lifetime of the strata. (Figure 2.11f). During quiescence, strata in fan apices are continuously rejuvenated by small increments of erosion and deposition because the fluvial slope is close to its equilibrium value and most material is bypassed. The layer's top age information is therefore permanently updated, resulting in a long lifetime of this layer. If the layer's base is removed by erosion the layer is represented in time-space as a hiatus. Obviously the sea-level signal is recognisable in the alluvial stratigraphy. Some authors have even postulated that a fluctuating baselevel signal can be transmitted as transient knickpoint and depositional waves to the bedrock floored catchment (e.g. Humphrey and Heller, 1995). In order to investigate whether this is also the case in our model, time-series frequency analysis of the average bedrock erosion rate was done. No frequencies close to the sea-level signal are present in the time series. Most likely the sea-level signal is subdued in our model due to the high rate of in accommodation space creation and the large differences between the detachability of bedrock and alluvial sediment.

### ***2.3.4 Lag time in the depositional response***

The dynamics of the systems are partially reflected by the shape of the sedimentation rate response curves (Figure 2.12). All curves show a gradual increase in the volumetric alluvial sedimentation rate in response to tectonic uplift, followed by an exponential decline after uplift cessation. The gradually rising curve of experiment 1 ( $R_{\text{thrust}} 2.0$  m/kyr,  $K_b 0.5 \times 10^{-4} \text{ yr}^{-2/3}$ ) shows its maximum in sedimentation rate 40 kyr after the end of uplift (Figure 2.12a). The higher  $K_b$  value experiments have their maximum alluvial fan sedimentation rate the moment activity stops at 200 kyr. The values of the maxima slightly vary. The shapes of the exponential decline curves are almost identical, just as the post-tectonic geometric evolution of the catchments (Figure 2.6).

The experiments with a higher displacement rate (exp. 6 and 7,  $R_{\text{thrust}} 4.0$  and  $8.0$  m/kyr, respectively) reveal higher average sediment accumulation rates during decline. The maxima shown for experiment 7 are mainly the result of temporary ponding and subsequent release of sediment behind the 'bulge'



at the fault front (Figure 2.7). Pulsed tectonic activity is reflected as a succession of shark-fin-shaped response curves with increasing maximum sediment accumulation rate values (Figure 2.12c, exp. 8). A superposed sea-level fluctuation modifies the tectonic response curves to a more symmetrical form (Figure 2.12d, exp. 9).

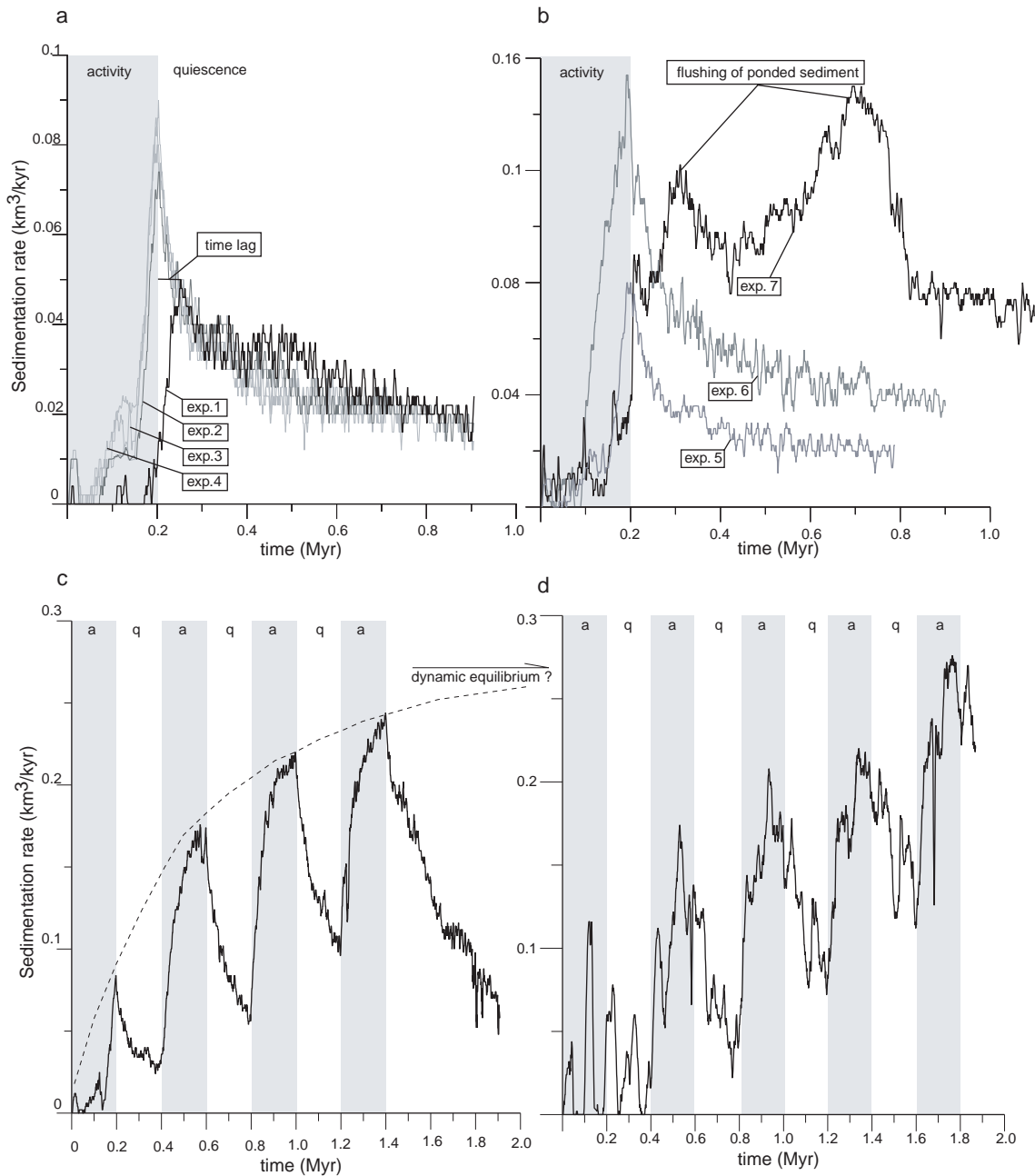


*Figure 2.12 Volumetric sedimentation rates (km<sup>3</sup>/kyr) on the alluvial plain as a function of time for all experiments. Shown are the trends during tectonic activity (grey) and quiescence for variable (a) bedrock erodability coefficient, (b) thrust displacement rate, (c) tectonic pulsation (exp. 8), (d) sinuous sea-level fluctuation superposed on tectonic pulsation (exp. 9).*

Another form of delayed sedimentary response, more useful to the field stratigrapher is the gravel arrival time, which is quantified for experiments 1-8. The arrival time is defined as the time difference between cessation of tectonic activity and the time of arrival of the gravel front at a specific position along a section perpendicular to the thrust fault. A number of synthetic logs are used to evaluate the lag time because they carry detailed age information about every deposited layer facilitating accurate dating of vertical changes in gravel fraction (example of logs in Figure 2.13). There is a resemblance in the arrival time response shown by experiments 2-6, indicated by the clustering of the trend lines (Figure 2.14a). The spread between the lines reflects the time-scale observed in repetitive lobe switching events on the fan surfaces (20~60 kyr). Again, experiments 1 and 7 are exceptions to the general behaviour, and are characterised by longer lag times (Figure 2.14a and b). In experiment 1 this is due to the slow rate of sediment creation by bedrock incision, whereas in experiment 7 it is due to the larger accommodation space that has to be filled before the fan is allowed to prograde. The arrival time is also quantified for the quiescence gravel progradations in the pulsed activity experiment. Successive phases of progradations show equal sloping trend lines, so comparable rates of gravel advance for every quiescent phase (~ 30 m/kyr). Note that the time lag in the distal regions of the basin is on the order of 200 kyr, so the presence of a gravel sheet in the distal stratigraphy can be deceiving. After all, a gravel sheet belonging to a previous tectonic quiescence phase can reach a certain geographic position at the moment a new tectonic pulse initiates.

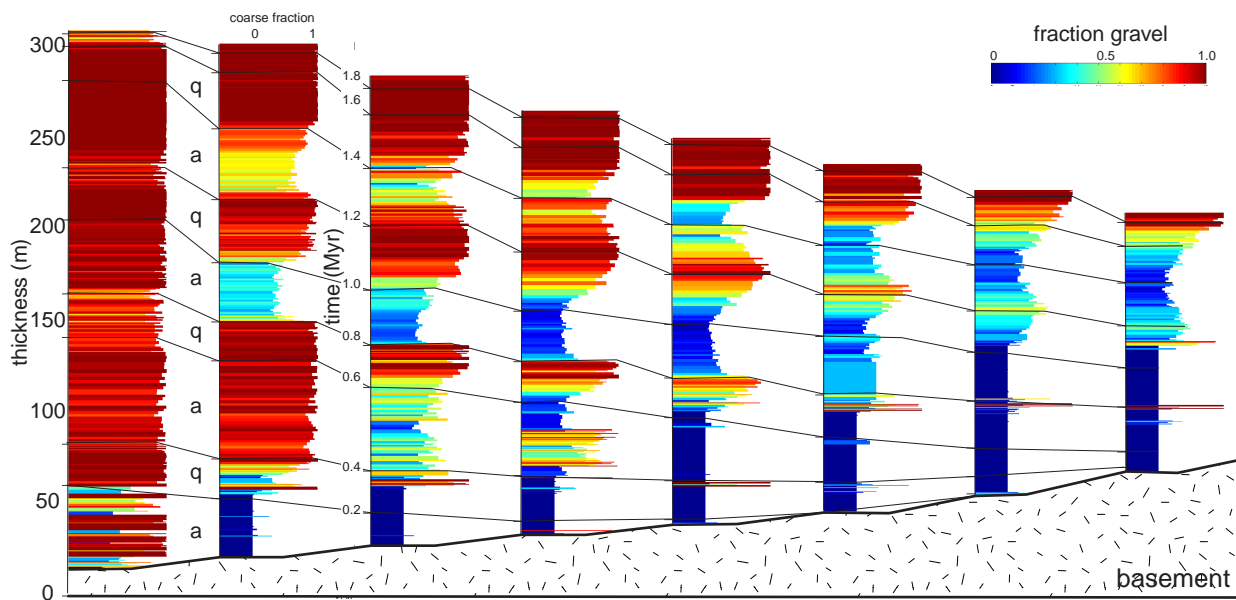


Figure 2.13 Synthetic sedimentary logs sampled from the pulsating tectonic activity experiment in a section line perpendicular to the fault zone illustrating the vertical resolution of the subsurface dataset (< 1.0 m). Indicated are phases of activity (a) and quiescence (q) and correlative time-lines (0.2 Myr time-intervals). Locations of the logs are indicated on figure 2.11.

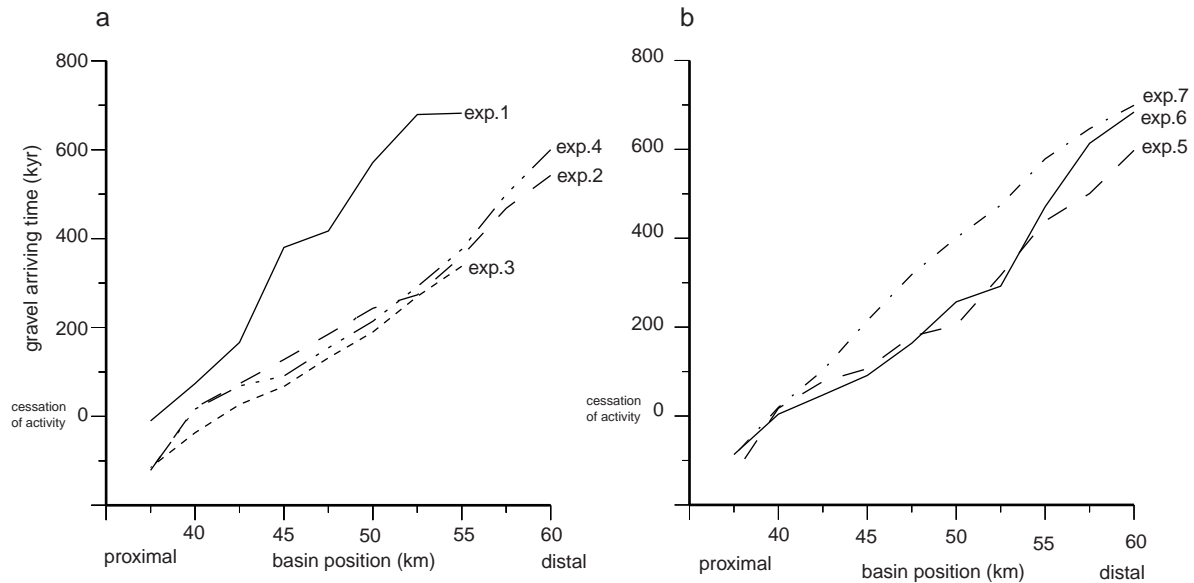


Figure 2.14 Time elapsed after tectonic cessation that the quiescence gravel front reaches a certain position in the basin.

## 2.4 Discussion

The number of catchments draining the up-thrusted fault block and the spacing between their outlets feeding the alluvial fans is approximately the same in the final stages of the experiments 1-7 (Figures 2.6 and 2.7). Average catchment lengths are 35 km whereas widths are 12.5 km, resulting in a length/width ratio of 2.8. This ratio is in the range found for natural uplifting fault block systems (1.4 – 4.1), (Talling *et al.*, 1997), but slightly higher than ratios determined for simple linear-shaped mountain belts (1.9 – 2.2) (Hovius, 1996). No physical explanation for this natural regularity has been suggested so far. Most likely the responsible mechanism is the same as the one underlying Horton's law of channel networks and the power law relationships between catchment length and area (Horton, 1945; Hack, 1957). The branching of the catchments networks in the model is caused by the convergent, steepest descent routing rule, which is the dominant water and sediment routing rule in the eroding areas (Figure 2.3a). The geometries of the catchments and the spacing of outlets can deviate from the above average value due to model parameter changes (Tucker, 2000; Tucker, 2003). From sensitivity experiments not shown here it is clear that initial conditions are also an important factor. If initial slopes between cells due to the surface noise are larger than the slope created by tectonic displacement, the networks grow slower. In addition, the final networks are wider, because sideward extension is favourable above landward extension. A higher *tectonic offset rate* increases the potential of cells at the faulted front to form elongated catchments by vigorous headward erosion. Consequently the outlets are more closely spaced and a continuous depositional apron or bajada is formed (Figure 2.8). *Tectonic style* is also important. Drainage networks are persistent features, once established they hold their position and only incise. As thrust activity

translates the hanging wall towards the depositional basin and channel erosion keeps pace with uplift in the zone of frontal deformation, the outlet channel is stretched in the direction of the displacement. This enhances the typical wine glass shape of the catchments (Schumm, 1977, 1981). If this model behaviour is analogous to a natural situation, settings bounded by normal faults are expected to have more and shorter outlets feeding alluvial fans.

The networks respond in an unexpected manner to changes in bedrock erodability (experiment 1-6). A change from  $K_b$   $0.5 \times 10^{-4}$  to  $2.0 \times 10^{-4} \text{ yr}^{-2/3}$  results in faster network growth and different configurations at 0.9 Myr. Changing erodability from 2.0 and  $8.0 \times 10^{-4} \text{ yr}^{-2/3}$  does not result in noticeable changes in network evolution, its final state or the response of the fan deposition rate curves (Figure 2.12). The explanation is found in the size of the incremental tectonic displacement step versus the general erodability of the bedrock substratum. The incremental vertical displacement is 3.2 m. Bedrock catchments with erodabilities of 2.0 to  $8.0 \times 10^{-4}$  are all able to counteract this incremental offset with an equivalent incision. As a result the morphological response and yield are limited by the offset size and not by the erodability. Even if this behaviour is an artefact of the incremental calls to the thrust displacement routine, it could mean that erodability versus incremental offsets created by single seismic events is important in shaping natural systems. Adding more material per tectonic increment by increasing the displacement rate again leads to different network configurations, higher sedimentation rates and even post-tectonic highs in sedimentation rates. A long-term dynamic equilibrium between uplift and erosion is not reached in all experiments. Levelling of the response curves, characteristic of an achieved dynamical equilibrium is not observed (Figure 2.12). If one extrapolates the trends, equilibrium is expected to occur after 2.0 Myr of constant uplift. Therefore, dynamic equilibrium is a very exceptional geomorphic situation, especially in natural situations which are prone to climatic and tectonic perturbations with higher frequencies than the time needed to reach equilibrium in the model (Whipple, 2001).

The model behaviour as result of pulsating tectonic activity is in agreement with model results obtained by Paola *et al.* (1992) and Marr *et al.* (2000), although they do not incorporate uplift and drainage basin excavation. Gravel front progradation corresponds with phases of tectonic quiescence, whereas retrogradation reflects (renewed) tectonic activity. Catchment yields increase during phases of active uplift but are of insufficient volume to fill the accommodation space created. Consequently, the coastline and the gravel front retreat. As the creation of accommodation space due to subsidence stops, the fans are forced to prograde into the basin in order to disperse their sediment while maintaining an equilibrium slope. Intervals of tectonic activity are recognised in stratigraphic section by vertical stacking of layers with comparable grain-size fractions. Active creation of accommodation space near the faulted margin prevents fans from prograding. The catchments are not able to supply enough sediment to fill the accommodation space that has been created. The transition from activity to quiescence is characterised by gentle progradation of coarse sediment. The fans first try to

accommodate the sediment by increasing their slope, and when the ideal slope is reached, they prograde. This transition takes at least 100 to 150 kyr in the model. The stratigraphic response to a transition from quiescence to activity is more abrupt. As new accommodation space is created along the entire section line, fans retrograde. Within 100 kyr, finer-grained sediments deposited by the retrograding fans, cover the coarse quiescence deposits. Using a time-dependent, visco-elastic flexure equation to create accommodation space would modify the general pattern, depending on the viscosity value chosen.

One of the most tangible results from our modelling exercises is the quantification of the gravel arrival time (Figure 2.14). Although we think that the magnitude of the response is of the right order, prudence is called for if applying these values directly to field situations. The model lag time is very dependent the local accommodation space and on the choice of the fluvial coefficient  $K_f$  (eq.15) in the model.  $K_f$  should be calibrated better using well-dated fan stratigraphic patterns and simple forcing histories, but such data are sparse in the coarse-grained sedimentary record. The chosen  $K_f$  value results in an average propagation velocity of the gravel front (30 m/kyr) which is in good agreement with those observed in natural alluvial fan systems in rapidly subsiding basins (Eocene Tresp Basin 25-40 m/kyr, Nijman 1998; Himalayan foreland basin 30 m/kyr, Brozovic 2000). Perhaps the dual-lithology system is described more appropriately using two values for  $K_f$ , one for the coarse and one for the fine fraction, e.g. Riveneas (1997) and Marr *et al.* (2000). However, this would complicate the computational effort.

Natural, comparable settings of our modelled fans are, for example, the large fan-deltas along the Catalan Coastal Ranges because of the resemblances in average drainage basin erosion rate (0.15 m/kyr), fan size ( $> 100 \text{ km}^2$ ), fan deposition and episodic progradation rate (0.30 m/kyr and 0.10 to 5.0 m/kyr, respectively, Lopez-Blanco, 2000). Of course, the model does not capture the facies detail described for these fans, or the complete suite of interfering external forcings and processes responsible for their formation. However, basin-wide retraction of the gravel front and fine-grained sedimentation in these settings is interpreted as non-periodic variations ( $10^5$ - $10^6$  yr) of subsidence and sediment supply (Burns *et al.*, 1997; Lopez-Blanco *et al.*, 2000). Often these retractions are accompanied with onlap of carbonate sediment and abrupt changes of the clast composition close to the thrust front. These additional depositional features are often used for unravelling the relative contributions of climatic and tectonic control on the stratigraphic record and are partly added to the model version shown in Chapter 3 and 4.

## **2.5 Conclusions**

Experiments show that it is possible to capture the main morphological and stratigraphic features of drainage basin excavation and synchronous alluvial fan deposition with a three-dimensional forward model. Drainage basin networks developed are dendritic and, when established, show a tendency to incise without shifts in location. Channel re-organization occurs solely by occasional drainage basin capture events. In contrast to drainage basins, the alluvial fan surfaces are characterized by rapidly shifting braided stream patterns. Repetitive switching of coarse-grained depositional lobes on the fan surfaces is non-periodic and occurs every 20 to 60 kyr.

The balance between bedrock erosion rate and tectonic uplift determines the geometrical evolution of the catchments and possible time lags between the end of tectonic activity and fan sedimentation rate highs. Pulsed tectonic activity is reflected in the alluvial fan stratigraphy as a stacking pattern of prograding and retrograding gravel fronts. Progradation phases are synchronous with tectonic quiescence, whereas retrogradation phases are synchronous with tectonic activity. Progradation of the front during quiescence is a transient process. The greater the distance from the tectonic boundary, the larger the lag time before arrival of the front. The order of magnitude of the gravel arrival time after tectonic cessation is several tens to hundred kyrs. The stratigraphic response to the onset of tectonic pulses is a rapid retrogradation due to the surplus in accommodation space created compared to the catchment yields. Due to the basin-wide character of the subsidence, retreat is faster than progradation and noticeable in the entire basin. Simultaneous variation in sea level results in a more complex stratigraphic record. The tectonic response is then masked by smaller-scale progradation sequences synchronous with sea-level fall.

## **Differentiating the effect of tectonic pulsation and eustatic sea-level fluctuation in foreland basins filled by alluvial fans and axial deltaic systems**

### **Abstract**

Many studies of foreland basins have recognized a hierarchical organisation in the stacking of sequences deposited by axial-deltaic and alluvial fan systems. The hierarchy is often explained in terms of the competing control of eustasy and pulsed tectonic subsidence and the different frequencies at which these processes operate. Unravelling the relative contributions of tectonic and eustatic control on the sequence stacking pattern is a fundamental question in foreland basin analysis, yet difficult because of the lack of independent stratigraphic evidence. In this study we present a 3D numerical tool, which aids in the interpretation of alluvial successions in foreland basins filled by both depositional systems, under conditions of variable tectonism and eustatic sea-level change. The tectono-sedimentary model is capable of simulating the hierarchical stratigraphic response to both external forcings, and is of higher resolution compared to previous models of foreland basin filling. Numerical results indicate that the onset of tectonic activity is reflected by rapid retrogradation of both depositional systems, widespread flooding and onlap of marine sediments. Syntectonic fluvial patterns on the axial-delta plain are dominated by bifurcating channels, swiftly relocating in response to the general rise of relative sea level induced by flexural subsidence. The resulting surface morphology of the axial delta is conical. Syntectonic eustatic sea-level fluctuations result in parasequence-scale packages of retrograding and prograding fan and deltaic sediments bounded by minor flooding surfaces and Type-2 unconformities. Incised channels are rare within the syntectonic parasequences and are formed only during phases of tectonic quiescence when eustatic falls are not longer compensated by the subsidence component in the rise of relative sea level. Suites of amalgamating axial channels corresponding to multiple eustatic falls delineate the resulting Type-1 unconformities. Coarse-grained, incised channel fills are found in the zone between the alluvial fan fringes and the conical body of the axial delta, as the axial streams tend to migrate towards this zone of maximum accommodation.

### 3.1 Introduction

Foreland basins are commonly filled by a combination of two depositional elements: transverse alluvial fans and longitudinal structure-parallel rivers (Kuenen, 1957; Miall, 1981). *Modern examples* of this association are found on the Po, Indo-Gangetic and Mesopotamian plains (Geddes, 1960; Allen, 1965; Baltzer and Purser, 1990; Ori, 1993; Sinha and Friend, 1994; Gupta, 1997), while *Ancient examples* are well-studied in the sedimentary records of the Alpine Molasse Basin (Figure 3.1) (Jin *et al.*, 1995; Schlunegger *et al.*, 1997; Zweigel *et al.*, 1998) and the Pyrenean Foreland Basin (Bentham *et al.*, 1992; Dreyer and Falt, 1993; Nijman, 1998). A fundamental problem in interpreting the stratigraphy of these foreland basins is to understand and differentiate the relative importance of tectonism and eustasy on sequence development and architectural stacking patterns of both depositional systems (Bhattacharya, 1991; Schwans, 1995; Nijman, 1998; Robinson and Slingerland, 1998; Zweigel *et al.*, 1998; Dreyer *et al.*, 1999).

Sequences in these basins contain both depositional elements and are often bounded by unconformities and carbonate horizons. The sequences usually reflect continuous deposition at rates of 0.2-0.6 m/kyr (Mutti *et al.*, 1988; Bentham and Burbank, 1996; Brozovic and Burbank, 2000), while the bounding horizons that indicate temporal flooding, low sedimentation rates or erosion.

A well-studied example of the internal fluvial architecture of such sequences comes from the Eocene Montanyana Group of the Pyrenean Foreland Basin (Marzo *et al.*, 1988; Nijman, 1998). Here

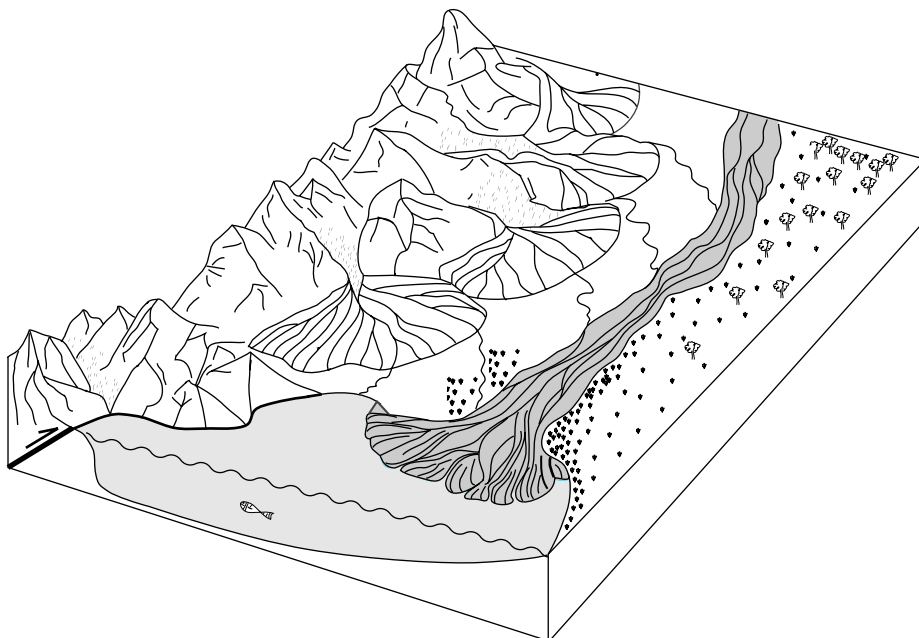


Figure 3.1 Example of the foreland basin configuration modelled in this chapter. The German Molasse basin during the Oligocene, occupied by transverse alluvial fans and an axial river, draining into a marine embayment. Redrawn after Jin *et al.* (1995).



sequences are characterised by retrogradational and progradational changing positions of the alluvial fan gravel fronts, accompanied by shifts of axial-channel deposition. Both systems move in phase with each other, almost in a tandem-like fashion. Abrupt changes in the architectural stacking pattern are found around the sequence unconformities. The basin-wide sequence unconformities are marked by sudden shifts of both depositional systems and their relative positions, often concurrent with onlap of shallow marine sediments, such as carbonates. The distribution of the unconformities through time is a-cyclic and their re-occurrence interval in the order of 0.2 to 2.0 Myr. Therefore, both the unconformities and the observed architectural patterns are often explained in terms of pulsating tectonic activity (Puigdefabregas and Souquet, 1986; Mutti *et al.*, 1988; Kamola and Huntoon, 1995; Nijman, 1998).

During the late eighties it was recognized that the above-mentioned depositional systems respond differently to the onset of tectonic activity (Blair and Bildeau, 1988; Heller *et al.*, 1988). Thrust-load emplacement causes rapid flexural subsidence in the proximal regions of the basin; the newly created accommodation space is occupied first by the finer-grained axial-depositional system and subsequently by alluvial fans. The expected response of the alluvial fans in terms of gravel front progradation will lag behind the onset of a tectonic activity because these systems depend on the relatively slow denudation of the newly created topography for their sediment supply (Schumm, 1963). In addition, their progradation is inhibited by the high rates of syn-tectonic subsidence close to the fault front. In most cases the rate of proximal accommodation space created exceeds the rate of sediment supply from the rejuvenated hinterland, and the alluvial fans retreat towards the thrust front (Heller *et al.*, 1988; Schlager, 1993). The externally sourced axial depositional system can take advantage of the sluggish alluvial fans by occupying the newly created depression swiftly because of their low depositional slope and continuous high supply of sediment. The onset of subsidence results in a punctuated, basin-wide flooding, marked by the deposition of coals, marls or carbonates, depending on the basin configuration. Later, during ongoing tectonic activity the balance between the rate of subsidence and the rate of alluvial fan progradation controls the position of the axial system as the axial streams preferably occupies the depression between fan fringes and the previously deposited convex body of the axial delta. The stratigraphic architecture in the Pyrenean example can therefore be interpreted in terms of tectonic pulsation, thrust emplacement-induced subsidence and the differential velocities of the depositional systems occupying the accommodation space created.

The stratigraphic response to tectonic processes in this and in other foreland basins is often complicated by a higher-order stratal pattern with a frequency close to 100 kyr. These are patterns of repetitive growth of the fans (Nijman, 1998), or in case of the axial deltaic deposits, upward coarsening and upward-shallowing, clastic progradational packages bounded by minor flooding surfaces (i.e., parasequences). The parasequences could reflect short-term variations in thrust propagation (Houston *et al.*, 2000) or climate-induced fluctuations in sediment supply (Weltje *et*

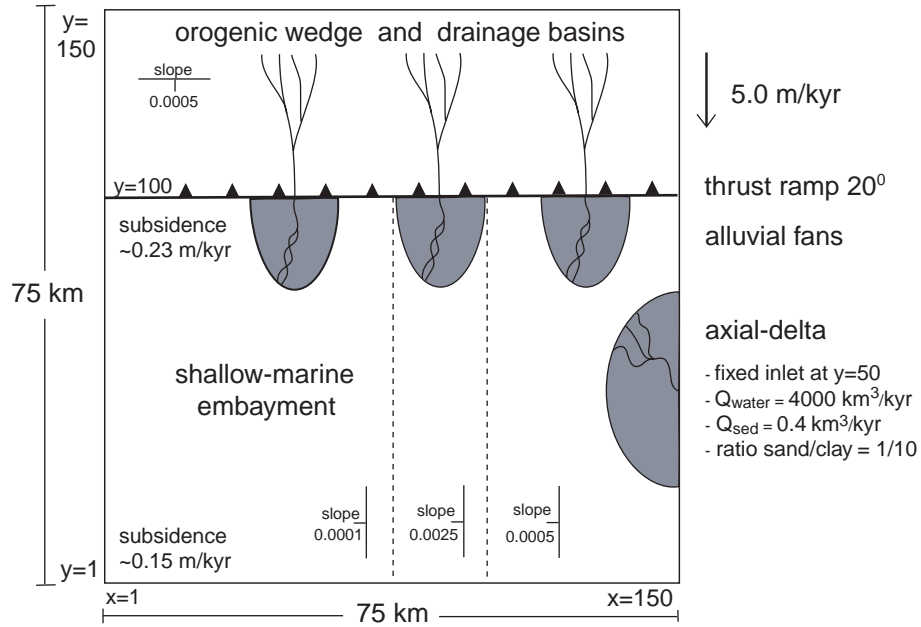


Figure 3.2 Geometric plan view of model set-up, representing a proximal foreland basin separated from the orogenic wedge by a hinterland-dipping thrust fault. Indicated are the initial surface slopes and the fixed inlet position of the axial system. Value of the syn-tectonic subsidence diminishes basinward due to the shape flexural response. Alluvial fans fed by orogenic drainage basins experiencing a constant rainfall of 1.0 m/yr. Dimensions of the set-up represent 75 x 75 km using a 150 x 150 rectangular matrix of 500 m cells.

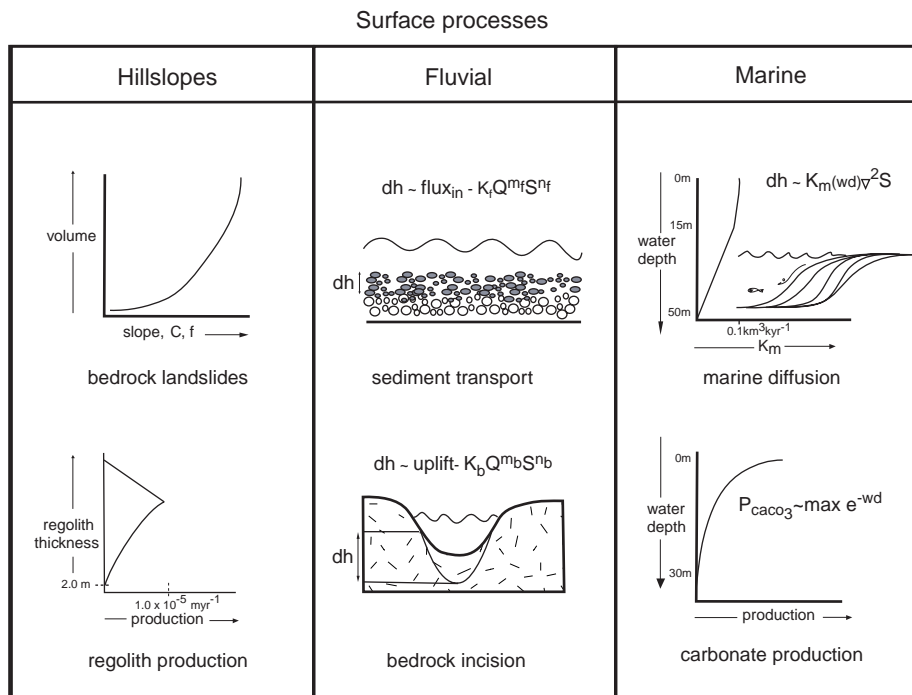


Figure 3.3 Diagram summarizing the main surface processes used to generate and transport sediment in the drainage basins and depositional realms of the modelled foreland setting. Selected literature sources for the used methods are: bedrock collapse (Spangler and Handy, 1982; Densmore et al., 1998), weathering (Heimsath et al., 1997), sediment transport (Howard et al., 1994; Tucker, 1996), bedrock incision (idem), marine diffusion (Kenyon and Turcotte, 1985), carbonate sedimentation (Boscher and Schlager, 1992).

*al.*, 1996), but are often explained by eustatic sea-level change (Bhattacharya, 1991; Chen *et al.*, 2001; Plint *et al.*, 2001). Interpreting foreland basin stratigraphy is therefore difficult because the relative importance of tectonism and eustasy on sequence development and architectural stacking patterns is not always apparent.

Therefore, a three-dimensional stratigraphic forward model is constructed to facilitate the interpretation of ancient alluvial successions generated under these two external forcings. The quantitative model simulates the interaction between pulsating thrust activity, sea-level change, flexural response, orogenic denudation and sediment transport across alluvial fans and axial channels towards a shallow marine realm. The modelled foreland basin fill is visualized and studied by means of fence diagrams, individual cross-sections, Wheeler diagrams, synthetic wells and voxel representations of subsurface sediment characteristics. Animations of the landscape evolution, recorded time series of the denudation and deposition rates, facilitate to relate geomorphic processes and the associated stratigraphic response. Limited by computational capacity the model only applies to the proximal section of a foreland basin.

## **3.2 Modelling method**

### ***3.2.1 Earlier modelling studies***

During the previous decade, process-based models of long-term sedimentation have become widely used tools in theoretical and applied basin studies. A thorough overview of the developments in the field is provided by Paola (2000). The early generation of two-dimensional foreland basin models increased our understanding of sedimentation responses to tectonic loading and unloading (Flemings and Jordan, 1990; Sinclair *et al.*, 1991; Peper, 1993). The following three-dimensional models echoed their conclusions and added along-strike variation in tectonic convergence rate, subsidence, drainage patterns and stratigraphy (Johnson and Beaumont, 1995; Garcia-Castellanos *et al.*, 1997; Garcia-Castellanos, 2002). Despite the numerical complexity involved in these models the spatial and vertical resolution of the synthetic stratigraphic sections generated is often poor and they show no discrimination in depositional facies or grain sizes. Consequently, these model results are only suitable for illustrating large-scale, geodynamic concepts, and are difficult to compare directly with sedimentological field studies that gather data on a smaller scale.

### ***3.2.2 Model used in this study***

In this study we present a model developed to bridge the gap between both spatial scales of interest by increasing resolution and realism of the stratigraphic record. Due to computational limitations the modelled time span and spatial extensions are smaller than those in the larger foreland basin models. The model operates on a 150 x 150 rectangular grid with a spatial resolution of 500 m, using timesteps of 10 yrs for the geomorphic processes (Figure 3.2). Consequently, workable time spans of basin-fill simulations are on the order of 2.0-3.0 Myr. The three-dimensional model incorporates several geomorphic processes to produce, transport and deposit sediments (Figure 3.3

Parameter	value	equation/figure
$\Delta x$	500 m	Figure 3.2
$\Delta t$	10 yr	3.1
$K_f$ axial delta	$0.1 \text{ m}^{-3/2} \text{ yr}^{1/2}$	3.1
$K_f$ alluvial_fans	$0.01 \text{ m}^{-3/2} \text{ yr}^{1/2}$	3.1
$m_f, n_f$	3/2 and 1	3.1
$K_b$	$1.0 \times 10^{-4} \text{ yr}^{-2/3}$	3.2
$m_b, n_b$	1/3 and 2/3	3.2
$R_{\text{regolith}}$	$1.0 \times 10^{-5} \text{ myr}^{-1}$	Figure 3.3
$\theta_c$	$30^\circ$	3.7
C	$6 \times 10^4 \text{ kgm}^{-1} \text{ s}^{-2}$	3.7
$K_{\text{marine}}$	$0.1 \text{ km}^3 \text{ kyr}^{-1}$ at 15 m	3.10
$\text{Carb}_{\text{max}}$	$0.1 \text{ mkyr}^{-1}$	3.11
Thrust fault ramp	$20^\circ$	Figure 3.2
$\text{EET}_{\text{flexure}}$	15 km	2.16

Table 3.1 Constants used in the foreland basin model in this chapter. For time-dependent variables see Figure 3.5.

and Table 3.1). Orogenic denudation is performed by bedrock collapse, bedrock incision, and bedrock to regolith conversion (i.e., weathering). The released sediment is distributed over alluvial fans following steepest descent and bifurcating routing schemes while using streampower-type equations for stream transport capacity. An important additional sediment source enters the space in the form of an axial fluviio-deltaic system. Water and sediment supply rates to this system are held constant throughout the scenario presented below at  $4000 \text{ km}^3/\text{kyr}$  and  $0.4 \text{ km}^3/\text{kyr}$ . As a basis for these values, the time-averaged volumetric sedimentation rates of the Montanyana Group (Trempe Basin) are used, because the basin's size matches the dimensions of the model. The ratio is derived from the general notion that the average sediment / water discharge ratios for large rivers fluctuate around 1:10,000 (Milliman and Syvitski, 1992). The axial sediment entering the system is composed of 10 % sand and 90 % finer-grained sediment (Burgess and Hovius, 1998). Both alluvial fan and axial sediments are routed toward the marine area where they are deposited in the delta or leave the western grid boundary, which operates as a sediment sink. Marine cells, deprived of clastic input simulate carbonate production *in situ*.

### 3.2.3 Surface Processes

#### 3.2.3.1 Streampower law sediment transport

Sediment transport in both alluvial fan and axial channels is evaluated with a streampower-type equation, which states that the capacity to carry sediment is proportional to the product of slope  $S$  and water discharge  $Q$  in the channel (Howard, 1994; Tucker, 1996b). In absence of tectonic subsidence or uplift, the change of height of a channel cell is a function of the changes in carrying capacity along the transport path

$$\frac{\partial h_{\text{all}}}{\partial t} = -\frac{K_f}{W} \left( \frac{\partial Q^{m_f} S^{n_f}}{\partial x} + \frac{\partial Q^{m_f} S^{n_f}}{\partial y} \right) \quad (3.1)$$

where  $W$  is the channel width, which can be approximated using an empirical equation (Leopold and Maddock, 1953), and  $K_f$  the fluvial transport coefficient. Based on a study of extensional

basins it is argued that a ten-fold difference in diffusivity coefficient is suited to model the difference in transportability between coarse fan deposits and finer axial sediments (Marr *et al.*, 2000). Their approach is adopted in this study by applying two values for  $K_p$ , one for the alluvial fans (0.01) and one for the axial fluvio-deltaic system (0.1). Analogue to diffusion-based stratigraphic modelling, there is most likely a wide range in applicable values of the transport coefficient  $K_p$ , depending on the spatial and temporal discretization used (Anderson and Humprey, 1990; Quiquerez *et al.*, 2000). The form of equation 3.1 is derived from engineering time-scale formulae for bedload transport, and the values of  $m_f$  and  $n_f$  are determined empirically. Several recent publications give a thorough theoretical background of the method (Whipple, 1999; Tucker, 2000; Whipple and Tucker, 2002). Here, a slope exponent of  $n_f = 1.0$ , ensuring numerically stable transport while distributing sediment over multiple downstream cell directions and  $m_f = 1.5$ , because it enhances channalisation and incision of flow at emerged delta break-in-slopes and stream confluences (Murray and Paola, 1997; Crave and Davy, 2001). Each fluvial system carries a sediment load composed of two grain size fractions. During the multiple evaluations of erosion and deposition along the stream paths through the computational grid the coarse fractions are segregated from the finer ones using the perfect sorting principle, which is based on selective deposition of the least transportable fractions (Paola *et al.*, 1992).

### 3.2.3.2 Bedrock incision

In the absence of a sediment cover, the change of height of a cell is determined by the rate of bedrock incision, which is again a function of discharge and slope (Howard, 1994)

$$\frac{\partial h_b}{\partial t} = -K_b Q^{m_b} S^{n_b} \quad (3.2)$$

where the  $K_b$  is the bedrock erodability coefficient ( $1.0 \times 10^{-4} \text{ yr}^{-2/3}$ ). Exponents  $m_b$  and  $n_b$  are 1/3 and 2/3 respectively, as these values resulted in a well calibrated fit between modelled and observed topography of the Zagros fold-and-thrust belt (Tucker, 1996a). Sediment produced by bedrock incision is composed of 50% coarse and 50% fine grain size fraction and distributed further downstream by fluvial transport (eq. 3.1).

### 3.2.3.3 Bedrock collapse

In actively deforming regions bedrock landsliding is an important contributor to the volumes denudated (Hovius *et al.*, 1997). However, landslides are complex sporadic events for which it is hard to derive a time-average denudation rate. It depends on the interaction between hillslope gradient, rock strength, internal friction, and the occurrence of seismic events (Schmidt and Montgomery, 1995; Densmore *et al.*, 1998). The local potential failure is assessed using the Culmann slope stability criterion (Spangler and Handy, 1982) (Figure 3.4). This criterion states that the maximum stable slope of a hillslope will be reached when the effective weight ( $F_{\text{eff}}$ ) on the potential failure plane is balanced by the shear resistance on this plane ( $F_r$ ):

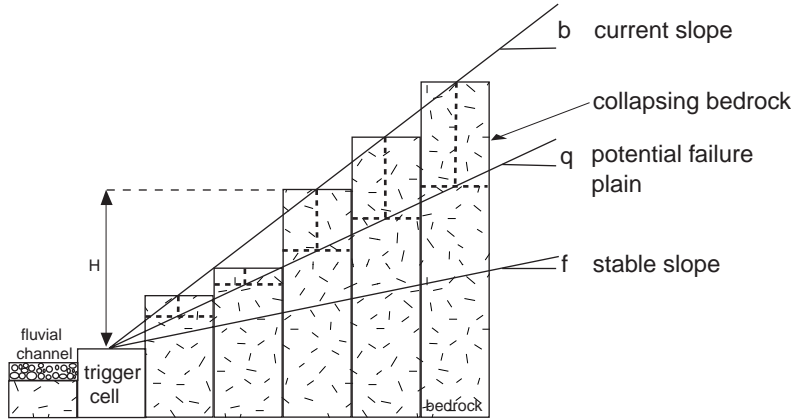


Figure 3.4 Two-dimensional diagram of the geometry involved in the evaluation of a bedrock landslide envelope. If collapse takes place, the failure plain becomes the new surface slope and the material is routed via the target cell towards a nearby fluvial cell as sediment.

$$F_{eff} = F_w \sin \theta \quad (3.3)$$

$$F_r = CL + F_w \cos \theta \tan \phi \quad (3.4)$$

Where  $F_w$  is the weight of the material,  $\theta$  the slope of the failure plane,  $L$  the length of the failure plane,  $C$  the cohesion and  $\phi$  the friction angle on the plane (Spangler and Handy, 1982; Densmore *et al.*, 1998). Failure will occur at the critical fault plane if  $F_{eff} = F_r$ . In this situation the cohesion on the failure plane is expressed as:

$$C = \frac{1}{2} \rho g H \frac{\sin(\beta - \theta_c) \sin(\theta_c - \phi)}{\sin(\beta) \cos(\phi)} \quad (3.5)$$

where  $\rho$  is the density of the rock,  $g$  the gravitation constant,  $H$  is the elevation difference between a stable cell and the collapsing cell and  $\beta$  the surface slope of the landslide envelope (Figure 3.4). The derivative of the cohesion with respect to the failure plane slope is:

$$\frac{\partial C}{\partial \theta} = \frac{1}{2} \rho g H \frac{\sin(\beta - 2\theta_c + \phi)}{\sin(\beta) \cos(\phi)} \quad (3.6)$$

so that  $C$  is maximized at  $\theta_c = 1/2(\beta + \phi)$ . The stable maximum height of the hillslope is found by substituting  $\theta_c$  into equation 3.6:

$$H_c = \frac{4C}{\rho g} \frac{\sin \beta \cos \phi}{[1 - \cos(\beta - \phi)]} \quad (3.7)$$

The probability of failure and the resulting landslide can now be expressed as the ratio actual hillslope height versus the maximum critical height according to equation. 3.7.

$$P_{collapse} = \frac{H}{H_c} \quad (3.8)$$

This landslide probability ranges between 0 and 1, and is evaluated using a random number routine. A positive test for a single hillslope cell results in application of the criterion on surrounding potentially unstable hillslope cells. The size of the landslide is determined by accumulating all failed mass around the trigger cell of the landslide. The receiving cell of the landslide is the cell holding the steepest slope with the triggering cell (Figure 3.4). The landslide is distributed further

downstream as a sediment mass flow. The shape of the mass-flow deposit is determined by an empirical determined run-out length (~ 5 km, Blair, 1999) and the possibility to spread in multiple directions. During mass-flow routing over the grid, the debris fills in irregular topographies and subsequently increases the amount of sediment on valley floors and alluvial fan apices. Mass flow sediments are subsequently reworked by fluvial erosion and deposition.

#### 3.2.3.4 Bedrock to regolith conversion

Regolith is produced by in situ chemical weathering of bedrock. Recent studies based on the decay of cosmogenic nuclides indicate that regolith production rates are around  $1.0 \times 10^{-5}$  to  $5.0 \times 10^{-5}$  m/yr for semiarid areas, e.g. Western United States (Bierman, 1994), and  $5.0 \times 10^{-6}$  m/yr for Alpine areas (Small *et al.*, 1999). These studies confirmed that weathering rates are faster beneath a certain regolith cover (Heimsath *et al.*, 1997), but decay with increasing cover thickness. Following Densmore *et al.* (1998) the regolith production curve in the model starts with a bare bedrock production rate, increasing linearly to a maximum rate at the regolith thickness optimum, followed by an exponential decrease with increasing regolith thickness (Figure 3.3). Regolith is produced in model cells, which do not act as drainage outlets for upstream cells. The composition of the regolith produced is 10% coarse and 90% fine-grained sediment.

#### 3.2.3.5 Marine deposition

In the model a fluvial channel entering the marine realm is instructed to dump all its bedload until the local accommodation space below sea level is filled. Excess sediment is distributed to neighbouring marine cells proportional to gradient. Within the marine realm sediment transport is modelled by diffusion because of its ability to produce realistic looking clinoform profiles in delta fronts (Kenyon and Turcotte, 1985; Syvitski and Daughney, 1992). Making the diffusivity coefficient  $K_m$  water-depth dependent enhances this property, simulating the decrease of erosive energy in the coastal area with increasing water depth. The values of  $K_m$  are maximum above wavebase depth ( $0.1 \text{ km}^3/\text{kyr}$  at 15m) and decreases linearly below this depth. The marine sediment flux is a function of the water depth-dependent diffusion coefficient  $K_m$  and the local slope in three-dimensions,  $\nabla S$ :

$$Q_{sed} = K_m(wd)\nabla S \quad (3.9)$$

Combined with the continuity equation, this transport equation gives the rate of elevation change for a marine cell:

$$\left. \frac{dh}{dt} \right|_{marine} = -K_m(wd)\nabla^2 S = -K_m(wd) \left( \frac{\partial^2 h}{\partial x^2} + \frac{\partial^2 h}{\partial y^2} \right) \quad (3.10)$$

#### 3.2.2.6 Carbonate deposition

Carbonate producing organisms are dependent for their growth on the intensity of light penetrating through the water column and are hindered by the presence of clastic sediment. Therefore, a depth-

dependent carbonate production law (Demicco, 1998) is applied to the marine model cells, but only to those that do not receive any clastic input during the specific time step. The carbonate production rate  $P$  decreases exponentially with increasing water-depth  $wd$

$$P_{carb} = \max_{carb} e^{-wd} \quad (3.11)$$

There is a high variability in the maximum carbonate production rate ( $\max_{carb}$ ) proposed by various authors (see Boscher and Schlager, 1992, for an overview). In our experiments we adapt the relatively low, average sedimentation rates obtained from the Morillio and Guarra Limestone (0.1 m/kyr, Eocene Pyrenean foreland) as these are formed in a basin with high clastic supply rates (Bentham *et al.*, 1992; Molenaar and Martinius, 1996; Nijman, 1998).

### 3.2.4 Tectonic processes

Thrusting of the orogenic block over the developing foreland is modelled by using a velocity description of deformation (Figure 2.5) (Hardy and Poblet, 1995). Flexural subsidence upon thrust and sediment loading is calculated in multiple sections using a 2D analytical solution of broken plate flexure (Slingerland *et al.*, 1993).

### 3.2.5 Tectonic and eustatic forcing

During the scenario modelled the foreland basin setting was subjected to a periodic tectonic forcing composed of alternating intervals of tectonic activity and quiescence, both having a duration of 250 kyr (Figure 3.5). Although there are no indications from the stratigraphic record that tectonic activity is periodic, it is applied as such in the model in order to facilitate recognition of the related stratigraphic response. The horizontal displacement rate of the thrust fault is 5.0 m/kyr, which is in the range of average Eocene convergence rates obtained from balanced cross-sections in the Pyrenees (Burbank *et al.*, 1992; Meigs, 1997). The corresponding vertical uplift rate over the 20 degrees dipping thrust ramp is about 1.6 m/kyr. The flexural adjustments upon thrust-load emplacement result in a subsidence rate of 0.23 m/kyr in the proximal basin area. Oscillations of the eustatic sea level with a frequency of 100 kyr and amplitude of 7.5 m are superimposed on the pulsating tectonic activity. The eustatic and tectonic component together give the relative sea level or the basin average development in accommodation space (Figure 3.5). Many authors suggest that the rate of relative sea-level change rather than the absolute relative sea level is a key factor in controlling the formation of sequence-bounding unconformities and incised valleys (Posamentier and Vail, 1988; Shanley and McCabe, 1994). This value as function of time is therefore also depicted for comparison with the modelled stratigraphy (Figure 3.5). From this curve it is clear that the most rapid rises in relative sea level are found during intervals of tectonic activity combined with eustatic rise, while the most rapid decreases in relative sea level are limited to eustatic falls during tectonic quiescence (-0.5 m/kyr).



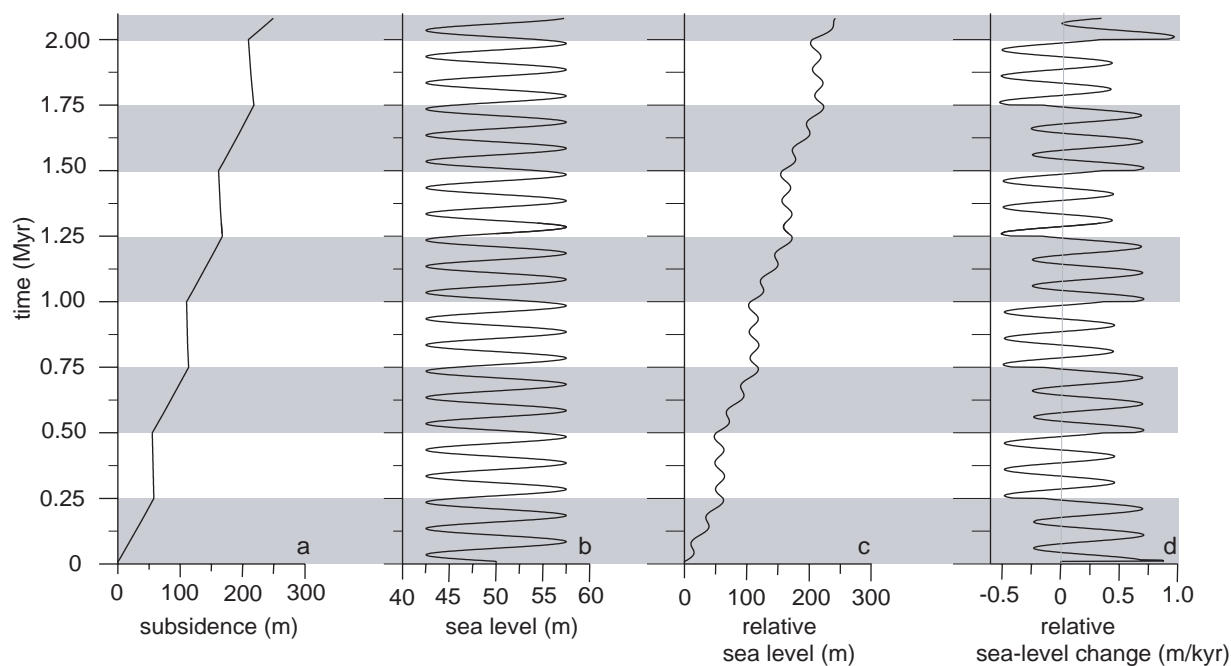


Figure 3.5 Curves of the external forcing applied to the model space as a function of simulation time (~2.0 Myr). The stepped flexural subsidence curve is the effect of pulsed thrust-load emplacement with a periodicity of 250 kyr (a). The superposed eustatic sea-level fluctuation had a periodicity of 100 kyr and amplitude of 7.5 m (b). The resulting composite curve of the relative sea level is depicted in (c) but also its derivative, the rate of relative sea-level change (d). Compare to Figures 3.9-3.11.

### 3.3 Experimental results

#### 3.3.1 Geomorphic response to tectonic and eustatic change

The main geomorphic processes respond to a different degree to the tectonic and eustatic perturbations applied to the model space (Figure 3.6.a-d). The number of bedrock collapse events shows a good correlation with the history of alternating tectonic activity and quiescence intervals. Collapses start after approximately 10 kyr, because at the beginning of the run there was insufficient relief to initiate slide events. Immediately after the first transition of activity to quiescence the number of collapses in the system is reduced to a few events per kyr. In the successive activity-quiescence couplets the distribution of the number of collapse event takes the shape of typical response curve, with a gradual increase during activity, followed by a more rapid decline during quiescence (Figure 3.6a). The form of these asymmetric response curves slightly changes during the experiment. The maximum number of events rises per successive activity interval, due to the cumulative growth in relief of the thrusting hangingwall block. For the first two tectonic intervals the maximum number of events coincides with the transition from tectonic activity to quiescence, while in the last two activity intervals the maximum is already reached at  $\frac{3}{4}$  of the pulse. Also, the decrease in events is more gradual during the last quiescence intervals, and the number of events rises, as a signature of accumulated relief.

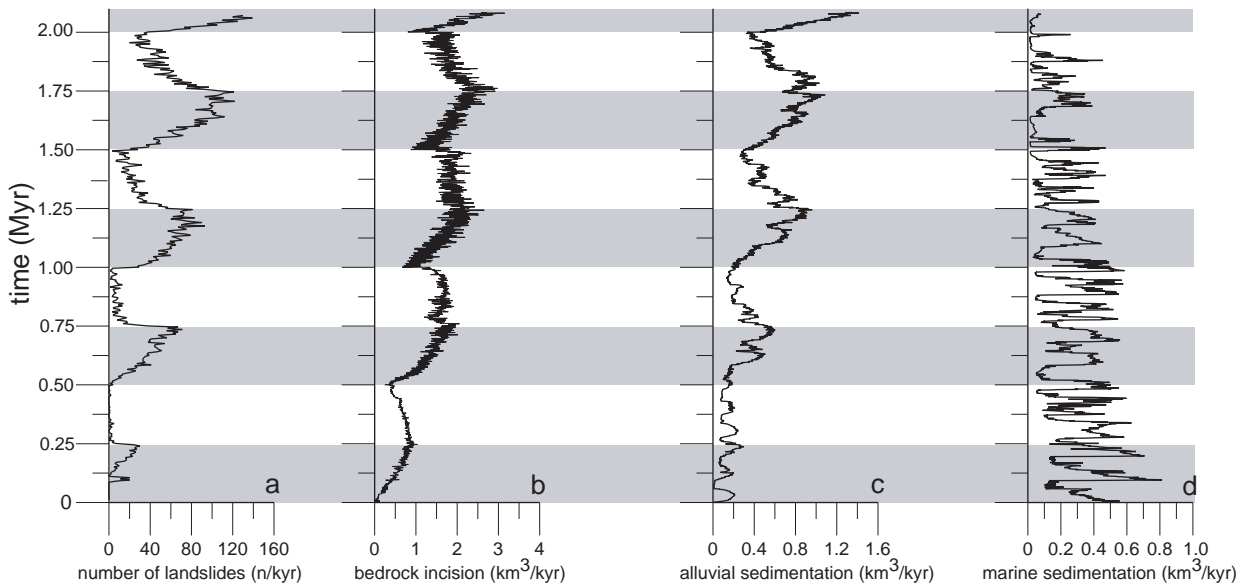


Figure 3.6 Response of the main surface processes to tectonic and eustatic forcing applied. The volumes transported by the different processes are increasingly a reflectance of eustasy while the tectonic signal loses in importance.

The rate of fluvial bedrock erosion is also influenced by the tectonic pulses, but to a lesser degree (Figure 3.6b). Again tectonic activity-quiescence couplets are responded by increases and decreases in the eroded volume. The shape of the curve is more symmetrical than that for the collapse events, indicating a more transient response. A notable feature of the curve is the sharp fall directly *after* the transitions to tectonic activity. Intuitively a rise is expected but the response is explained by interaction with the bedrock collapse events. The sediment liberated by the collapses is distributed through the catchment valleys as mass-flow sheets. Consequently, their sediment temporally blankets the valley floors during (renewed) tectonic activity and protects the bedrock temporally from exposure and removal by fluvial incision.

The control of sea-level variation on the geomorphic response varies. Neither bedrock collapse events nor bedrock incision show influence of the fluctuations in eustatic sea level (Figures 3.6a and b). In order to verify this quantitatively both time series were subjected to frequency analysis. Hence, in contrast to the model results obtained by Humphrey and Heller (1995), there is no evidence that sea-level-induced, transient waves of erosion and deposition are transmitted to the catchments. The processes operating in the adjacent sedimentary basin are, of course, influenced by the eustatic sea-level fluctuations (Figures 3.6c and d). The large-scale, undulating trend in the curve of the volumetric alluvial deposition rate corresponds to the tectonic history, and has a similar symmetry as the bedrock incision. Superimposed on the curve are smaller variations, reflecting the eustatic sea-level fluctuations. Responses to the sea-level fluctuations are dominant in the marine deposition

curve. Single responses often have a sharp base, followed by a decline reflecting rapid flooding and gradual filling of the new marine accommodation space.

### **3.3.2 Response of the axial-alluvial system to tectonic and eustatic change**

The axial-alluvial system in the foreland basin is sensitive to the tectonic pulses and the eustatic sea-level variations (Figure 3.7). During tectonic activity, the increase in flexural subsidence causes a rise of the relative sea level and basinwide retreat of the shoreline. Channels on the axial-delta plain respond to the relative sea-level rise by rapid backfilling, frequent abandonment of positions and splitting of flow in order to spread the carried sediment load as efficient as possible. Consequently, many short-lived, shallow, braided channels dominate the delta plain, which eventually takes the form of a cone. During tectonic quiescence no accommodation space is created by flexural subsidence and the delta is forced to prograde rapidly in order to keep its preferred equilibrium depositional slope ( $\sim 0.0025$  m/m). Initially, during this progradation phase the system is still covered by many, unstable channels and the surface of the deltaic cone is everywhere close to its equilibrium slope. As a consequence, the prograding delta system is critical with respect to any changes local discharge ( $Q$ ) or surface slope  $S$  (eq.3.1). Occasional confluences of streams lead to local increases in capacity, incision and the formation of a single channel out of the widespread channel pattern. This automatic evolution of the modelled delta from disperse to single channel sediment distribution is analogous to the phased transitions described for flume fans (Bryant *et al.*, 1995; van Heijst and Postma, 2001) and is in the model caused by applying a discharge exponent  $m_f$  higher than unity (eq.3.1). Most of the time channalisation during the delta's quiescence progradation is achieved beforehand. Incorporation of steep sloping terrain such as clinofolds by the delta flow during progradation, possibly accelerated by emergence of the structures during eustatic sea-level falls, may change the state of coastal cells from aggradational to erosive. Once triggered, the erosion propagates hindward as a transient wave and focuses the deltaic flow in one or two major streams. The rate of knickpoint retreat is dependent on local discharge and sediment load carried by the flow and ranges between 1.0–100.0 m/yr. These rates are in agreement with values derived from Quaternary deltaic systems (van Heijst and Postma, 2001, their figure 18). The axial channels preferably form during tectonic quiescence in the depression between the fringes of the alluvial fans and the slightly conical delta body, which was shaped by the diffusive channel pattern during a previous phase of active flexural subsidence.

### **3.3.3 Foreland basin landscapes**

Two snapshots (0.9 Myr and 1.9 Myr) in the development of the foreland basin landscape belonging to the scenario are shown in Figure 3.8. Both landscapes represent eustatic lowstands simultaneous with a phase of tectonic quiescence, but in different stages of filling of the basin. At 0.9 Myr (Figure 3.8a) the axial channel is deflected toward the fault front and located in the depression adjacent to the alluvial fan fringes. Downstream the axial system changes in fluvial morphology

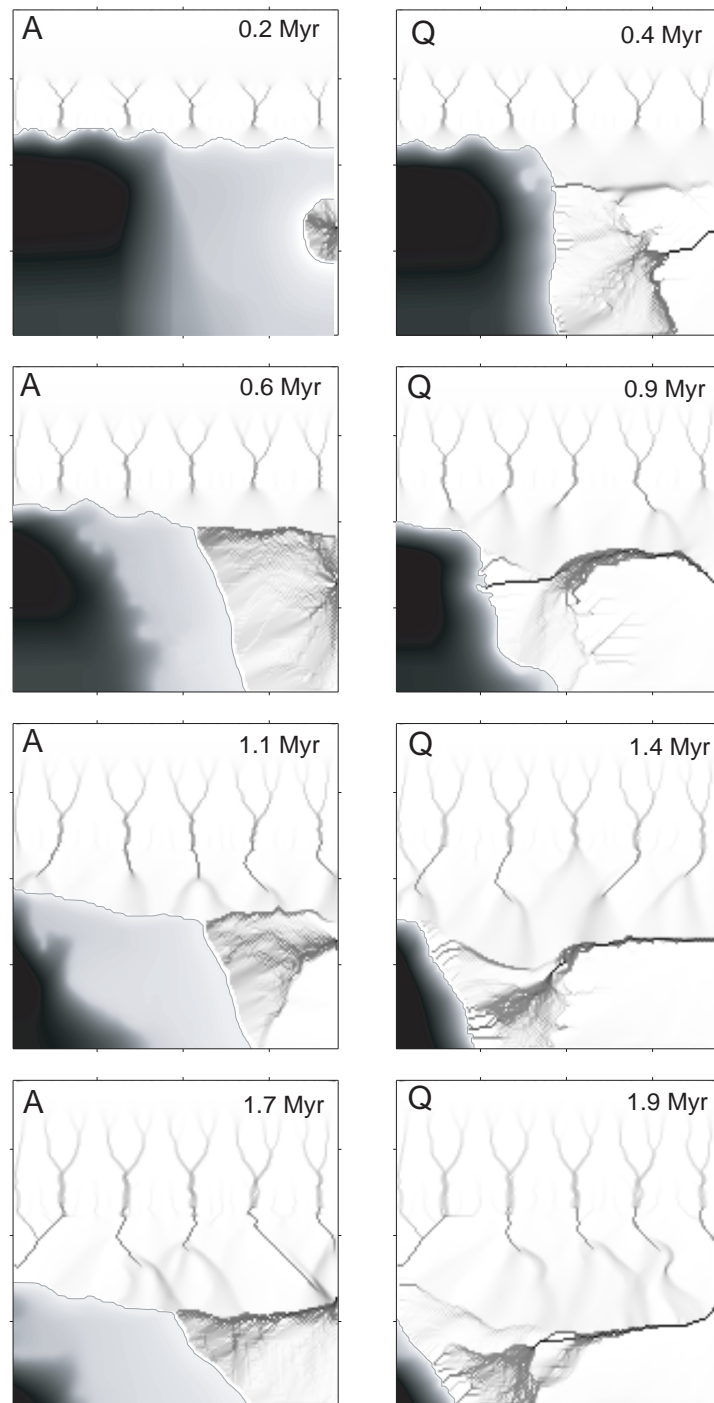


*Figure 3.7 Time steps in the water discharge patterns of the axial delta and the alluvial fans draining into the shallow marine embayment of the foreland basin. Tectonic phases of active flexural subsidence (A) are characterised by a dominance of braided channel patterns on the axial delta plain as a result of the rise of relative sea level. During tectonic quiescence (Q) phases, fluvial patterns are more diverse and show single channels in the proximal deltaic plain. Single channels and funnelling of the flow at the delta front are the result of incision triggered by simultaneous eustatic sea-level lowstands.*

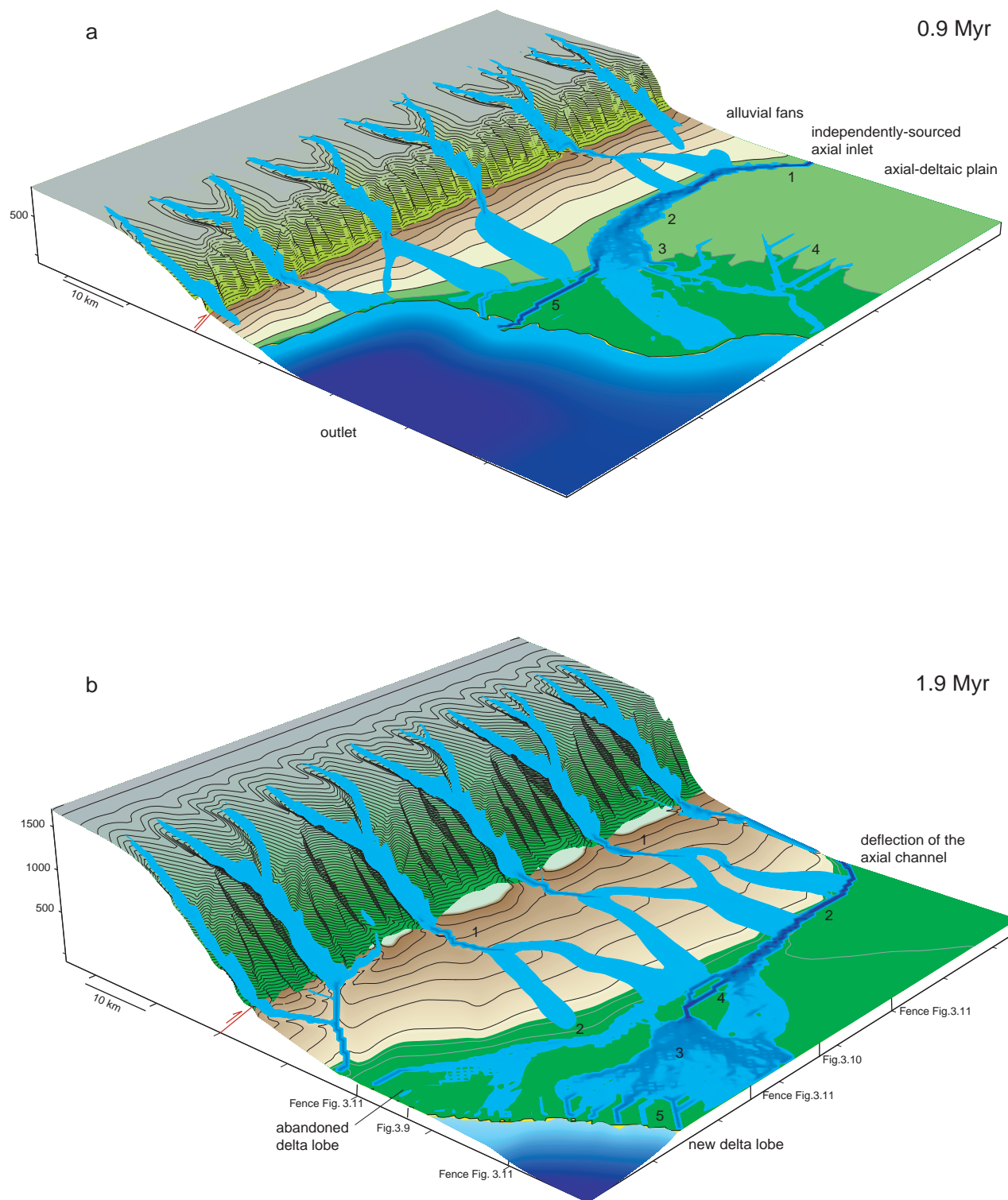


*Figure 3.8 Two examples of the modelled foreland basin landscape at 0.9 Myr (a) and 1.9 Myr (b). Both show the configuration of the main depositional elements filling the basin; transverse alluvial fans and an axial river discharging into the marine embayment as a delta. The main axial channel has a fixed inlet position but is drawn to the zone of high accommodation space creation close to the fan fringes. Eventually the fans deflect this channel basinward. See text for discussion and explanation of the numbers. Positions of the stratigraphic cross-sections, figures 3.9-3.11, are indicated along the edges of the landscape.*

from a single channel, via a confined braidplain to a true delta distributary (Figure 3.8a<sup>1,2,3</sup>). Two types of response to eustatic fall during quiescence are recognisable on the alluvial plain. First, small dendritic networks are formed on a part of the alluvial plain where the sediment supply is insufficient to dampen the erosive wave (Figure 3.8a<sup>4</sup>) triggered by eustatic fall. Secondly, the delta system reacts by propagation due to the high sediment load. However, a large portion of the water discharge is locally funnelled into a straight channel suggesting some incision on the deltaic distributary (Figure 3.8a<sup>5</sup>). At 1.9 Myr, the marine embayment is almost entirely filled by sediment and the alluvial fans have prograded further onto the alluvial plain, while their apices show signs of fan-head entrenchment in the proximal regions (Figure 3.8b<sup>1</sup>). The transport regime on the fans changes downstream from erosive or bypassing to depositional and the feeder channels bifurcate while depositing lobes. On the axial-deltaic plain, the main channel is deflected to the right-hand side by the progradation of the alluvial fans but still shows a preference for a position close to the fan fringes (Figure 3.8b<sup>2</sup>). An earlier but now abandoned delta distributary system is found in the continuation of this axial direction. The new distributary has formed in a more basinward position by a complex of upstream avulsions (Figure 3.8b<sup>3,4</sup>). Four eustatic lowstand-induced channels, funneling the drainage to the coastline, mark the new delta front (Figure 3.8b<sup>5</sup>).

### **3.3.4 Three-dimensional basin fill**

The modelled basin-fill stratigraphy can be visualized as individual sections (Figures 3.9 and 3.10) or as fence-diagrams (Figure 3.11). Rendered animations of such a fence-diagram give a good impression of the 3D stratigraphic variability in the synthetic basin fill. However, for a thorough generic analysis, individual cross-sections are preferred because of the stratigraphic detail present in the dataset. The sections are complemented with timelines, which can be drawn at user-defined time intervals, here 50 kyr.

#### **3.3.4.1 longitudinal section**

A longitudinal stratigraphic section, parallel to the basin axis, is selected to describe the difference between tectonic and eustatic dominated sequences (Figure 3.9). This section resembles that of a classic prograding delta where the timelines in the alluvial delta-top facies change into shingles of marine clinofolds, and where their inflection point reflects the position of the shoreline (Figure 3.9a<sup>1</sup>) (Postma, 1995). In the top of this section the interfering alluvial fan deposits are recognisable (Figure 3.9a<sup>2</sup>).

Within this section two types of axial-deltaic progradational sequences can be distinguished, both corresponding to a different intensity of tectonism. The first type corresponds to tectonic quiescence (Q) intervals and is characterised by, 1) a large shift of the shoreline position together with superposition of coarse alluvial over fine-grained sediments (Figure 3.9a<sup>3</sup>), 2) entrenchment of the relatively coarse alluvium (Figure 3.9a<sup>4</sup>) and, 3) coarsening-up trends in the marine delta lobes (Figure 3.9a<sup>5</sup>). Three of these progradational sequences are recognisable before the alluvial fan

deposits enter the plane of the section. The second type of sequences is stacked in between these large-scale progradational sequences. They are deposited during tectonic activity (A) and consist of coarsening-up trends without down-cutting channels, alternated with marine onlap (Figure 3.9a<sup>6</sup>).

The signature of eustatic variation on both types of sequences is explained using figure 3.5d and its graphical derivative, figure 3.9c, where the section is coloured according to rate of relative sea-level change during deposition of the individual strata. Three individual progradational sequences of the second type are recognised in the base of the section each corresponding to successive eustatic sea-level lowstands during the first interval of thrusting and related flexural subsidence (0-250 kyr, Figure. 3.5). Their deposition is synchronous with moderate rate of fall of relative sea level (Figure 3.9c<sup>1</sup>). Periodically these alluvial plain deposits submerge due to a combination of eustatic and subsidence-induced sea-level rise (Figure 3.9c<sup>2</sup>). The resulting maximum flooding surfaces are indicated by thin bands of onlapping carbonate sediments, often occupying a position at the clinofolds-topset transitions (Figure 3.9a<sup>6</sup>). Because here the relative sea level does not fall below the clinofold breaks during the deposition of these sequences and consequently no fluvial incision is triggered, their boundaries are of Type-2 (Van Wagoner *et al.*, 1988).

The channelized delta top progradations are deposited concurrently or shortly after the most rapid decreases in the relative sea-level curve (Figure 3.9c<sup>3</sup>). They are coeval with the tectonic quiescence intervals, which involve a cessation of flexural subsidence and therefore a reduction in the creation of accommodation space. As a result, the axial delta is forced to prograde in order to spread the sediment load carried under its preferred equilibrium slope conditions. Fluctuations in the eustatic sea level are no longer compensated by subsidence-induced sea-level rise, and eustatic falls stimulate the formation of incised channels by knickpoint retreat. Indicative of this incisive, channel-forming process are the colours of the channel lags in the section; they are coincident with the most rapid falls in relative sea level (Figure 3.9c<sup>4</sup>), which reached a level well below the clinofold break. Therefore, and because of the grain size facies dislocation, the horizon of composite incision represents a Type-1 unconformity (Van Wagoner *et al.*, 1988). So, both progradation types reflect phases of low accommodation space during basin evolution, controlled by the changing relation between eustatic oscillation and tectonic subsidence.

Multiple generations of axial channels amalgamate (Figure 3.9a<sup>7</sup>) and are filled with coarse sediment, because the approximate channel position is reused during the two cycles of eustatic change present in one interval of tectonic quiescence. Alternatively, channel positions may relocate by increased active bifurcation and avulsion during eustatic sea-level highs, leaving a previously incised channel abandoned and filled with fine-grained, shallow marine sediments (Figure 3.9a<sup>7</sup>). Which type of channel fill the modeller observes depends on the relative positions of the successive channels and the cross-section drawn through the synthetic basin fill. Animations of multiple surface drainage evolutions and stratigraphic cross-sections indicate that the zone close to the alluvial fan toes offer

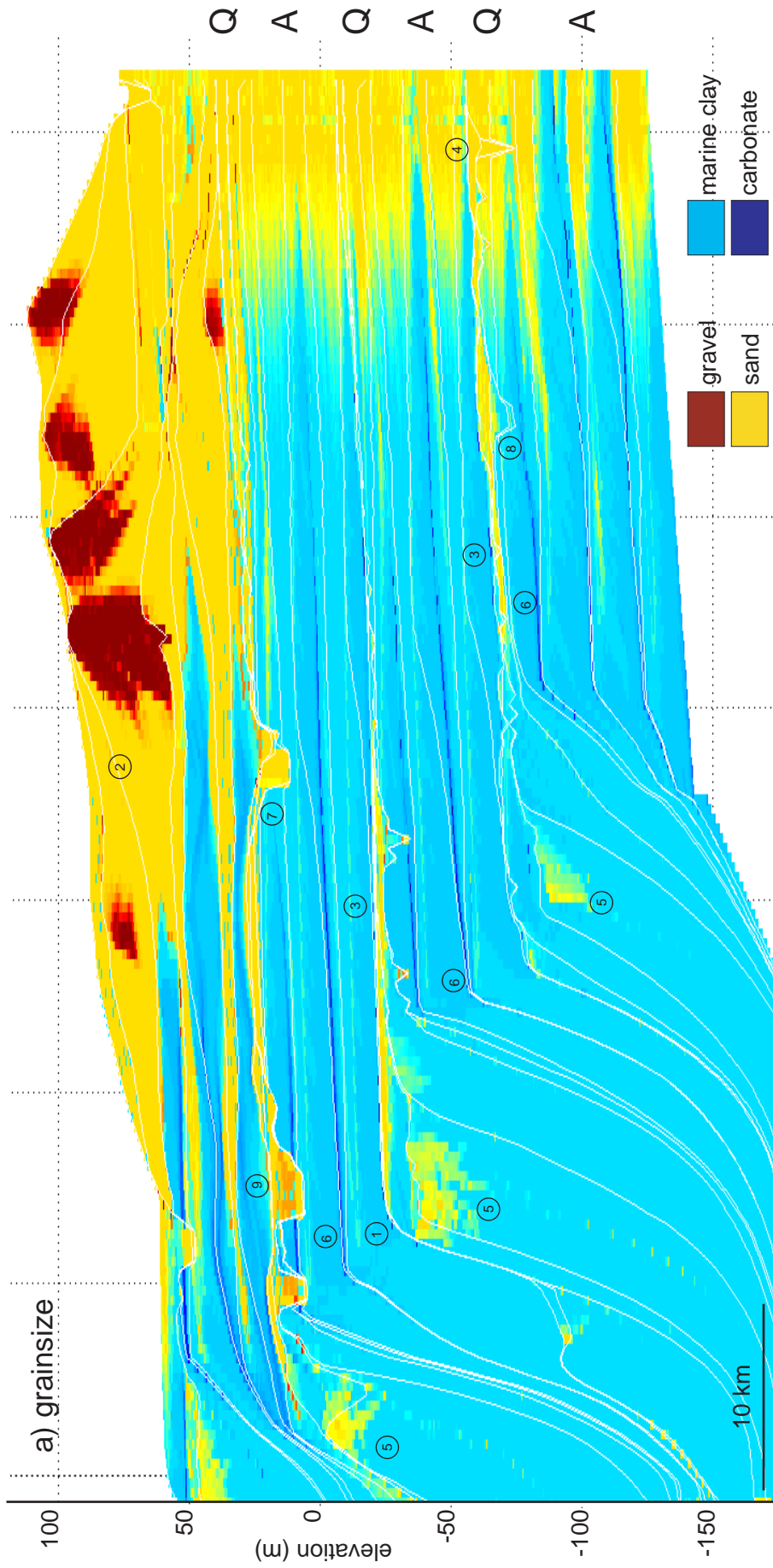
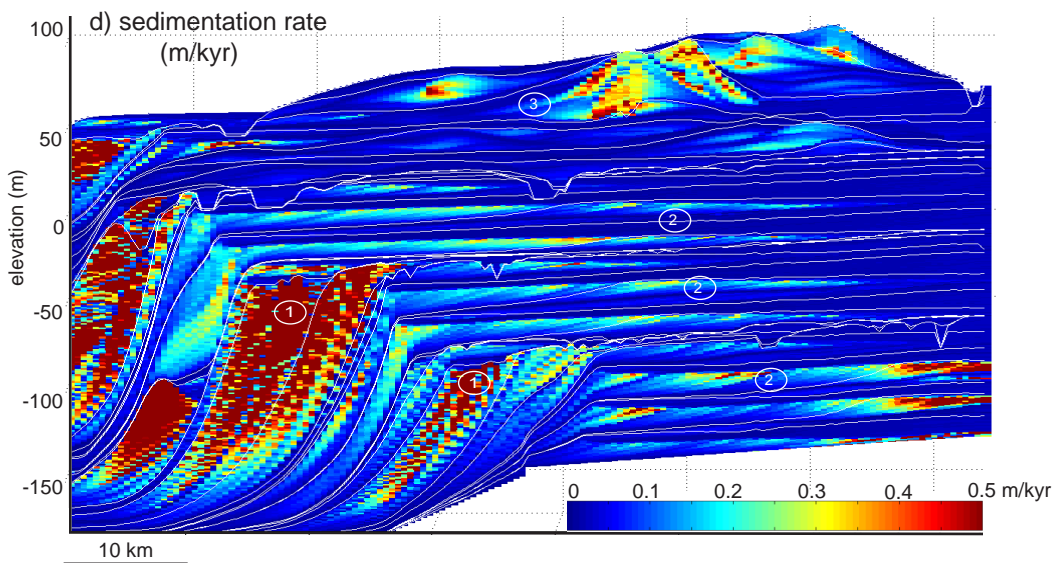
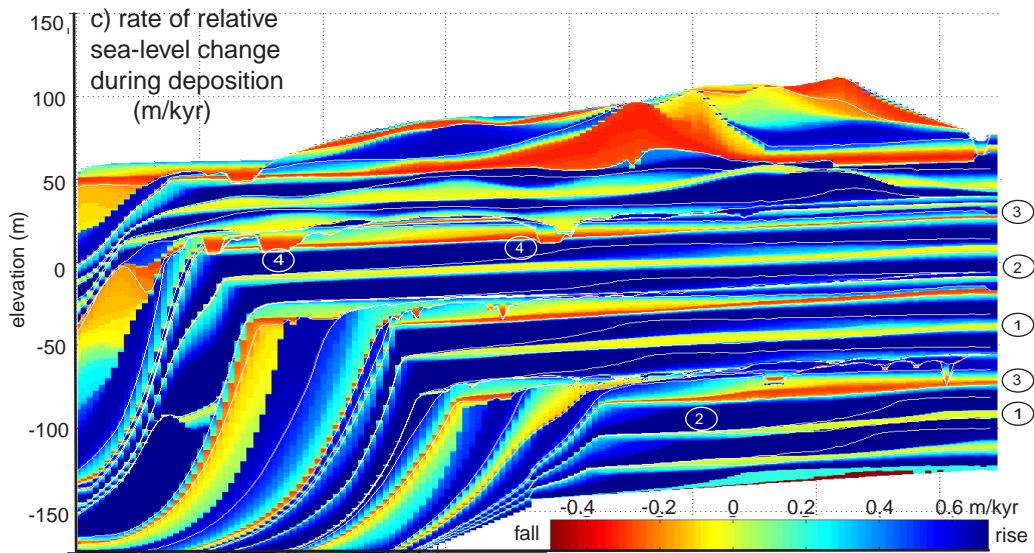
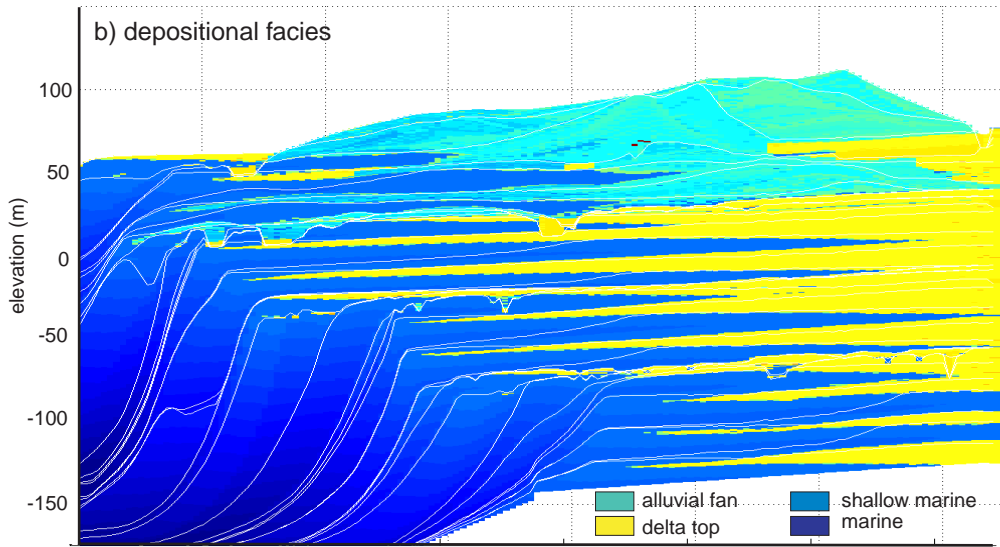


Figure 3.9 Longitudinal stratigraphic section through the basin fill dominated by axial-delta sediments. Section is coloured according to (a) grain size, (b, next page) facies, (c, next page) rate of relative sea-level change of the individual strata during their deposition and (d, next page) sedimentation rate. A is tectonic activity, Q quiescence. See text for explanation of the numbers.





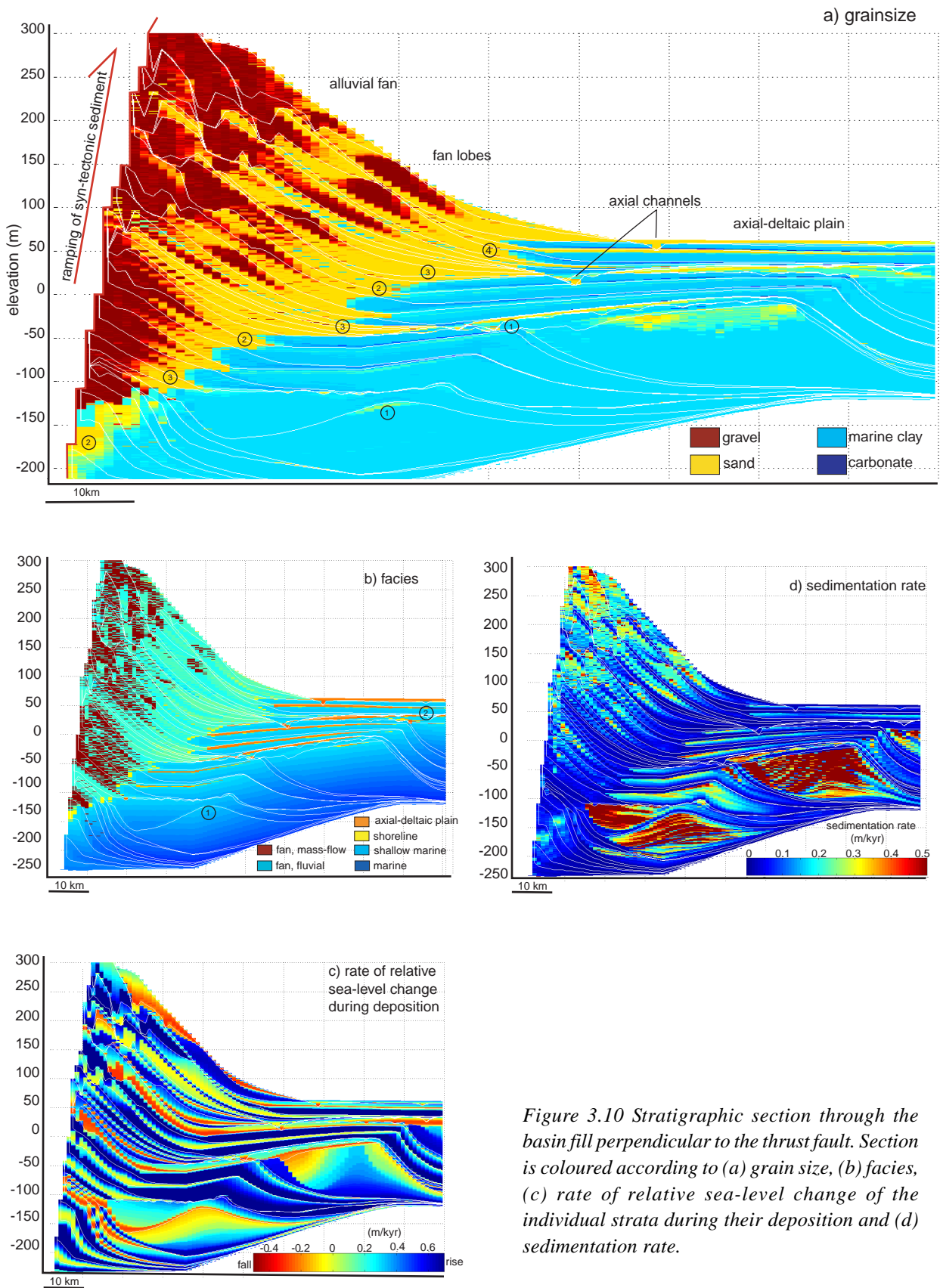


Figure 3.10 Stratigraphic section through the basin fill perpendicular to the thrust fault. Section is coloured according to (a) grain size, (b) facies, (c) rate of relative sea-level change of the individual strata during their deposition and (d) sedimentation rate.

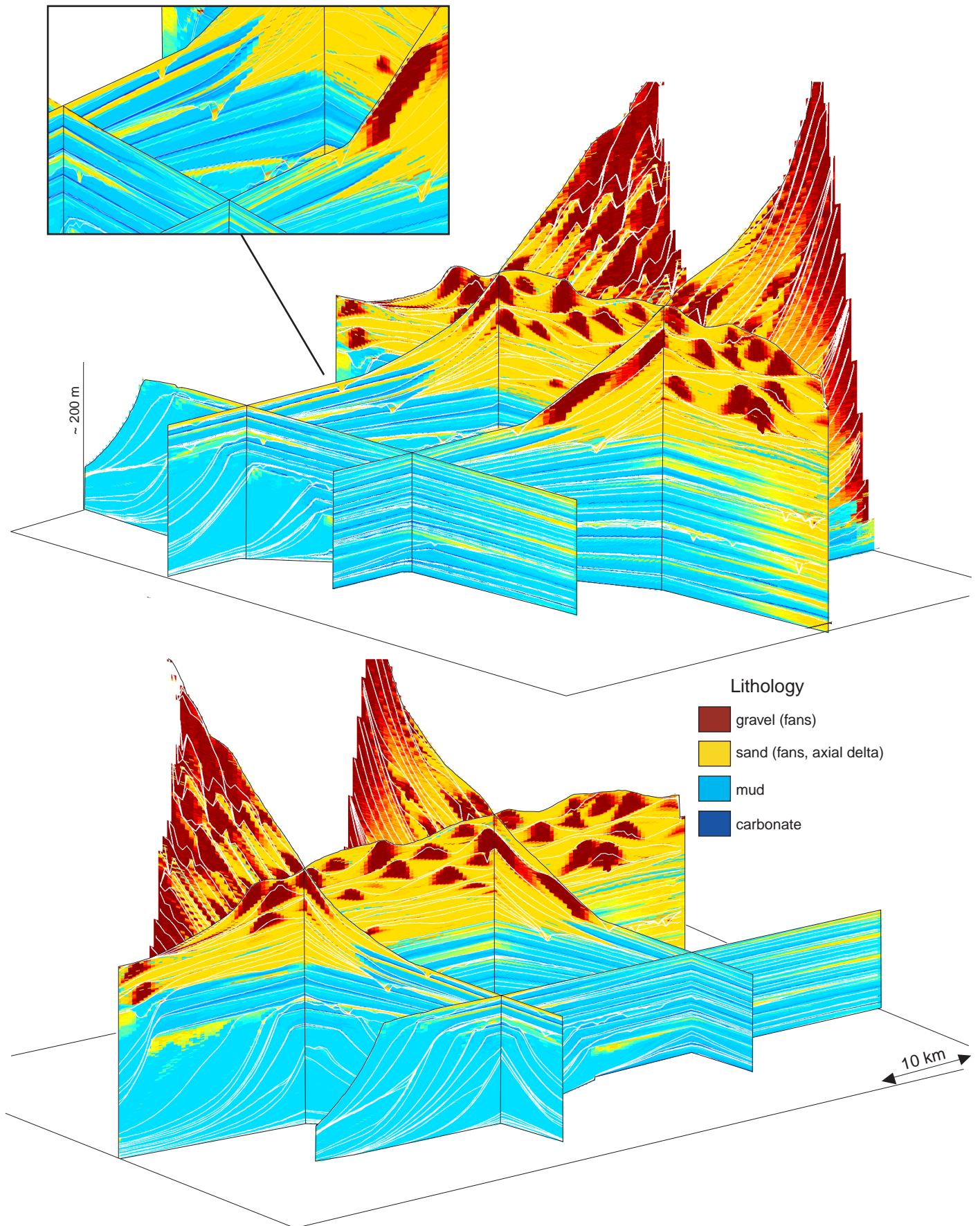
the best chance of finding a suite of incised, axial channels filled by coarse-grained sediment. This is because during tectonic quiescence and associated progradation the axial stream preferably migrates into the topographical depression between the alluvial fan fringes and the slightly conical axial delta body. Locked in this position and connected to the break in slope to deeper water, the axial channel is very susceptible to incision triggered by eustatic lowstands. During these lowstands, most of the sediment load is bypassing the alluvial plain and dumped at high sedimentation rates as delta lobes in marine waters (Figure 3.9d<sup>1</sup>). The coarsening-up grain-size trend visible in some of these delta lobes is the result of grain size sorting by progressive selective deposition (Posamentier and Vail, 1988) as these structures build up and emerge (Figure 3.9a<sup>5</sup>).

Renewed onset of subsidence during tectonic activity causes active sedimentation to rapidly retreat over the delta plain and subsequently the delta lobes starve and become covered by a thin sheet of carbonate. During the syn-tectonic falls in eustatic sea level that follow, the axial system periodically progrades, resulting in a foreset-like pattern in the sedimentation rate cross-section (Figure 3.9d<sup>2</sup>). Inevitably the alluvial fan lobes overwhelm the delta plain. During their advance they use the incised channels created by the delta streams (Figure 3.9a<sup>7</sup>). Indicative for this process is superposition of coarse alluvial fan sediment over channel lags of axial-deltaic provenance. The alluvial fan lobes are marked by sideward decreasing grain sizes and sedimentation rates (Figure 3.9a<sup>2</sup> and 3.9d<sup>3</sup>). Delta flows curving around the fan bodies result in intercalated patches of delta sediment in between the fan bodies while both systems are competing for the same zone of high subsidence, especially during tectonic quiescence.

#### *3.3.4.2 Thrust-perpendicular section*

In the section perpendicular to the strike of the thrust front, the basin is asymmetric due to the differential subsidence rate across the basin, which is increasing towards the thrust fault (Figure 3.10). The stratigraphic patterns indicated by the time lines in the basin centre show a transition from lobate to tabular stratification. This transition from marine delta-lobe clinofolds to horizontal delta tops reflects the decrease in accommodation space at the location of the section by progressive infilling of the basin with sediment. In the lower half of the section coarse-grained sediment is only found in the tops of lobes or in the incised channels (Figure 3.10a<sup>1</sup>). The upper half of the section is marked by intercalations of sandier, channelized alluvium with fine-grained sediment and carbonate onlaps, reflecting the eustatic sea-level fluctuations.

Coalescing alluvial fans form a line source that is marked by a continuous but indented progradation of gravel and sand into the basin. The small-scale growth and retreat patterns of the fans (Figure 3.10a<sup>2</sup>) are the result of the successive eustatic sea-level falls and rises, whereas the large fan progradations occur during intervals of tectonic quiescence (Figure 3.10a<sup>3</sup>). Identical to the behaviour of the axial delta, the main reason for fan progradation is the decrease in accommodation space during quiescence. Competition between the two depositional systems for the limited accommodation space during quiescence is fierce. Coeval axial stream patterns preferably



follow the basin axis and occasionally trim the fan toes, which is visible stratigraphically as a steepening and merging of the fan time lines (Figure 3.10a<sup>4</sup>). Normally, fans tend to react more slowly to a decrease in accommodation space, because they are able to store sediment under their steeper-sloping profiles. Consequently, they prograde slightly later and overlie the axial alluvium, which was initially deposited close to the thrust front (see inset of the fence diagram Figure 3.11).

### **3.3.5 Three-dimensional visualization of subsurface channel belts**

In order to illustrate the potential of forward models for applied reservoir studies a second basin filling experiment by transverse and axial sources was conducted, focusing at the analysis and visualization of the main axial-channel stacking pattern (Figure 3.12). The scenario variables consisted of 400 kyr tectonic pulses and a high-frequency sea-level fluctuation of 40 kyr, in order to create multiple incised channels. These sea-level oscillations are rare in the sedimentary record but they are inferred, for example, from the Quaternary deposits of Taiwan (Chen *et al.*, 2001). In this particular foreland basin their preservation in the stratigraphy is facilitated by high rates of subsidence and sediment supply.

After 2.5 Myr of simulation time the axial channel strata are selected from the 3D synthetic stratigraphic dataset and visualized using two criteria. First, they have to be deposited by the axial system at water discharge conditions that approximate the discharge of the axial inlet cell. Secondly, they have to be composed of more than 50 % sand. The resulting 3D distribution of coarse-grained channel voxels delineates the successive positions of the main axial-deltaic channel belt in the subsurface (Figure 3.12). Three channel belt horizons are visible, all corresponding to periods of axial-delta progradation due to limited accommodation space during phases of tectonic quiescence (0.4-0.8 Myr, 1.2-1.6 Myr and 2.0-2.4 Myr). They originate from a vertical stack of voxels at the left hand side of the figure that indicates the location of the fixed inlet cell. The lower channel belt is relatively thick (~ 20 m) but thins distally by branching. These distributaries are the result of successive deflections of the axial streams due to the emergence of offshore delta lobes. Chronologically, the individual branches are younging towards the foreland because the obstructing lobes fill-up the high-subsidence zone close to the thrust fault first, and then relocate to a more basinward position as the offshore accommodation space fills up (see also Figures 3.7 and 3.8).

*Figure 3.11(previous page) Fence diagram of the foreland basin fill coloured according to grain size fraction present in the individual strata, viewed from two different angles. Timelines are spaced 50 kyr. Alluvial fan gravel and sands are clearly recognisable by the stacked and shifting lobate bodies. They progressively cover the axial-delta deposits as part of their general progradation. Thin, near-horizontal delta-top sheet sandstones alternate with shallow marine clays and thin carbonates represent axial-deltaic deposits. Incised channels mark widespread progradations of these sandy delta-top horizons during phases of tectonic quiescence together with simultaneous deposition of coarsening-up offshore lobes. The inset shows the covering of incised axial channels by alluvial fan toe sands during a phase of tectonic quiescence. This is indicative of the differential response times of both systems upon reduction of accommodation space.*

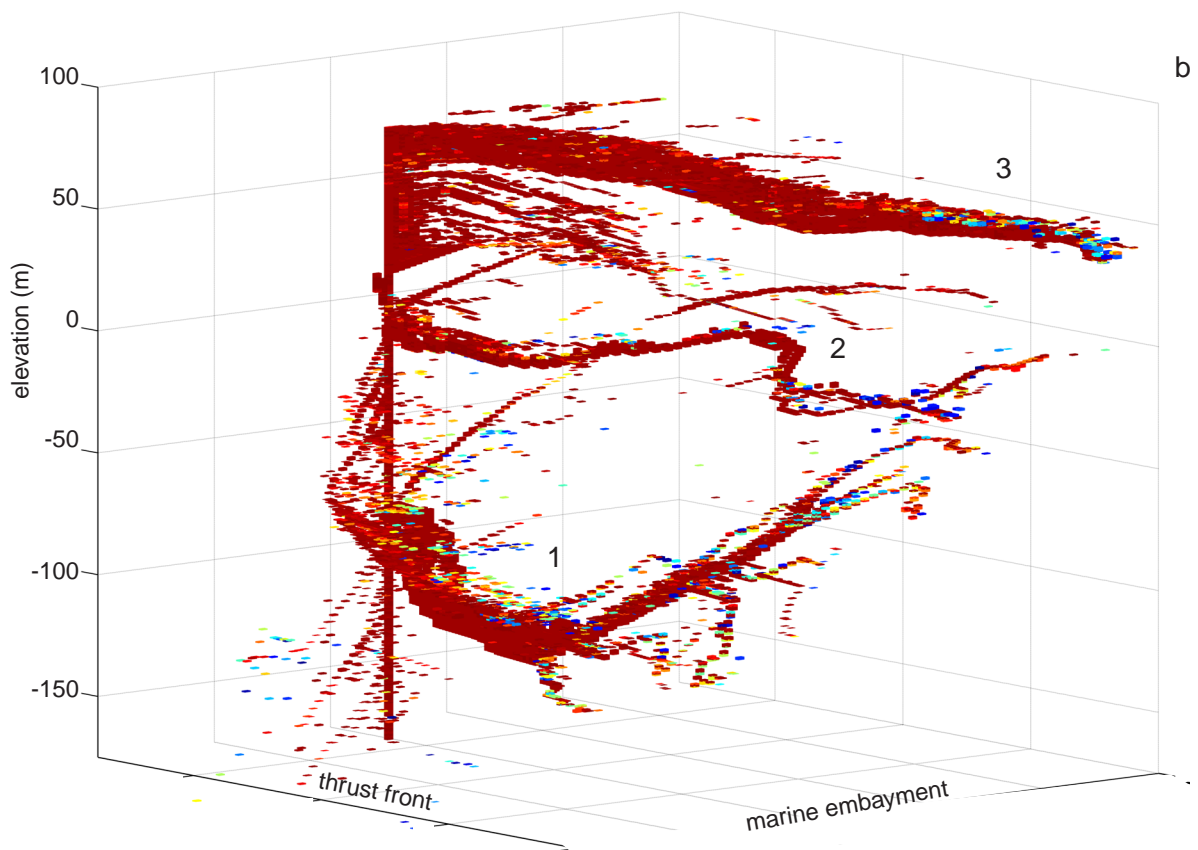
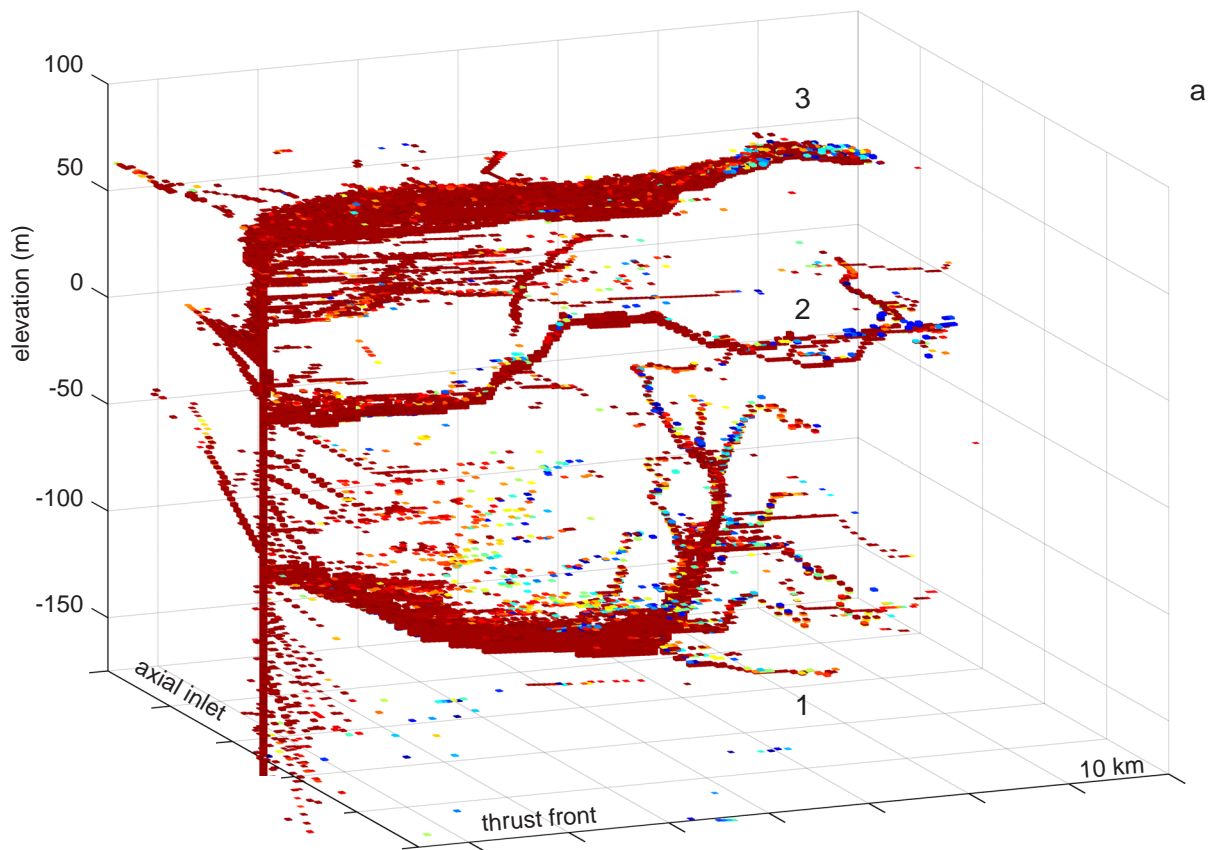


*Figure 3.12 (previous page) Changing subsurface position of the main channel belt deposited by the axial–delta system. Three channel belts are recognisable (1, 2 and 3), all formed during tectonic quiescence phases of low accommodation space generation. They are situated spatially between dominantly fine-grained sediments corresponding to phases of higher subsidence rates during tectonic activity. The upper channel belts are successively displaced basinward with respect to the lower one due to the progradation of the alluvial fan front (Figure 3.8). Multiple deflections and branching of the lower channel belt are the result of progressive basinward deflection by emerging delta lobes.*

The second and third channel belt are progressively located in a more basinward position but this is due to the deflection of the entire axial system by the continuous progradation of the alluvial fans.

### 3.4 Discussion

The here presented high-resolution model of foreland basin filling resembles that of a natural foreland basins in three ways (cf. Bentham *et al.*, 1992; Remacha *et al.*, 1998; Ramos *et al.*, 2002). Firstly, the basin is progressively filled by an axial delta due to the long-term dominance of clastic supply over the accommodation space created, causing a regression (Bentham *et al.*, 1992; Remacha *et al.*, 1998). Secondly, transverse alluvial fans become more important as a source of clastics with time, and they push away the axial system and bury the sediments previously deposited by the axial delta during the final overfilled basin phase (Brozovic and Burbank, 2000; Ramos *et al.*, 2002). In the model the small size of the computational grid ultimately limits the distal position of the axial system. In natural foreland basins the axial system is expected to relocate in a more basinward position, following the length axis of the widening flexural depression (Puigdefabregas and Souquet, 1986; Jin *et al.*, 1995). Thirdly, the final stratal patterns have a wedge-shape geometry due to the asymmetrical generation of accommodation space by flexural subsidence, just as in natural foreland basins.

One of the fundamental issues addressed in this model study is the question what controls gravel advance in foreland basins. The initial advance of fan gravels in foreland basins is a direct function of the interaction between proximal accommodation space generation and the increasing orogenic supply from nearby catchments. In this early phase vertically-stacked fan (delta) bodies with a progradation pattern, reflecting the balance between both components, will dominate the basin fill. However, in a following, overfilled basin stage care should be taken in interpreting the stratigraphic pattern directly in terms of competing local flexural accommodation and orogenic supply. The externally sourced axial system is volumetrically an important component in filling the local accommodation space, and its supply is most likely unrelated to the intensity of tectonic activity at this position. Consequently, axial-induced overfill and conditions of constant local supply and subsidence could cause fan progradation to accelerate, resulting in thin gravel sheets in the distal foreland without any change in tectonic activity.

### Chapter 3

The long-term rate of gravel advance in the modelled basin fills is 100-150 m/kyr, which is relatively high, compared to natural fan gravels deposited under similar subsidence rates (Trempe Basin, 40 m/kyr, (Nijman, 1998) ). This is partly due to the rapid infilling of the basin by axial sediments but also the result of the technique that was used to simulate thrusting in the model. From several synthetic sections it is concluded that this horizontal component in the tectonic displacement contributes for 20 % to the long-term fan gravel propagation rate. This is because the thrusting algorithm employed incorporates active ramping of syn-tectonic sediment, and consequently the fan apices increase in elevation and propagate basinward (Figures 3.10 and 3.11). Many conceptual models of basin filling neglect this obvious component in their explanations of gravel progradation, although it is an important contributing factor.

Pulsating tectonic activity in the model results in a pattern of repetitive alluvial fan retrogradation and progradation, where the latter corresponds to phases of tectonic quiescence, in coherence with other forward model studies of gravel dispersal in foreland basins (Paola *et al.*, 1992). Onset of tectonic activity is marked by retrogradation of gravels and onlap of finer-grained marine or axially sourced sediment on the fan surfaces. Syn-tectonic alluvial fan bodies show a higher density of landslide over streamflow deposited strata (Figure 3.10b), due to the good correlation of bedrock collapse events with the phases of active tectonic uplift (Figure 3.6a). Together with fan retreat and transitions in clast provenance this is probably a diagnostic feature of active uplift and (re-)juvenation of source terrains (Heller and Jones, 2001).

The model has shown to be able to simulate a hierarchical sequence stacking arrangement of the axial-delta system by simultaneously applying tectonic pulsation and eustatic sea-level variation as forcing. Many authors have identified such hierarchical arrangements in the stacking of sequences and facies patterns in the shallow marine to deltaic deposits of foreland basins (Plint, 1991; Nijman, 1998; Dreyer, 1999; Chen 2001). Although the model results cannot be seen as a direct proof for any of the conceptual interpretations in these field situations, it illustrates a possible mechanism and the diagnostic features of the sequences and their unconformities. The synthetic 100-kyr sequences, which are controlled by eustatic sea level in the model, lack basal incision if deposited during active tectonic phases. The bounding unconformities are of Type-2 due to the simultaneous subsidence component in the relative sea level, causing decreases in eustatic sea level to be suppressed and not to fall below the clinoform breaks. The Type-2 sequence boundaries are hard to recognise in the model though the consequent carbonate onlaps corresponding to syn-tectonic eustatic sea-level highs are well developed. Therefore, carbonate onlaps are probably good markers to delineate sequences deposited in high-subsidence rate foreland basins as a result of high-frequency sea-level variations.

The eustatic-controlled pattern is less observable in the sequences deposited during tectonic quiescence phases when limited accommodation space inhibits their recording in the stratigraphy.



However, the major 3<sup>rd</sup> order progradation of the delta-top facies during quiescence is punctuated by phases of basal incision as result of simultaneous eustatic sea-level lowstands. The resulting unconformity is defined by these incised channels and appears on cross section similar to the Type-1 unconformities of the classic Exxon model of sequence stratigraphy (Van Wagoner *et al.*, 1988; Emery and Myers, 1996). Note that these Type-1, 3<sup>rd</sup> order unconformities in the model are of composite origin, generated by multiple sea-level lowstands during quiescence. Further, the resulting unconformity horizons are discontinuous because their intensity is dependent on the distance to the incising axial-deltaic channel. Therefore, these unconformities are of limited value in delimitating the large-scale sequences or putting exact time-constraints on sequence boundaries. The major flooding surfaces, as a result of renewed tectonic activity and subsidence, are better discriminators because of their basin-wide character and relative instantaneous development (e.g. Galloway, 1989).

The relatively high stratigraphic resolution of the modelled basin fill facilitates correlation of the stratigraphic patterns with the external forcing but also allows visualization of sediment bodies of high reservoir potential in a foreland basin setting, such as the axial channel belts. Their general position always follows the zone of maximum subsidence. However, in order to investigate the model's predictive capabilities, several channel belt locations, generated in more than one model experiment should be evaluated statistically. Exact channel positions may vary slightly throughout multiple runs under conditions of identical model input due to internal random behaviour of the cellular model approach (cf. Meijer, 2002).

### **3.5 Conclusions**

It is shown that it is possible to capture the basic tectono-geomorphic evolution and simultaneous filling of a proximal foreland basin by independent axial and transverse sediment sources in a 3D forward numerical model. The synthetic stratigraphy accumulated in the basin is of relatively high resolution when compared to existing foreland basin models. A scenario of tectonic pulsation and superposed eustatic sea-level oscillation produces a hierarchical stacking pattern of axial-delta and alluvial fan sequences separated by thin carbonate onlap and unconformities, patterns which are characteristic of many natural foreland basins.

Basic controlling mechanism behind the large-scale stacking of these sequences is the balance between supply and flexural-created accommodation space. Due to the elastic flexure solution applied and the constant axial-delta and the increasing alluvial fans sediment supply, alternating phases of tectonic activity and quiescence in the scenario correspond to retrogradation and progradation of both systems. Syntectonic eustatic sea-level fluctuations result in a set of internal, parasequence-scale packages of prograding and shallowing-upward delta sediments bounded by Type-2 unconformities. Incised channels are rare within these sequences, but are characteristic features of tectonic quiescence phases where eustatic fall are not longer dampened by the subsidence component in the rise of relative sea level. Suites of amalgamating, axial channels mark the resulting

### *Chapter 3*

Type-1 unconformities. Coarse-grained incised channel fills are preferentially formed in the zone of maximum accommodation space between the alluvial fan fringes and the slightly conical body of the axial delta. These potential reservoir bodies can be easily distilled from the subsurface dataset and visualized in 3D, illustrating an application of stratigraphic forward modelling in foreland basin settings.

## Stratigraphic signatures of translation of thrust-sheet top basins over low-angle detachment faults

### Abstract

Low-angle detachment faults and thrust-sheet top basins are common features in foreland basins. However, in stratigraphic analysis their influence on sequence architecture is commonly neglected. Usually, eustatic sea level and changing flexural subsidence get all attention, and when deformation is considered, the emphasis is on the generation of local thrust-flank unconformities. This study focuses on the effects of detachment angle and repetitive detachment activation on stratigraphic stacking patterns in a large thrust-sheet top basin by applying a three-dimensional numerical model. Model experiments show that displacement over low-angle faults ( $2\sim 6^\circ$ ) with moderate rates ( $\sim 5.0$  m/kyr) results in a vertical uplift component sufficient to counteract the background flexural subsidence rate. Consequently, the basin-wide accommodation space is reduced, fluvio-deltaic systems carried by the thrust sheet prograde and part of the sediment supply is spilled over towards adjacent basins. The intensity of the forced regression and the interconnectedness of fluvial sheet sandstones increases with the dip angle of the detachment fault. In addition, the delta plain is susceptible to the formation of incised valleys during eustatic falls because these events are less compensated by regional flexural subsidence.

### 4.1 Introduction

Foreland basins are often envisaged as asymmetric systems experiencing maximum subsidence rate and accommodation space generation adjacent to the main thrust front, decreasing away from the deformation front (Heller *et al.*, 1988). This view is too simplistic to explain stratigraphic patterns in the proximal domains of such basins, as subsidence patterns are often complicated by local tectonic deformation and the activity of thrust-sheet top basins (Ori and Friend, 1984; Ricci-Lucchi, 1986).

Thrust-sheet top basins are very common features in foreland basins (Beer *et al.*, 1990; Puigdefabregas, 1992; Talling *et al.*, 1995; Hogan and Burbank, 1996), and are large phenomena, which sometimes affect more than 75% of the entire foreland basin (Vergez and Burbank, 1996; Wagreich, 2001).

Temporal variations in sea level and therefore the stratigraphic stacking patterns in these basins are controlled by eustatic and tectonic processes, of which the latter is a combination of thrust displacement and regional flexural subsidence. To unravel the relative contribution of each process on the sequence architecture is difficult, because individual rates and frequencies of the components cannot be estimated independently. This interplay in thrust-sheet top basins is suited for evaluation by numerical forward models that couple the important processes, where the relative importance of a single component on basin architecture is highlighted by systematic variation. However, thrust-sheet top basin stratigraphy is not commonly addressed in modelling studies because of the numerical complexity involved in coding horizontal thrust-sheet translation and erosion at the same time. This is rapidly changing due to the increasing interest in tectono-geomorphic interaction, the availability of new dating methods (luminescence dating) in convergent neo-tectonic settings, and new modelling techniques sufficiently flexible to simulate thrusting and surface processes (Chaleron and Mugnier, 1993). A notable example is a recent study in which the TIN-based CASCADE model (Braun and Sambridge, 1997) is used to explain drainage diversion or incision along the Nepal Himalayan foothills as a function of detachment angle and lateral differences in displacement rate along the deformation front (van der Beek *et al.*, 2002). They conclude, that the direction and slope of the transverse drainage is primarily a function of lateral differences in propagation rate over an inclined detachment. Minor differences in convergence rate and detachment angle determine whether downstream fault-bend folds in the foothills are safeguarded from fluvial incision and the formation of wind gaps or not. In their study, the thrust-sheet top basin is fully continental and dominated by erosion of the frontal fault-bend fold and the basin itself. However, thrust-sheet top basins are known to develop early in immature foreland basins and to accommodate sediment due to their position below (Ricci-Lucchi, 1986; Huyghe *et al.*, 1999) or close to base level (Talling *et al.*, 1995; Ramos *et al.*, 2002). The balance between two fundamental processes: regional flexural subsidence and basin-wide uplift created by horizontal translation over a shallow hinterland-dipping detachment fault (Talling *et al.*, 1995) has a major impact on their stratigraphy.

Aim of this chapter is to investigate the effect of alternating activity and quiescence of a detachment fault on the evolution of a thrust-sheet top basin as a function of the detachment-fault angle. The consequent evolution of accommodation space, fluvial drainage directions, and stratigraphic patterns recorded in the basin are investigated with a numerical model. The influence of the detachment-fault angle is critically evaluated. This fundamental variable is commonly overlooked in foreland basin analysis, which traditionally focusses on rates of tectonic displacement and subsidence.

The results of the numerical model are compared to the Eocene Tresp thrust-sheet top basin of the Spanish Pyrenees (Marzo *et al.*, 1988; Nijman, 1998). In the interpretation of the alluvial stratigraphy in this setting the role of detachment fault dip has been fully neglected up to now. The basic structural geological geometry used in the model set-up is analogous to the one observed in the Tresp Basin in order to facilitate the comparison of the modelled stratigraphy with this field situation, and the re-evaluation of existing theories.

## 4.2 Numerical model

### 4.2.1 Basin geometry

A quantitative three-dimensional model has been developed to gain insight into tectono-geomorphological interaction and the stratigraphic response in foreland basins. The standard version of the model incorporates uplift by thrusting of an orogenic wedge and simultaneous erosion by bedrock collapse and fluvial bedrock incision. Erosional products are routed downstream and deposited in a flexurally created foreland basin by transverse alluvial fans and an axially flowing fluvio-deltaic system. In this study the model is adapted by incorporating a frontal fault-bend fold and a shallow hinterland-dipping sole-thrust detaching the foreland basin, creating a thrust-sheet top basin. (Figure 4.1). The model set-up consists of a grid of 150 x 150, 500m cells in which both thrust structures are bounded to the left by a marine basin, which is not experiencing deformation,

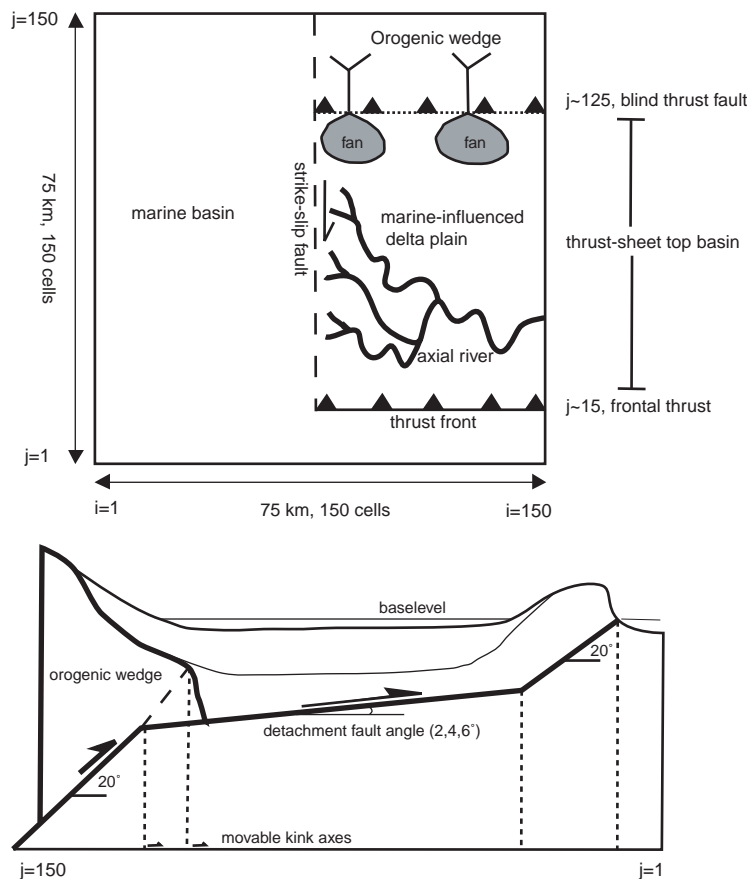


Figure 4.1 Basin geometry used in the numerical experiments (150 x 150 cells, 75 x 75 km). The initial model landscape starts as a flat surface positioned at baselevel (0 m). The basin is divided into two domains by a strike-slip fault. The domain on the right experiences deformation by a moving orogenic front and displacement of the thrust-top basin along a detachment fault. The marine basin on the left solely experiences regional flexural subsidence. The segmented foreland basin is filled by an axial-delta system entering from the right-hand side with a constant supply, and by the erosional debris shed off from the uplifting orogenic wedge. The grid boundary at the left-hand side is open and functions as an ultimate sediment sink.

only flexural subsidence. The configuration of the modelled thrust-sheet top basin is based on Tremp-Ainsa Basin in the Spanish Pyrenees (Figure 4.2 and 4.3). This basin has been filled by the Eocene fluvio-deltaic Montanyana Group, which was deposited by southwestward prograding alluvial fans merging with an axial fluvial system, flowing parallel to juvenile Pyrenean Orogen (Friend *et al.*, 1981; Marzo *et al.*, 1988). The Montanyana Group passes into the turbidite systems of the Hecho Group deposited in the adjacent marine Ainsa Basin (Mutti, 1985). A considerable fraction of the material constituting these turbidite systems has been derived from the nearby structurally oversteepened deltafront, positioned above a lateral ramp of the underlying Cotiella-Montsec thrust sheet (Nijman, 1998).

In stratigraphic cross section, the Montanyana Group is partitioned into several megasequences characterised by unconformities along the basin margins. These unconformities pass into conformable stratigraphic relationships, axial sheet sandstones or marine flooding surfaces in the basin centre (Figure 4.3).

As a result of the complexity of the selected set-up, three routines had to be added to the existing foreland basin model (Chapter 2 and 3) handling the:

- syn-sedimentary horizontal translation of the detailed stratigraphic fill of the thrust-sheet top basin.
- three-dimensional flexural response upon thrust, sediment and water loading.
- delta slope collapse, delivering sediment to the adjacent marine basin.

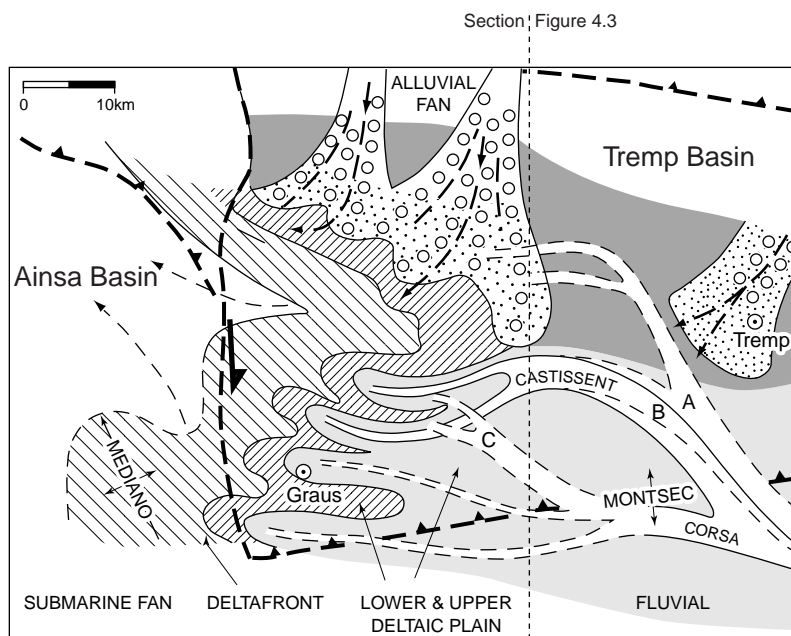


Figure 4.2 Planview of the drainage organisation in the Eocene Tremp thrust-sheet top basin (Spanish Pyrenees) during the deposition of the Montanyana Group. The basin is occupied by two depositional systems, transverse alluvial fans and an axial fluvio-delta system, which converge in the axis of the basin. The basin is bounded in the west by the lateral ramp of the carrying Coteilla-Montsec thrust-sheet, which marks the facies transition to the turbidite systems of the Hecho Group in the Ainsa Basin (modified after Nijman, 1989).

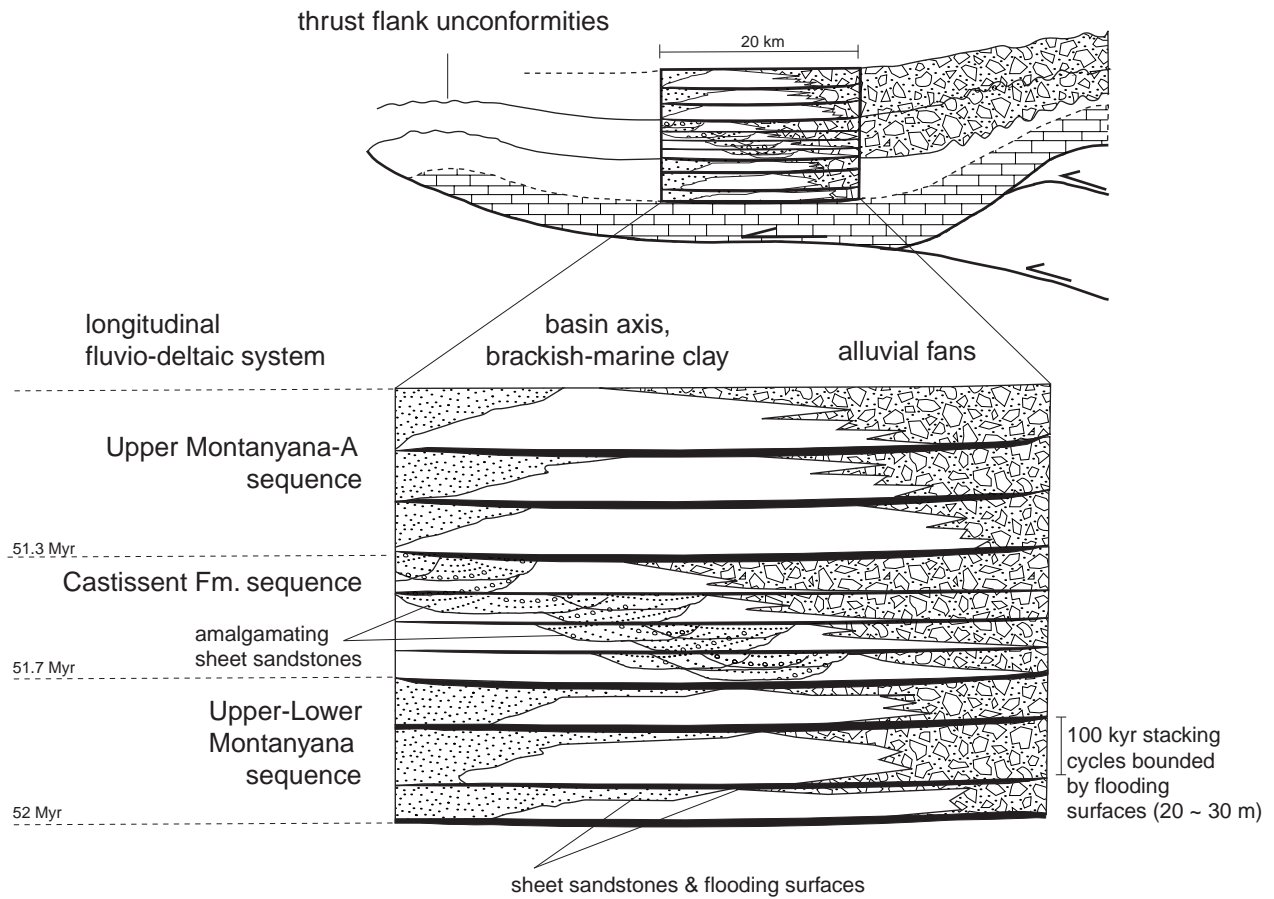
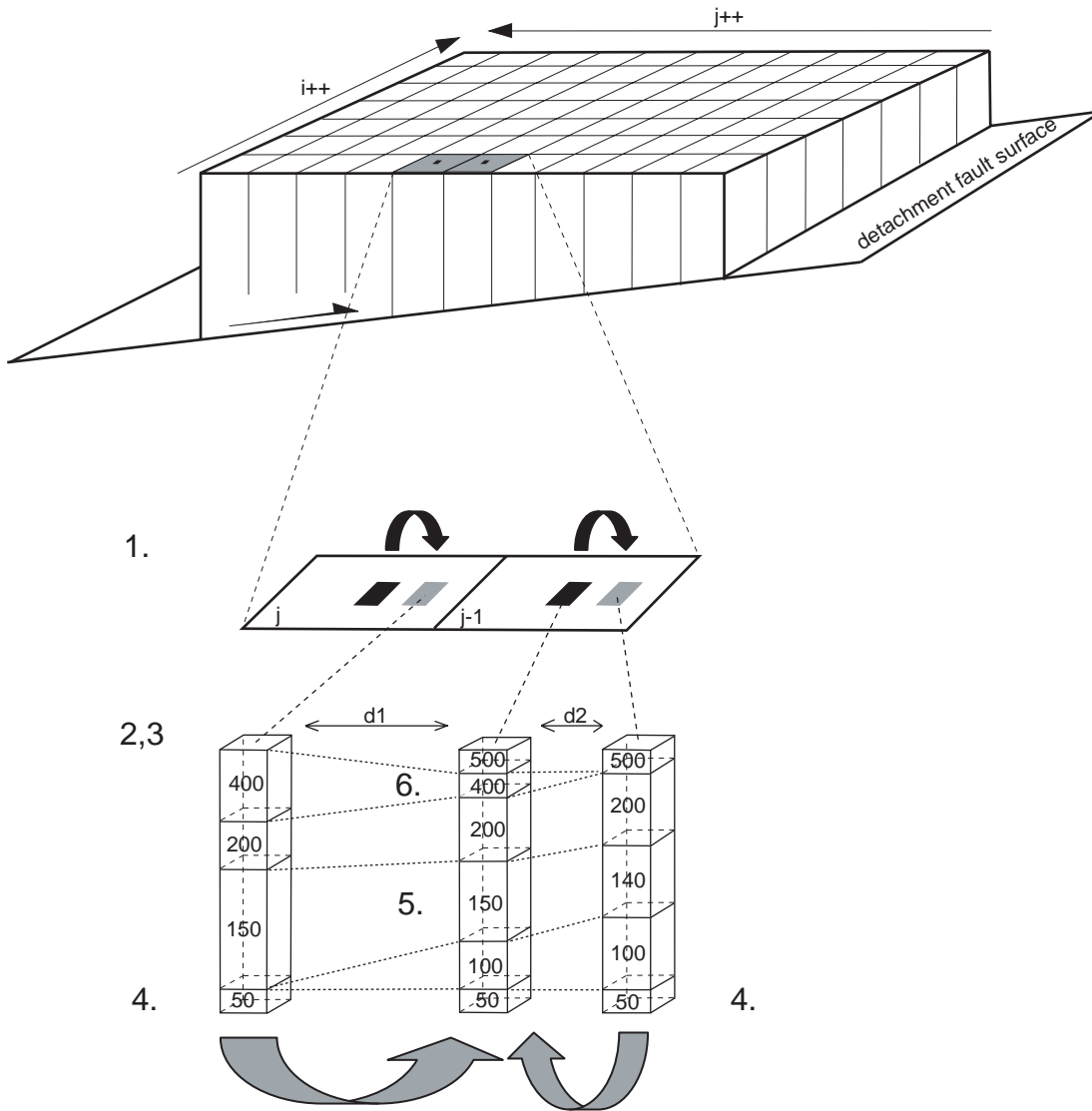


Figure 4.3 Schematic representation of the Montanyana Group sequence architecture in the Tremp thrust-sheet top basin. The fine-grained basin fill is partitioned into megasequences by pronounced unconformities at the basin margins, which pass into conformable stratigraphic relationships in the basin centre. Here, amalgamating sheet sandstones and marine flooding surfaces mark the boundaries. The sequences are subdivided into fan/axial-fluvial couplets bounded by flooding surfaces, each representing approximately 100 kyr (modified after Marzo et al, 1988). For a thorough 3D analysis of the basin fill architecture see Nijman (1998).

#### 4.2.2 Horizontal translation of thrust-sheet top stratigraphy

The tectono-sedimentary model is based on a static rectangular grid (Figure 4.4). As a consequence translation of geologic structures always involves spatial interpolation, because the displacement during a single tectonic step is usually smaller than the grid discretisation. A simple interpolation method is used to model the topographic development of a single fault-bend fold (Figure 2.5). The same technique is applied here to simulate the frontal thrust structure in the foreland basin. The frontal thrust ramp is connected to the orogenic wedge by a hinterland-dipping sole thrust, detaching the foreland basin and transforming it to a thrust-sheet top basin (Figure 4.1). The stratigraphic fill of the detached basin is translated using a comparable, but more computational intensive technique, which is a modification of the routine originally developed for relocating individual nodes during



Create a new stack of layers for the static grid cell centre position  $j-1$  by interpolation between the properties of two displaced stacks

Figure 4.4 Simplified explanation of the stratigraphic interpolation routine used to translate the stratigraphic information of the piggyback basin fill. 1) New node positions are calculated as function of the tectonic displacement field. 2) The distances between the new node positions and the static grid are calculated. 3) These distances are used in weighted interpolation of layer properties. 4) Comparison of the layers, starting at the base of the stratigraphy 5) If layers fall in the same age range (arbitrary value of 10), new layer properties are calculated using weighted interpolation between two matching layers. The age of the composite layer is set to the youngest value. 6) If layers do not match in age range the new layer is advected into pile, so that the sequence of layers in of the column is still in chronologic order.



the creation of a meander bend (Tucker *et al.*, 1999). Instead of a few nodes, here an entire mesh of nodes needs to be moved.

Each of the grid nodes representing the basin landscape is connected to a linked-list data structure (Oualine, 1997) which stores the stratigraphic stack of layers at the specific location (Figure 4.4). Every layer in such a linked list carries lithological information about its texture and provenance (marine, alluvial fan or axial delta) and chronological information about depositional age and if the layer was recently involved in an erosion or sedimentation process. This chronological information is used in the translation of the thrust-sheet top basin fill. The tectonic displacement field predicts new positions for the piggyback basin nodes, but because the model is based on a fixed, equidistant grid, they are not allowed to move. The solution is to assign new locations to the stratigraphic linked lists, temporally, and to interpolate a new stack of layers for the static node positions by weighted distance interpolation between two displaced locations. Interpolation, and averaging of properties between layers is allowed if they fall in the same age range, which is a user-defined variable. If this requisite is not fulfilled, the layers are advected into the newly created stack, according to chronological age (Figure 4.4). The technique is here applied to simulate the translation of a thrust-top basin fill. Of course it is applicable to other tectonic processes involving a horizontal component, such as strike-slip or normal faulting.

#### 4.2.3 Three-dimensional flexure

The activation of intra-foreland basin thrust structures results in spatially highly variable loading of the lithosphere due to the discontinuous nature of the frontal thrust (Figure 4.1) and the subsequent redistribution of the sediment. The pseudo three-dimensional flexure solution adapted in a previous model version proved to be inadequate to adapt to this more complex structural setting. The model is therefore extended with a full three-dimensional flexure solution based on the Fourier Transform method (Karner, 1982; Wees and Cloetingh, 1994; Hodgetts *et al.*, 1998; Watts, 2001). The two-dimensional theory (equation 2.16, Chapter 2) is extended to three dimensions:

$$\left( \frac{\partial^2}{\partial x^2} + \frac{\partial^2}{\partial y^2} \right) D \left( \frac{\partial^2 w_{(x,y)}}{\partial y^2} + \frac{2\partial^2 w_{(x,y)}}{\partial x^2 \partial y^2} + \frac{\partial^2 w_{(x,y)}}{\partial x^2} \right) + (\rho_m - \rho) g w_{(x,y)} = L_{(x,y)} \quad (4.1)$$

where  $D$  is the flexural rigidity,  $w_{(x,y)}$  is the lithospheric deflection resulting from the load  $L$ , both being a function of spatial coordinates  $x$  and  $y$ . Expressed in the wave number domain, equation 4.1 becomes

$$W_{(i,j)} = R_{(i,j)} \mathcal{F}L_{(i,j)} \quad (4.2)$$

where  $W_{(i,j)}$  is the Fourier transform of  $w_{(x,y)}$  and  $L_{(i,j)}$  the Fourier transform on  $L(x,y)$  while  $i$  is the wave number in the  $x$ -direction and  $j$  the wave number in the  $y$ -direction. The response function  $R(i,j)$  defines the isostatic compensation for a certain load

$$R(i, j) = \frac{1}{(\rho_m - \rho)g + D(i^2 + j^2)^2} \quad (4.3)$$

The equations are solved using a 2D Fast Fourier Transform algorithm (FFT) (Press *et al.*, 1992). Such algorithms are developed for signal processing studies and are not directly applicable for solving the flexure problem, because the method assumes that the input data series is periodic. Of course this does not hold for the spatial distribution of a tectonic load, which is non-periodic and spatially confined. Boldly applying a FFT algorithm could result in series of interference patterns because deflections are felt at large distance from the load ( $n \times 10$  km) and will interfere. One way solving this FFT ‘artefact’ is to wrap up the actual load in a synthetic load, which on average equals the minimum load. This technique is called ‘copy padding’ (Hodgetts *et al.*, 1998). The expanded data series used for padding should have dimensions larger than the wavelength  $\lambda$  over which the lithosphere flexes due to the load itself.

$$\lambda = 2\pi\alpha \quad (4.4)$$

where  $\alpha$  is the flexural parameter defined as

$$\alpha = \left( \frac{4D}{(\rho_m - \rho)} \right)^{1/4} \quad (4.5)$$

This large area ( $n \times 100$  km) is not entirely modelled with the surface process equations due to computational limitations. Flexure-related phenomena such as forebulge uplift and migration are calculated but occur outside the area addressed by surface processes and are therefore not recognisable in the model results. An assumption in the lithospheric response algorithm is that the isostatic adjustment upon an increment of thrust or sediment loading is applied to the model space for 90-95 % within a time-span of 10 kyr. This rate of lithospheric response is comparable to the pace of crustal rebound associated with postglacial ice cap melting (Forman, 1990; Peltier, 1990), and is therefore a good assumption.

#### **4.2.4 Submarine slope collapse and mass-flow deposition**

A simple marine slope collapse routine is added to the surface process equations in order to simulate sediment supply from the structurally oversteepened delta front to the deeper marine part of the basin configuration (Figure 4.1 and 4.2). A relevant question is to what extent the number of collapse events and the spatial distribution of mass-flow deposits correspond with the timing of thrust sheet translation and eustatic sea-level variation. In the model, gravity-flow transport to deeper water is predicted using an adapted version of the Cullman slope-stability criterion, wherein the probability of slides is dependent on the cohesion of the delta front sediments (600 Kp) and their critical slope of  $1^\circ$  (Loseth, 1999). Assuming that remobilisation of shoreface sediment is most effective at depths around the wave base, the collapse criterion is active below a water depth of 15 m. The material

supplied by the collapsing delta front is distributed to deeper water according to a runout length of 10 km. This distance is chosen because it results in the bulk of the mass flows to be deposited within the model set up and to be visualized.

#### 4.2.5 Model scenarios

Four scenarios are modelled in order to analyse the influence of the balance between regional flexural subsidence and displacement-induced uplift along the detachment fault on the stratigraphic patterns recorded in the thrust-top basin (Table 4.1 and Figure 4.5). In the first three experiments the angles of the detachment fault are 2, 4 and 6°, while keeping the effective elastic thickness (EET) constant at 15 km. The corresponding regional subsidence rate is approximately 0.35 m/kyr.

Exp.	Effective Elastic Thickness, EET (km)	Average flexural subsidence (m/kyr)	Detachment angle	Vertical uplift component detachment angle
1	15	0.35m/kyr	2°	0.16 m/kyr
2	15	0.35m /kyr	4°	0.32 m/kyr
3	15	0.35 m /kyr	6°	0.48 m/kyr
4	30	<b>0.18 m/kyr</b>	4°	0.32 m/kyr

Table 4.1 Flexural subsidence rate and displacement-induced vertical uplift in the thrust-top basin applied in the model experiments.

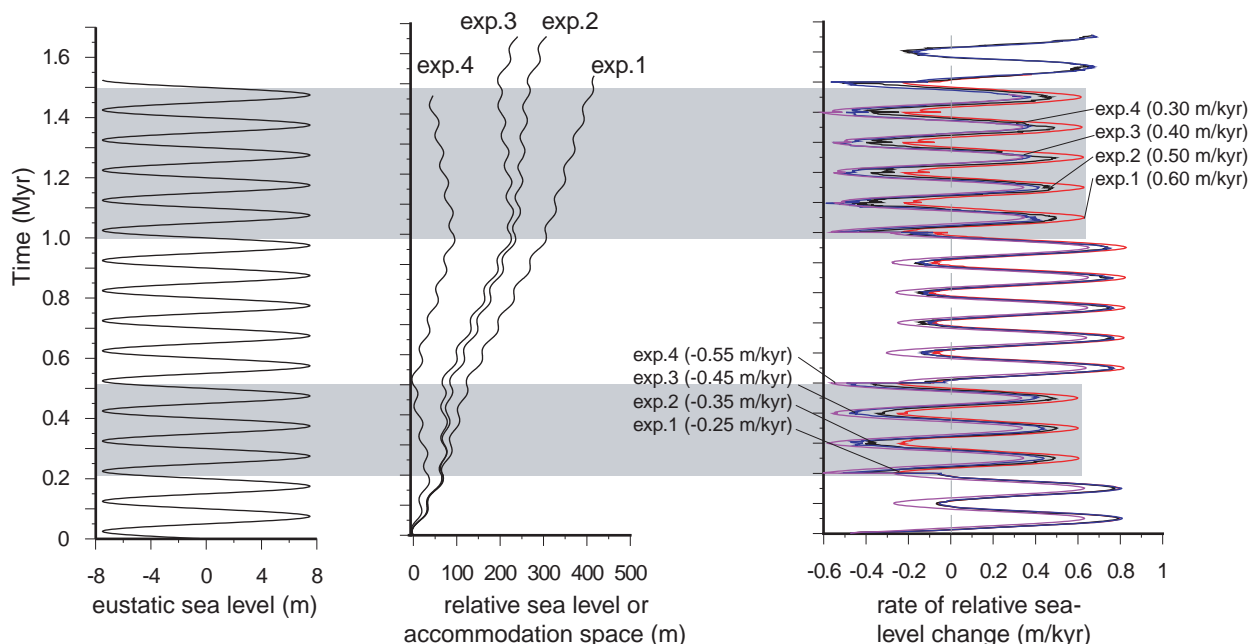


Figure 4.5 The combined effect of flexural subsidence, detachment activity and eustatic sea-level fluctuation on the thrust-top basin accommodation space and the rates of relative sea-level change. A stepwise increase in detachment angle (exp.1-3) results in reduced accommodation space and higher rates relative sea-level fall, promoting incision of the thrust-top basin fill.

In the fourth experiment, a detachment angle of  $4^\circ$  is applied, and double the value of the flexural rigidity, resulting in a lower average subsidence rate of  $\sim 0.18$  m/kyr. The activity history of both thrusts is identical in all scenarios. The activity of the structures alternates; the thrust separating the orogenic wedge from the thrust-sheet top basin is active from 0 to 0.2 Myr and 0.5 to 1.0 Myr. The frontal thrust emerging in the foreland basin is active twice during the simulation, first between 0.2 and 0.5 Myr, secondly between 1.0 and 1.5 Myr. Both thrust structures accommodate a shortening rate of 5.0 m/kyr during activity. A eustatic sea-level variation is added with an amplitude of 7.5 m and a wavelength of 100 kyr.

The angles of the detachment fault, displacement and subsidence rates generated are comparable to values inferred from the Eocene Treppe Basin. The duration of the tectonic intervals ( $\sim 0.3$ - $0.5$  Myr) is an average for the time span covered by the mega-sequences in the Montanyana Group. Individual units in the architectural stacking pattern have an approximate duration of 100 kyr (Figure 4.3) (Marzo *et al.*, 1988; Nijman, 1998). In this model study this frequency component is introduced as sinusoidal sea-level variations.

Analysis of balanced cross sections indicates that displacement rates over the basal detachment during the deposition of the Montanyana Group range from 2.0 to 20.0 m/kyr (Munoz, 1992; Holl and Anastasio, 1995; Bentham and Burbank, 1996; Poblet *et al.*, 1998). The average, long term translation rate proposed is 5 m/kyr (Vergez *et al.*, 2002). These displacement rates, in combination with a  $3$ - $4^\circ$  slope of the Cotiella-Montsec detachment fault (Munoz, 1992), are able to generate a vertical uplift component of tectonic translation, which is sufficient to reduce the accommodation space created by background flexural subsidence (0.2-0.6 m/kyr Nijman, 1998).

## 4.3 Experimental results

### 4.3.1 Thrust-sheet top basin landscape evolution

The landscape evolutions of two of the four thrust-sheet top basins, experiment 2 and 3, are shown in figures 4.6 and 4.7. Initially, the basin is relatively shallow ( $\sim 30$  m) in both experiments and occupied by a conical delta body characterized by a disperse, braided channel pattern (0.2 Myr). During subsequent activation of the detachment fault and displacement of the basin, the delta progrades, while showing linear drainage structures on the lower delta plain (Figure 4.6, 0.5 Myr). The transition from these linear drainages on the lower deltaic plain to bifurcating channels on the upper deltaic plain marks the change in erosion/aggradation balance in the channels. The linear channels are dominated by sediment bypass or channel-bed erosion, while the bifurcating channels accumulate sediment. Geographically, the transitions delineate the position of a *knickpoint front*, triggered by the 0.45-0.50 Myr fall in eustatic sea level. The rate of migration of the knickpoint front is 5.0 km/kyr and diminishes in the basin centre (Figure 4.6, 0.5 Myr), where it represents a balance between incision, sediment supply and net accommodation space created. The front does not migrate further towards the inlet position of the axial delta, due to the slight dominance of

regional flexural subsidence over detachment-induced uplift, which compensates the incisive effect of eustatic sea-level fall. In experiment 3, the detachment-induced uplift component is larger, and activation of the detachment fault results in rapid formation (10-20 km/kyr) of a single incised channel connecting the delta to the axial inlet. The bulk of the axially fed material is bypassing the upper deltaic plain and deposited as a small deep-water delta.

After cessation of detachment activity at 0.5 Myr, regional subsidence is no longer counteracted by detachment-induced uplift (Figures 4.6 and 4.7, 0.75 Myr and 1.0 Myr). Consequently, the lower delta plain is flooded and the active delta retreats towards its inlet position, while showing bifurcating channel patterns again.

Subsequent activity of the detachment fault at 1.0 Myr results in decreased thrust-top accommodation space and renewed progradation of the axial delta (Figure 4.6, 1.25 Myr). Again experiment 2 is characterised by multiple linear drainages on the lower deltaic plain, but at 1.5 Myr a single, incised axial valley is created, implicating that all sediment is bypassing to deeper water (this already occurs at 1.25 Myr in experiment 3, Figure 4.7). In both experiments, the basin-margin alluvial fans prograde due to the gradual increase of orogenic topography and supply. Progradation is interrupted by shallow marine transgressions during detachment quiescence. During detachment fault activity and basin emergence, a collector river is formed at the toes of the alluvial fans in experiment 2, which is susceptible for incision by syn-tectonic eustatic sea-level fall (Figure 4.6, 0.5 and 1.25 Myr).

#### ***4.3.2 Evolution of the accommodation space***

The competition between regional flexural subsidence and local thrust-induced uplift controls the evolution of accommodation space in the thrust-sheet top basin (Figure 4.5). The resulting trend is modulated by the sinuous sea-level fluctuation. During activity of the frontal thrust, the accommodation space on the thrust-top platform is stepwise reduced with increasing detachment angle in the experiments (experiment 1, 2 and 3), or even periodically destroyed (experiment 4). During quiescence of the detachment, the flexural subsidence induced by thrust loading of the orogenic wedge predominates, increasing the accommodation space generated on the thrust-top basin.

During activity, a larger detachment angle results in increased incision susceptibility of the delta front by eustatic sea-level falls, as these are less compensated by regional flexural subsidence. The maximum rate of relative sea-level fall increases from 0.25 (experiment 1) to 0.45 m/kyr (experiment 3) with increasing detachment angle (Figure 4.5).

Indirectly, sea-level forcing does also influence the accommodation space trend by isostatic adjustment upon (sea level-induced) delta progradation and loading. However, this contribution is small, approximately 10 % of the flexural subsidence, and is therefore not visible in the curve of figure 4.5.

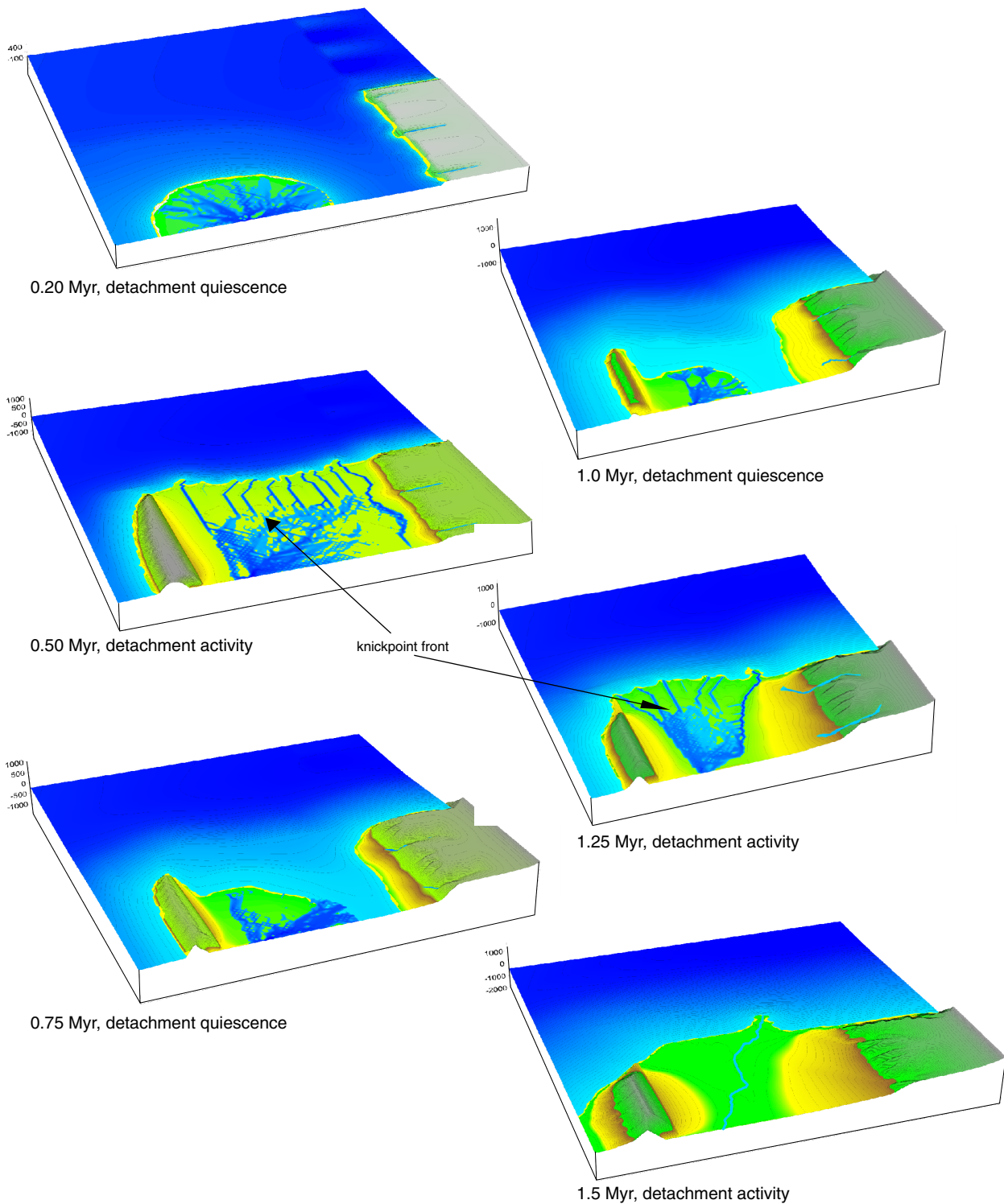


Figure 4.6 Successive steps in the landscape evolution of the exp.2 thrust-sheet top basin, applying a  $4^\circ$  detachment angle. Initially, the basin is occupied by a single delta cone (0.2 Myr). Upon activation of the detachment, the delta system progrades and becomes susceptible for eustatic-induced incision on the lower deltaic plain (0.5, 1.25 and 1.5 Myr). Detachment quiescence results in dominance of regional flexural subsidence and retreat of the delta across the thrust-top platform (0.75 and 1.0 Myr).

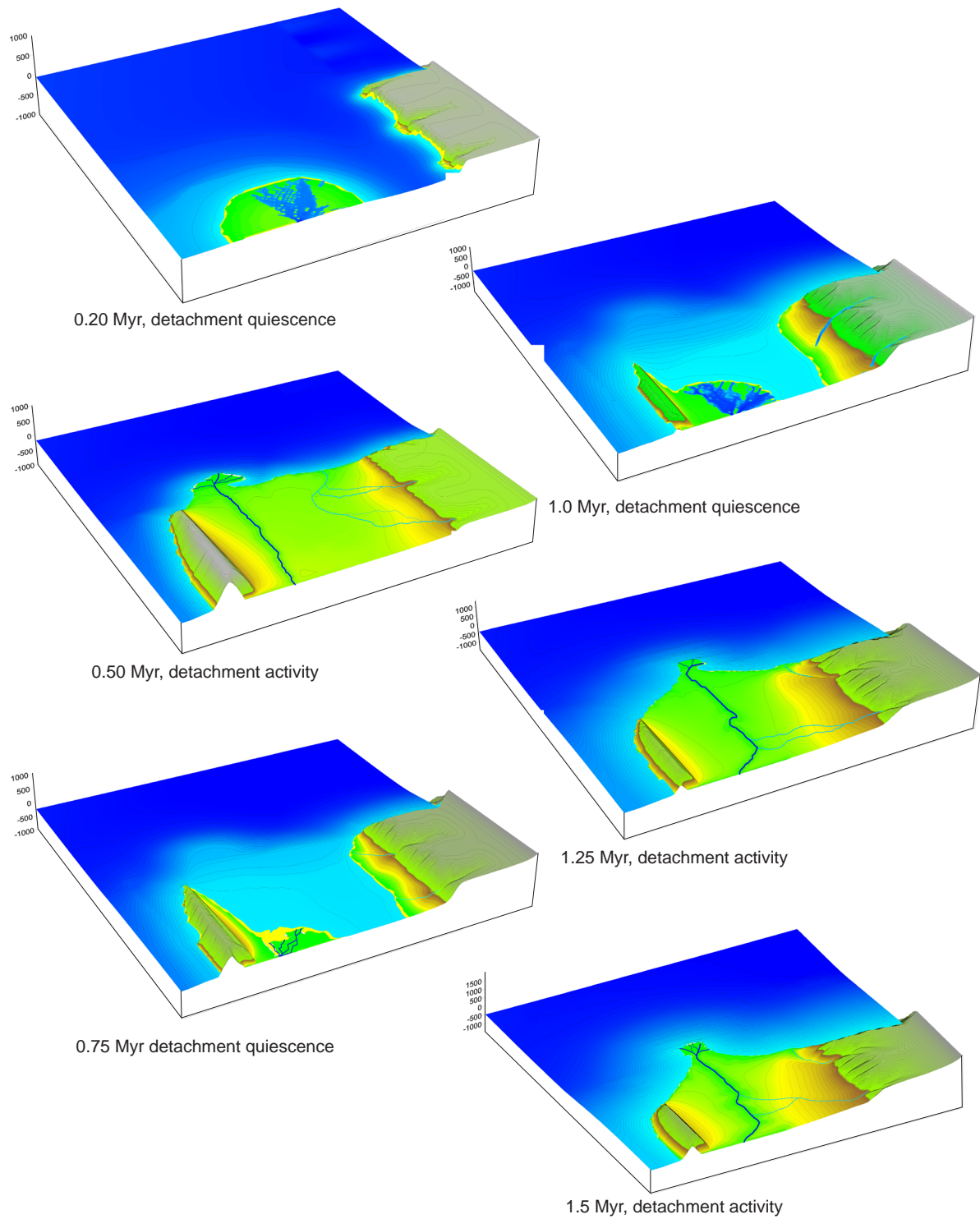
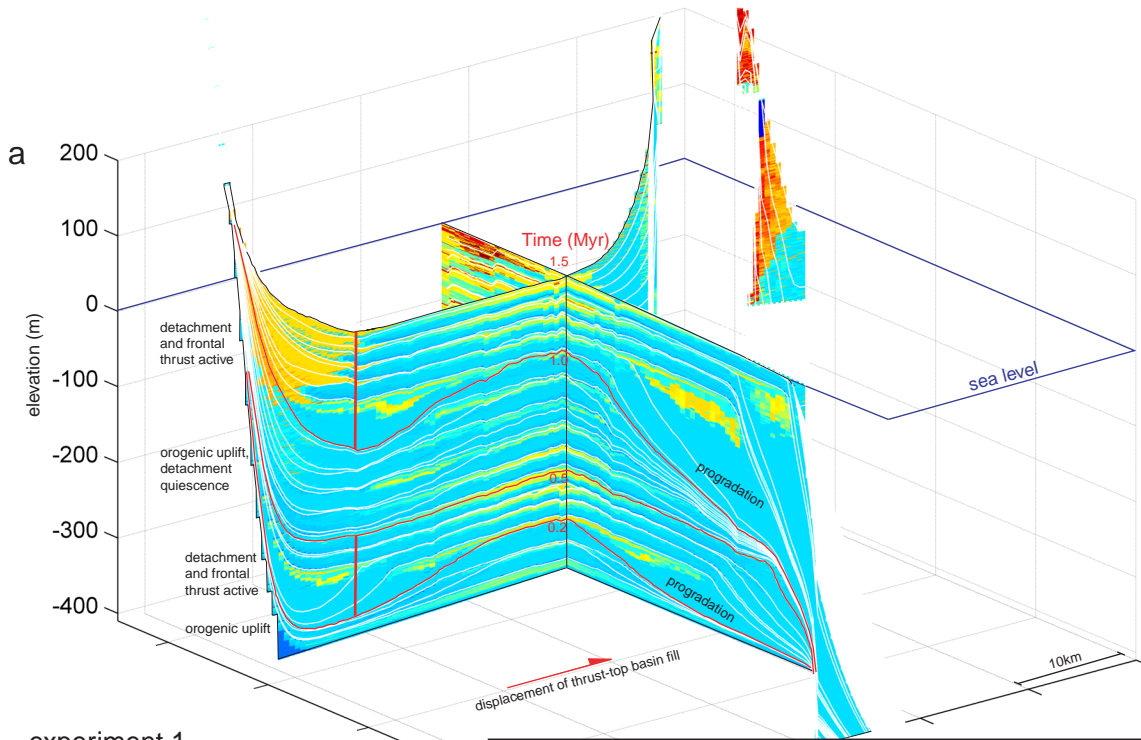
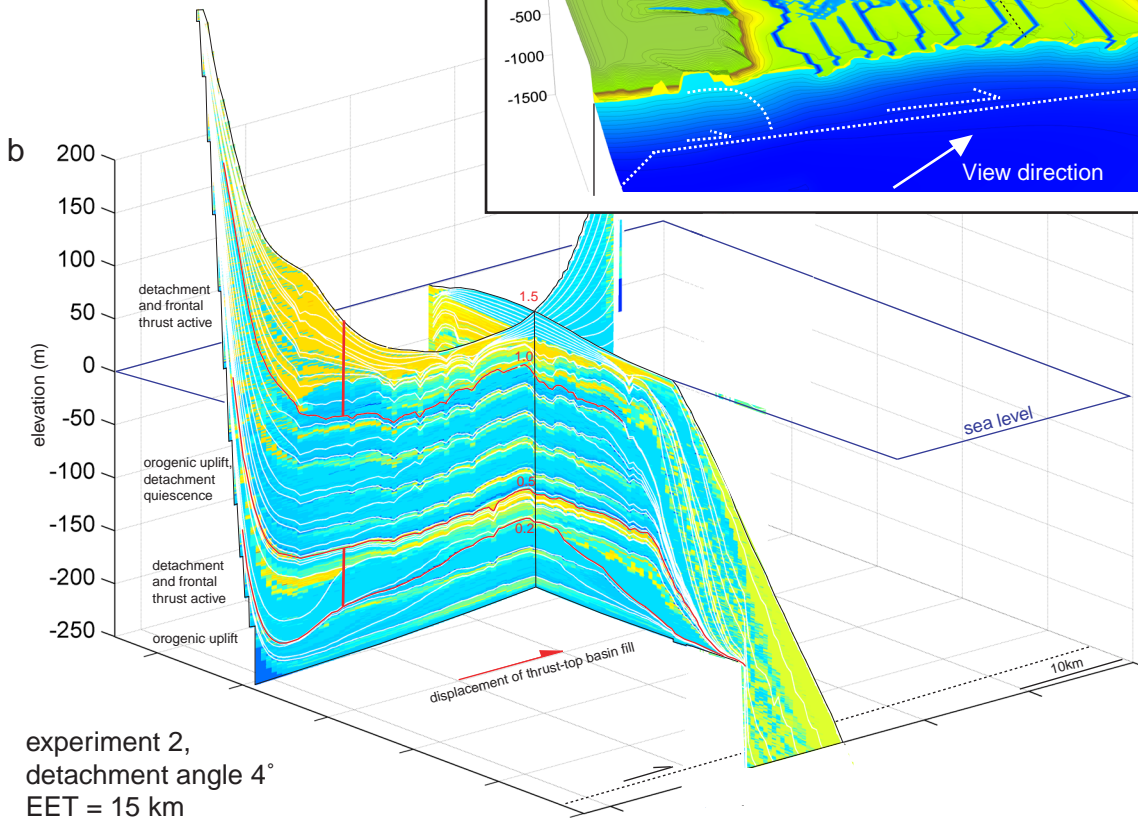
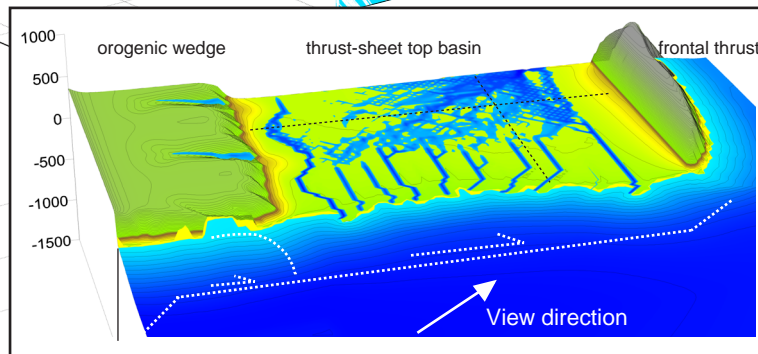


Figure 4.7 Successive steps in the landscape evolution of the exp.3 thrust-top basin, applying a  $6^\circ$  detachment angle. Evolution is similar to exp.2. although now syn-tectonic eustatic sea-level fall is able to carve a single incised valley into the delta plain. Much of the sediment fed to the system during the interval of detachment activity is bypassing to the adjacent marine basin.

Chapter 4



experiment 1,  
detachment angle 2°  
EET = 15 km



experiment 2,  
detachment angle 4°  
EET = 15 km



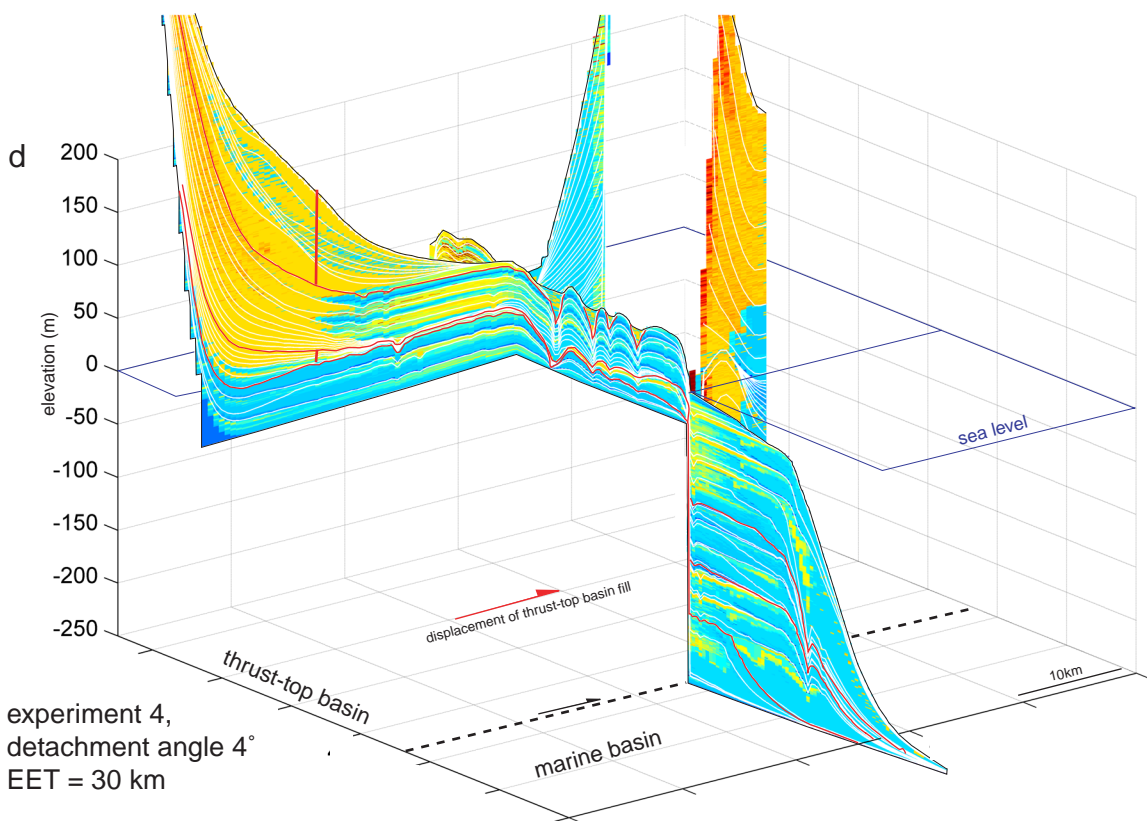
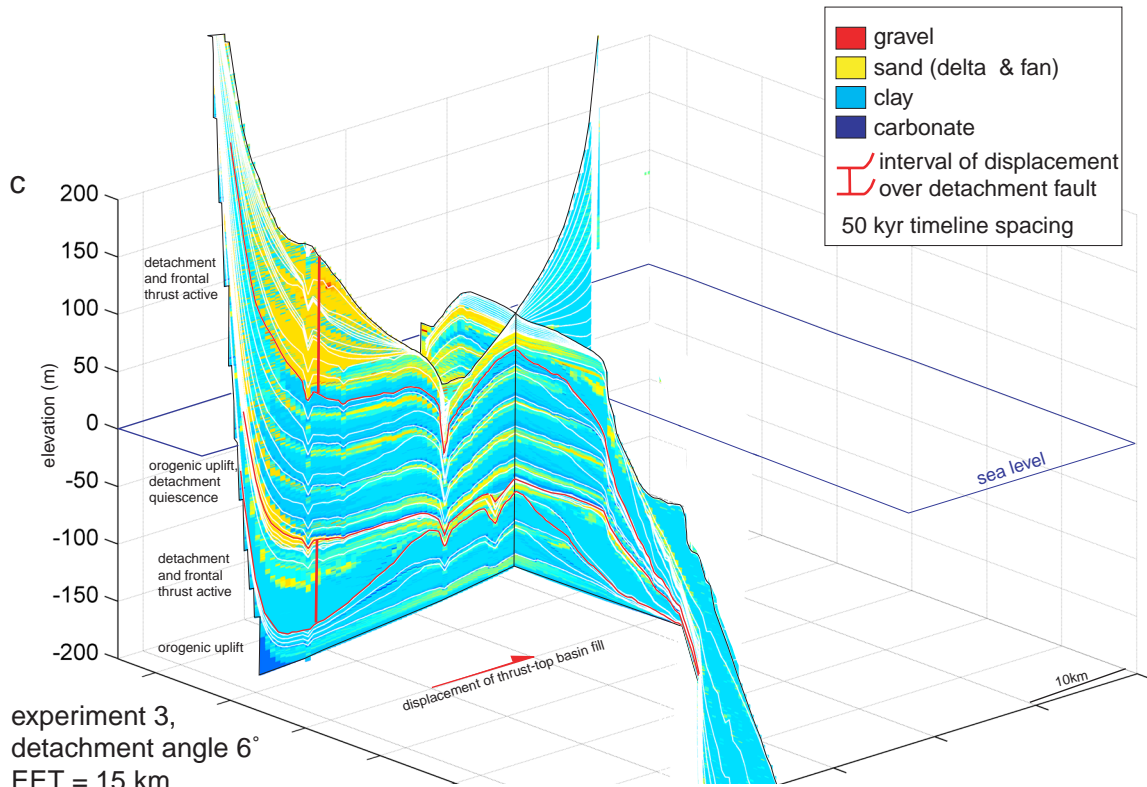


*Figure 4.8 (previous two pages) Fence diagrams illustrating the stratigraphic response to a shifting balance between regional flexural subsidence and detachment-induced uplift. A stepwise increased detachment angle (exp.1,2,3), or larger flexural rigidity results in enhanced delta progradation, increased interconnectedness of sandy fluvio-deltaic facies at the cost of fine-grained intervals, and susceptibility for incision by the longitudinal river. Nb. different vertical scales are used.*

### **4.3.3 Thrust-sheet top basin sequence architecture**

The sequence architecture of the thrust-sheet top basin fills is shown as a fence-diagram of two orthogonal lithological sections, selected from the 3D dataset at simulation time step 1.5 Myr (Figures 4.8). It is evident that the sediment thickness accumulated in the thrust-top platform decreases with increasing detachment angle or flexural rigidity (exp.1 ~400 m, exp.2 ~250 m, exp.3 ~175 m and exp.4 ~80 m).

The stratigraphy of experiment 1 is marked by multiple stacks of prograding, coarsening-up clinofolds overlain by delta-top sands and thin carbonate onlaps, reflecting the eustatic sea-level fluctuations. Timelines corresponding to initiation and cessation of activity of the underlying detachment fault are highlighted in red (Figure 4.8). In experiment 1, activity of the detachment fault is difficult to read from the stratigraphic pattern, because the eustatic signature dominates the stratigraphy. However, minor decreases in thickness of syn-tectonic eustatic-controlled cycles are recognisable together with enhanced progradation of coarsening-up clinofolds, implying reduction of the accommodation space on the thrust-sheet top basin. During the second phase of detachment activity, the clinofold break progrades within 0.5 Myr towards a final position above the strike-slip fault to the adjacent marine basin.

In experiment 2, the syn-tectonic strata clearly account for the decrease in general thickness. The eustatic cycles are thinner and the sea-level falls are characterised by increase of the sand content and high interconnectedness of the sandy delta-top layers at the expense of the fine-grained marine intervals. However, they are partly separated by thin marine carbonate onlaps, indicating a continuous marine influence into the delta-plain of the thrust-sheet top basin (~ 20 km) during syn-tectonic, eustatic sea-level highs. This type of response is comparable to the observations in parts of the Montanyana Group, where sheet sandstones are well developed but interleaved by thin marine intervals (Marzo *et al.*, 1988). The syn-tectonic timelines merge locally in the sandy intervals, due to erosion and incised-valley formation. The incision is developed at the transition from detachment quiescence to activity, marked by a Type-1 unconformity, developed during the first syn-tectonic, eustatic sea-level low.

Incisions are better developed in experiment 3, where timelines bend down in the basin centre, implying that the basin axis position is repeatedly used for incision, in particular during syn-tectonic intervals, where timelines merge. No carbonate onlaps are recognisable within the syn-tectonic sequences, implying that the delta plain is not influenced by sea-level highstands, only by the sea-

level fall-induced incisions. Note that at the end configuration of experiments 3 and 4 the complete thrust-sheet top basin is on average some 50 m above base level, due to the last phase of detachment-induced uplift.

#### ***4.3.4 The delta-slope stratigraphy in the adjacent basin***

Figure 4.9 shows the three-dimensional relationship between the incised valley fill systems of the thrust-sheet top basin (experiment 3) and the corresponding delta slope deposits in the adjacent basin. Two incised systems, a lower and an upper one, are represented as a string of voxels. Both are formed during phases of detachment fault activity. The lower fill (0.2-0.5 Myr) consists of two to three obliquely stacked channel belts, an amount that corresponds to the number of eustatic sea-level falls during the first syn-tectonic phase. The upper incised valley fill (1.0-1.5 Myr) also consists of multiple channel belts, but these are stacked vertically and only split in the downstream direction where they crosscut the cross-section. With respect to the lower valley fill, the upper one has been shifted to the left over a distance of 10 km. Vertical channel stacking and the shift are indicative of the axial river being locked in the thrust-sheet top basin axis during the second phase of detachment fault activity (see also figure 4.6 for the channel shift). Both valley fills are connected over the lateral ramp of the thrust-sheet top basin to a coarsening-up delta lobe, deposited in the deep-water sub-basin. In this basin, the successive phases of detachment activity and quiescence are recognisable as lobate bodies characterised by high sedimentation rate ( $> 0.5$  m/kyr, Figure 4.9b) separated by a condensed section of closely stacked timelines (0.5-1.0 Myr, Figure 4.9b).

#### ***4.3.5 Correlation of mass-flow events to the eustatic signal***

A synthetic well (Figure 4.10) through the deep marine basin fill illustrates the relation between mass-flow events and eustatic sea-level fluctuations. The well is complemented by a graph showing the eustatic sea level at the time of deposition of each individual layer. As a result the derived eustatic curve is not symmetrical, but stretched or compressed by differences in the sedimentation rate of the deposited stratigraphy. As in the fence diagram (Figure 4.9), the bulk of the deep-marine sedimentation in the well is synchronous with the phases of detachment activity, separated by a condensed section corresponding to detachment quiescence. The first interval (–575 to –450 m) represents a coarsening-up section through the lowermost deep-water delta lobe, topped by one of the axial channel lags and two carbonate-rich beds, indicating the transition from forced regression by detachment activity to transgression during detachment quiescence. In the second stratigraphic interval (–450 to –100 m) there is a correlation between the presence of mass-flow sand beds in the well and rises of the eustatic sea level.

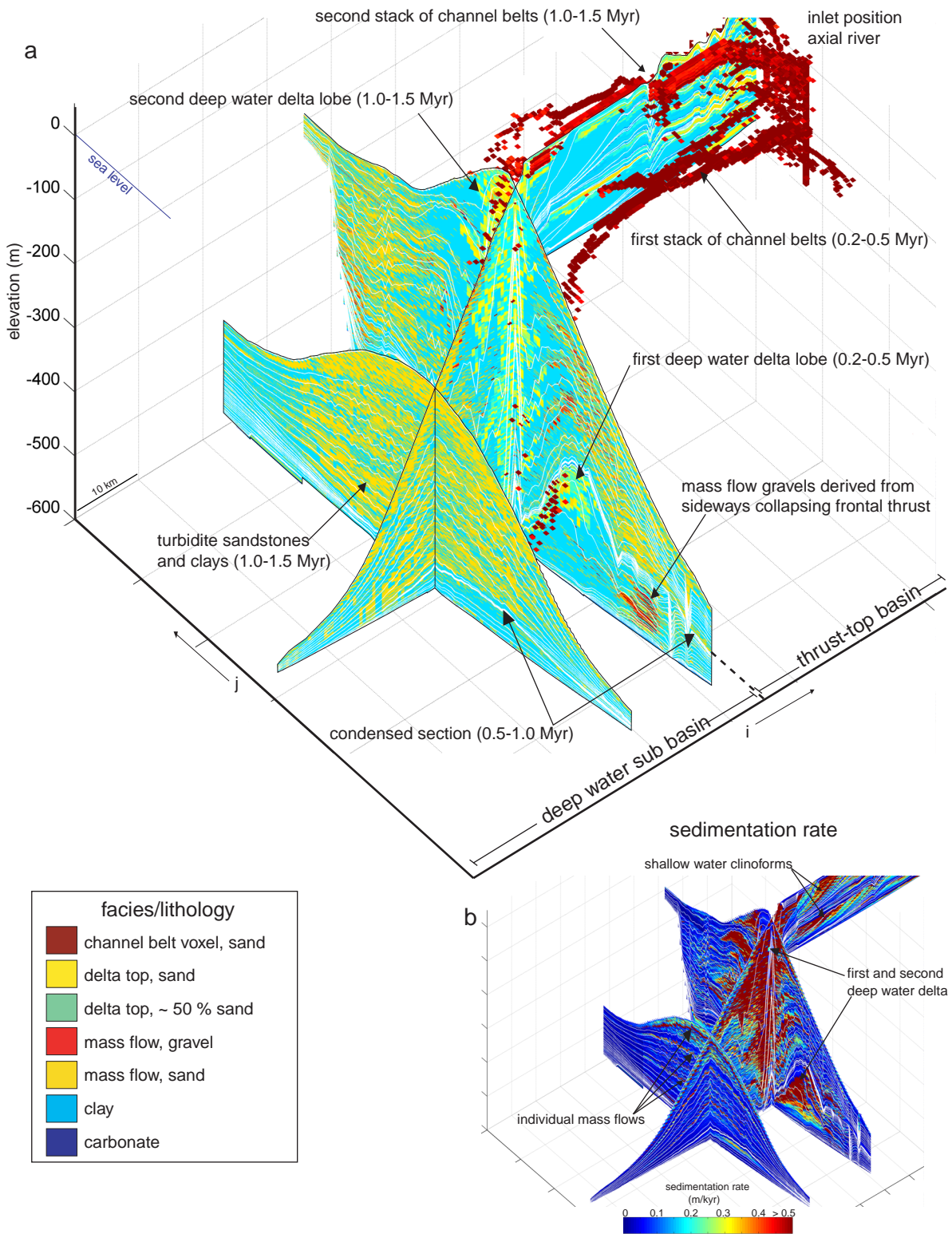


Figure 4.9 Lithological fence diagram of experiment 3 showing the connection between the thrust-sheet top basin and the deep-water sub basin. Two incised valley fills, corresponding to the phases of detachment activity, pass over the lateral ramp into deep-water delta lobes. These lobes are dominated by mass-flow beds and high sedimentation rates (~0.5 m/kyr), and are deposited during intervals of detachment activity. A condensed section represents the quiescence phase of the detachment fault (0.5-1.0 Myr).

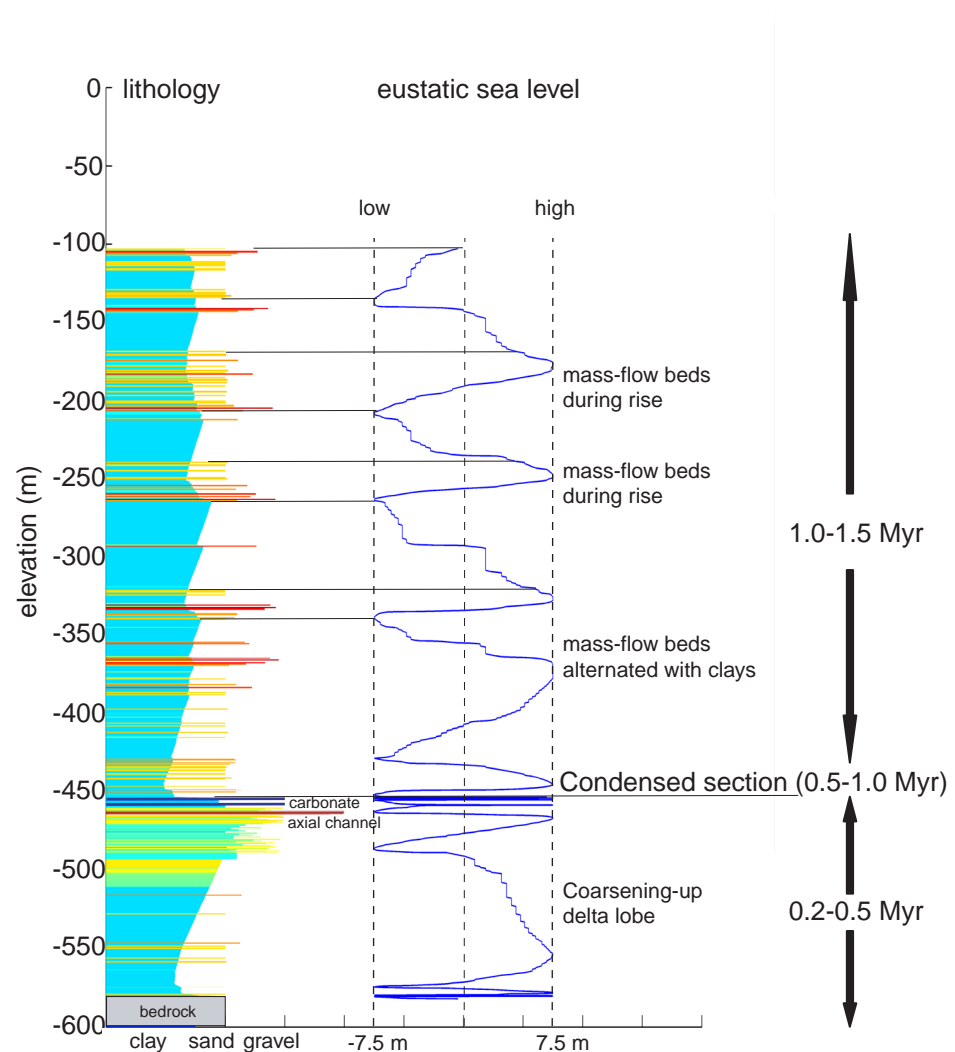


Figure 4.10 Synthetic well taken from the deep marine sub-basin, showing two intervals of syn-tectonic sedimentation, separated by the condensed section. Comparison of the well to the eustatic curve indicates that the timing of mass-flow deposition corresponds to syn-tectonic eustatic rise in the well top. Note that the curve is not symmetrical. This is due to the construction method of strata-specific age substitution into the eustatic-forcing curve (Figure 4.5).

## 4.4 Discussion

### 4.4.1 Fluvial patterns

It is clear from the above experiments that the fluvial drainage in thrust-sheet top basins is influenced by the angle and activity pattern of the detachment fault. During quiescence the rise of relative sea level due to regional flexural subsidence results in rapid backfilling, relocating fluvial channels and the formation of a single delta cone. During translation along the detachment, accommodation space is reduced, the fluvial system progrades and the clinoform break becomes a line source of

small deltas fed through a row of small, incised valleys. Alternatively, at a steeper detachment angle and faster fall of relative sea level (Figure 4.5 and 4.7) a single delta is formed at the clinoform break fed by a major incised valley system, which is locked between basin-margin alluvial fan profiles (Figure 4.7 and 4.8).

The syn-tectonic alluvial fan and longitudinal river progradation observed in the model, has an implication for the simplistic ‘two-phase’ concept of foreland basin fluvial patterns (Heller *et al.*, 1988). In this concept longitudinal flow close to the thrust front is associated with syn-tectonic subsidence, while dominance of transversal flow is indicative for quiescence or isostatic rebound by erosional unloading. In a foreland basin underlain by active hinterland-dipping detachments, transversal and longitudinal progradation of alluvial systems is rather due to a reduction of accommodation space along a considerable length of the foreland basin by translation over the detachment fault, instead of isostatic rebound.

#### **4.4.2 Stratigraphy**

The accommodation space in the modelled thrust-sheet top basin is sensitive to small increases in the detachment angle. The basin-scale stratigraphic stacking pattern is thus a function of the balance between regional flexural subsidence and thrust sheet displacement-induced uplift. Displacement results in sand-sheet amalgamation, unconformities or even incised valleys, the intensity of the response depending on the steepness of the angle of the detachment fault. This sedimentary response of detachment activity phases, punctuates the overall basin subsidence and fine-grained sedimentation, just as observed in the Montanyana Group (Figure 4.3).

A well-studied but controversial section of the Montanyana Group is the Castissent Formation or megasequence (Figure 4.3). Characterised by amalgamating sheet sandstones and pronounced progradation into the lower deltaic plain and the Ainsa Basin it has been interpreted as an incised valley-fill sequence (Marzo *et al.*, 1988), related to the Ypresian sea-level fall at 51.3 Myr. However, several characteristics of the Castissent Formation do not validate this interpretation. Improved dating constraints on existing correlations set the base of the formation at 51.7 Myr instead of 51.3 Myr (Nijman, 1998). There is no clear Type-1 unconformity at the base but a marine onlap that correlates with thrust-flank unconformities. The average sedimentation rate is only reduced, and not very different with respect to the underlying megasequence. Moreover, the individual sheet sandstones are sandwiched between widespread brackish-marine onlaps (Marzo *et al.*, 1988; Nijman, 1998), indicating a continuous marine influence throughout deposition. These inconsistencies within the incised valley interpretation were recognised earlier and the formation was interpreted as highstand progradation in response to a previous phase tectonic loading and subsidence (Nijman, 1998). Considering the model results, the Castissent Formation more likely represents a phase of displacement-induced reduction of accommodation space, resulting in forced regression and an increased interconnectedness of sandstones at the cost of fine-grained intervals, but without excluding marine influence.

*Other basins controlled by the same mechanism ?*

Paleomagnetic work in the late Cretaceous to Eocene Axhandle Piggyback Basin (Central Utah) indicates that sedimentation rates alternated between times of rapid (0.05 - 0.25m/kyr) and low (< 0.02 m/kyr) accumulation, while also periods of non-deposition or even incision occurred (Talling *et al.*, 1995). Lawton and Robinson (Lawton, 2003) identify two longitudinal fluvial systems supported by a detachment ramp and also characterised by a high net to gross aspect. These are the Santonian Straight Cliffs Formation in Southern Utah and the Mid-Late Campanian Price River Formation, which were both deposited during rapid advance of the thrust front. More extreme end members of the mechanism are probably found in the Plio-Pleistocene thrust-sheet depozones of the western Taiwan foreland basin, where accommodation space was not only reduced by tectonic translation, but even actively destroyed. Here, deposits are punctuated by phases of deep incised valley formation and creation of basin-wide unconformities every 200-700 kyr, which do not correspond to falls in eustatic sea level (Chen *et al.*, 2001).

**4.4.3 Temporal sediment storage on thrust-sheet top basins**

In segmented foreland basins, the timing of accumulation on the thrust-top basin and bypass to adjacent marine basins (Mutti, 1985; Ricci-Lucchi, 1986; Pickering *et al.*, 1995) is much debated. In the model experiments, bypass of the thrust-sheet top depozone occurs during detachment activity and is recognised by increased sedimentation in the deep-water subbasin (Figure 4.9). This behaviour of the model is conform the interpretation for tectonic-controlled sediment partitioning between the Tremp and Ainsa basins according to Mutti (1985). He concluded, based on correlation of sequence boundaries between both basins, that the Ainsa turbidite lobes are synchronous with phases of activity along the Tremp-Ainsa lateral ramp (Figure 4.2). The deep-water sediment geometries calculated by the model are a starting point for modelling this famous field-analogue for tectonically-influenced deep-water turbidite lobes. Adjustments need to be made in the model in order to incorporate the syn-sedimentary, blind thrusts which influence the orientation of the lobes and their stacking pattern.

The superimposed eustatic fluctuation in the model experiment leads to repetitive deposition of mass-flow beds. The timing corresponds to phases of syn-tectonic eustatic rise. This behaviour is easily explained. The collapse routine is only active at water depths over 15 m. During a phase of eustatic sea-level fall, an oversteepened delta front is created above this threshold depth. It becomes subject to drowning and collapses only during the subsequent eustatic rise. Obviously, changing the value of the water depth threshold or applying another, more sophisticated triggering threshold will lead to a change in timing of the mass flow events.

Despite the syn-tectonic spilling of sediment into the adjacent basin, the supply is insufficient to fill this continuously subsiding basin in experiments 1, 2 and 3. In experiment 4 the regional subsidence rate is reduced from 0.32 ~ 0.18 m/kyr by doubling the effective elastic thickness of the lithosphere. The resulting thrust-sheet top stratigraphy resembles that of experiment 3, showing

pronounced incisions, syn-tectonic sheet sandstones. Except that now a more complete delta stratigraphy is developed in the subbasin.

#### **4.5 Conclusion**

Model results show that the competition between rates of regional flexural subsidence, and local detachment-induced uplift controls the accommodation space evolution and the stratigraphic patterns in a marine-influenced thrust-sheet top basin. During activation of the detachment fault, the fluvio-deltaic system carried by the thrust sheet progrades and part of the sediment supply is spilled over into adjacent basins. The intensity of the progradation, the interconnectedness of fluvial sheet sandstones and the sensitivity to the formation of incised valleys increase with the angle of the detachment fault. The mechanism explains the Castissent Formation as a phase of reduced accommodation space by translation over the detachment, instead of an incised valley fill sequence formed by eustatic sea-level fall. During quiescence of the detachment fault, the flexural subsidence becomes the predominant component in the accommodation space balance above the thrust-sheet top basin. Sediment is temporally stored on the thrust-sheet as the deltaic system retreats, while leaving the adjacent deep-water basin starved.



## Stratigraphic modelling using CHILD

### 5.1 Triangular irregular network

Surface process models are widely used in geomorphology and geology, and the developments in the field follow each other rapidly. Much of the progress consists of the improvement of existing models, such as the addition of new surface processes (Densmore *et al.*, 1998), new sediment transport algorithms (Gasparini *et al.*, 1999), the recording of stratigraphy (Johnson and Beaumont, 1995) or complex scenarios such as stochastic rainfall (Tucker, 2000; Karssenber, 2002). Alternatively, effort is put in changing the backbone of the surface process model by changing the spatial discretization of the model landscape and the method by which water and sediment are routed downward over the surface. This resulted in a new generation of models based on a self-adapting irregular triangular network (TIN) instead of the commonly used static rectangular grid. Two notable examples applicable on the geologic timescale are CASCADE (Braun and Sambridge, 1997) and CHILD (Tucker *et al.*, 2002). In these models the nodes representing the landscape surface are connected to each other using Delauney triangulation (Fortune, 1995) (Figure 5.1). Delauney triangulation itself is not a new technique; it is applied in modelling of solid objects, fault surfaces and drainage basins. However, all these applications apply triangulation in a rather static way, in a sense that the object of interest is discretised only once or a limited number of times during a simulation. This is not the case in the two surface process models referred to here. They constantly update their landscape representation over geologic time by active remeshing. The triangulated landscape representation and the remeshing technique have several advantages above the 'classical' rectangular grid (Braun and Sambridge, 1997):

- 1) Reduction of the artificial symmetry in stream networks
- 2) Easy discretisation of complex geometries
- 3) Handling horizontal translation

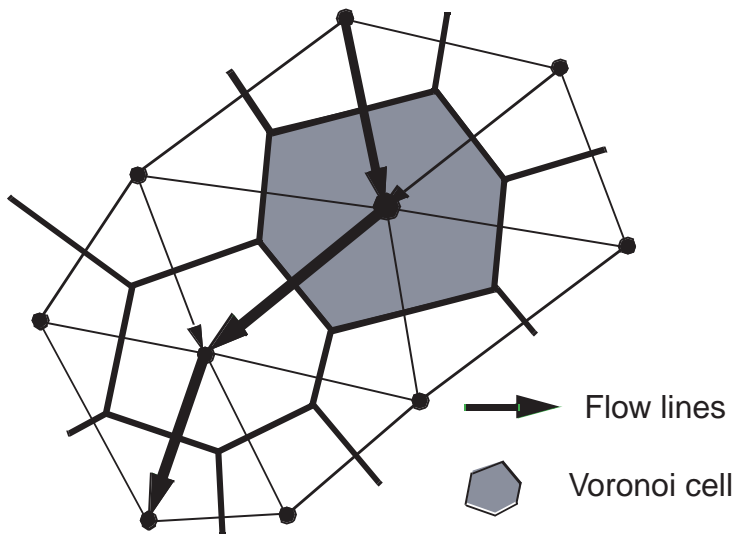


Figure 5.1 Illustration of the TIN framework used in the CHILD model. Indicated are the steepest descent flow routing over the nodes and the Voronoi areas represented by the nodes.

### 5.1.1 Reduction of artificial symmetry in stream networks

A routing scheme for water and sediment on a rectangular grid always involves 8 potential flow directions. Consequently, inter-node drainage paths make angles of 45 degrees, which is of course not realistic considering natural drainage situations. Commonly modelled drainage networks suffer from this geometrical bias, dictated by the rectangular grid, by showing an artificial symmetry in their organization. This does not affect models using a self-adapting triangular mesh, because their nodes have no fixed positions and nodes can be added anywhere during a simulation. The number of drainage directions is unlimited due to the ability of the model to ‘remesh’ by adding, deleting or re-locating individual nodes in between surface process timesteps.

### 5.1.2 Representation of complex geometries

The flexibility to add nodes at any position facilitates an improved representation of complex surface geometries by locally using a higher density of nodes. This is memory efficient in contrast to the classic rectangular grid models where resolution improvement is only achieved by increasing the number of nodes over the entire surface. In the TIN models a simple flat surface is adequately represented with a few widely-spaced nodes, whereas a more complex geometry such as a dendritic drainage network or a fault front is represented by a higher density of nodes.

### 5.1.3 Horizontal translation

An important advantage of moving nodes and remeshing is the capability to model complex geological problems that demand a high degree of geometrical flexibility, such as horizontal tectonic transport (thrusting and strike-slip) and river meandering. One of the first examples of thrusting simulated by a TIN based model is given by van der Beek *et al.* (2002). In this study the drainage development in response to active fault-propagation folding and variable detachment dip in the Himalayan foreland is addressed using CASCADE (Braun and Sambridge, 1997).

## 5.2 Channel Hillslope Integrated Landscape Development model, CHILD

Fascinated by these capabilities of the new meshing technique I visited Dr. Greg Tucker's group at MIT in the autumn of 1999 in order to work with their recently developed CHILD model (see the CHILD website: <http://platte.mit.edu/~child/>). CHILD (Channel Hillslope Integrated Landscape Development) is a unique triangular mesh-based surface process model, due to its modular design and the range of geomorphic processes that can be modelled (Tucker *et al.*, 2002). It addresses drainage basin evolution at different spatial scales, incorporates groundwater flow, transports and sorts multiple grainsize fractions, performs meandering and is capable of accumulating stratigraphy. Initially I intended to use CHILD as a basis for modelling foreland basins, but unfortunately this turned out to be practically impossible due to the complexity of CHILD and the long computer runtime involved for long geological scenarios. Part of the functions demonstrated in this thesis such as thrusting, 3D flexure and perfect sorting are already coded into CHILD, but wait on a computer potent enough to allow for geological timescale sensitivity analysis. It is to be expected that due to the steady increase in available computer power, TIN-based models will become the future standard for geologic time-scale modelling presented in this thesis. In order to illustrate the versatility and potential of CHILD, three examples of stratigraphic modelling using CHILD are shown at different temporal and spatial scales: 1) Alluvial Fans, 2) River Meandering, and 3) Basin Fill.

### 5.2.1 Alluvial fans

The alluvial fans modelled with CHILD (Figure 5.2) differ in three aspects from the fans shown in previous chapters. They are based on the irregular triangular mesh, use solely steepest descent flow paths on the alluvial fan surfaces (no bifurcation flow) and size-selective sediment transport along these stream paths is performed using a shear stress-based technique (Wilcock, 1998; Gasparini *et al.*, 1999). Within the simulation a fault block is uplifted at a steady rate, eroded by bedrock incision and the debris is deposited as alluvial fan cones. The exhumed bedrock is instructed to produce sediment with a composition of 50 % gravel (> 2mm) and 50 % sand (< 2mm). The sediment fractions are transported downstream according to individual transport rates of the two grainsizes

$$q_{gravel} = \frac{C_w f_g}{(s-1)g} \left( \frac{\tau}{\rho} \right)^{1.5} \left[ 1 - \frac{\tau_{crit\_gravel}}{\tau} \right]^{4.5} \quad (5.1)$$

$$q_{sand} = \frac{C_w f_s}{(s-1)g} \left( \frac{\tau}{\rho} \right)^{1.5} \left[ 1 - \sqrt{\frac{\tau_{crit\_sand}}{\tau}} \right]^{4.5} \quad (5.2)$$

where  $q_{gravel}$  and  $q_{sand}$  are the transport rates of gravel and sand (kg/ms),  $C_w$  a constant,  $f_g$  and  $f_s$  are the fractions gravel and sand in the stratigraphic toplayer,  $\tau$  the bed shear stress,  $\rho$  the density of water and  $\tau_{crit\_gravel}$ ,  $\tau_{crit\_sand}$  the critical entrainment shear stresses for gravel and sand. The sorting method is computationally very demanding because it requires very small timesteps (~1 yr) in order to maintain numerical stability. Therefore the simulation presented and the corresponding

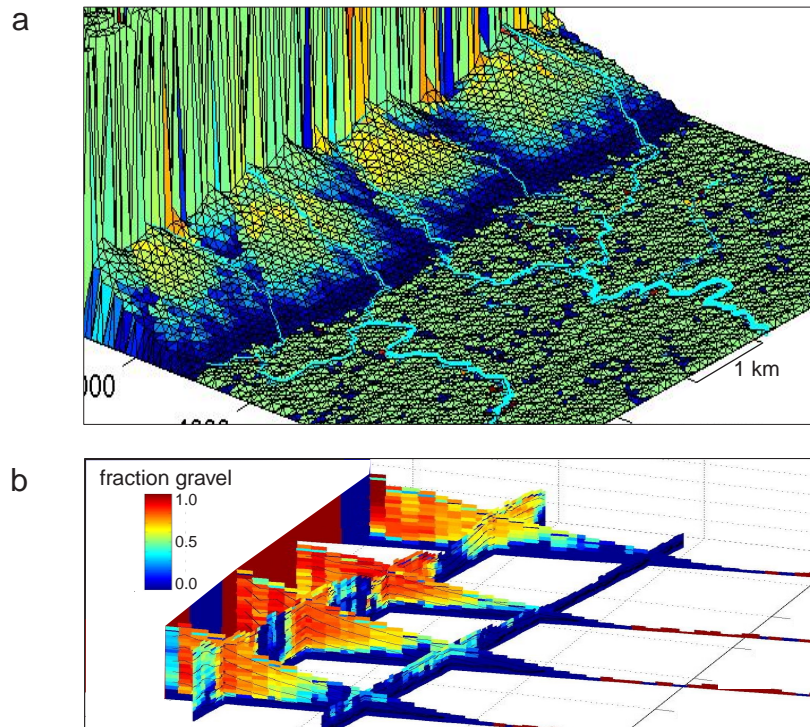


Figure 5.2 (a) Perspective view of TIN-based alluvial fans. Material for the aggradation of the fans is supplied by a set of switching feeder channels. The surface of the fans is coloured according to the fraction of gravel in the top layer of the stratigraphy. (b) Stratigraphic fence diagram through the alluvial fans after 0.6 Myr of aggradation. Timelines (black) represent 0.1 Myr each. Gradual progradation of the coarse gravel is the result of constant hangingwall uplift and erosion and steepening of the fan profile.

fence-diagram only represents a timespan of 60 kyrs. The fence diagram shows a gradual progradation of the coarse gravel fraction deposited by the alluvial fans as the result of steady uplift of the hangingwall block, subsequent erosion and steepening of the fan profile. Baselevel is kept at a constant level at all grid boundaries bounding the alluvial plain. TIN-based remeshing is not exploited in this example, but could be used to differentiate between floodplain and alluvial fan, or to study whether fan avulsion frequency is affected by differences in feeder stream and inactive fan cone resolution.

### 5.2.2 River meandering

The main process responsible for the morphology of a meandering river is gradual channel migration by erosion of the outer banks and deposition in the inner part of the channel loops (Allen, 1965). This process is appropriately simulated using the remeshing technique present in CHILD (Lancaster, 1998). For example, nodes representing the main thalweg channel are shifted gradually to shape meander bends, and obstructing outer bank nodes are deleted while additional nodes are created to form point bars. The rate at which the main channel is allowed to migrate ( $R_{\text{migration}}$ ) is defined by

the rate of bank erosion as function of the bank shear stress (Ikeda *et al.*, 1981; Odgaard, 1986; Lancaster, 1998):

$$R_{migration} = E\tau_w \hat{n} \quad (5.3)$$

where E is the bank erodability coefficient,  $\tau$  the bank shear stress and  $\hat{n}$  the unit vector perpendicular to the downstream direction. Besides active channel meandering, CHILD simulates a second process characteristic for the fluvial system, i.e. floodplain deposition (equation 5.4). The modelling method applied for floodplain deposition is geometrical and based on the observation that floodplain sedimentation rate decreases exponentially with distance from the main channel (Mackey and Bridge, 1995; Howard, 1996).

$$\frac{dh}{dt} = (H_{bfc} - H_{fp}) R_{max} \exp\left(-\frac{d}{\lambda}\right) \quad (5.4)$$

The change in elevation of a single floodplain node is a function of the difference in elevation between the floodplain node ( $H_{fp}$ ) and the bankful channel height ( $H_{bfc}$ ), its distance to the main channel ( $d$ ), a maximum sedimentation rate at the levees close to the channel ( $R_{max}$ ), and the decay distance ( $\lambda$ ) at which the sedimentation rate decreases to zero.

Figure 5.3 shows the evolution of a meandering river, encased in a narrow valley, during a period of 5000 yrs. The river is subjected to a general trend of baselevel rise, interrupted by two phases of baselevel lowering, the first at  $t=2000$  yrs and the second at  $t=4000$  yrs. During the simulation the baselevel rise is responded by alluviation of the valley by the combined effect of channel aggradation and floodplain deposition. Such phase of alluviation is associated with unrestricted meandering of the channel in the valley. An encounter of the channel with a valley wall results in carving out the meander bends and widening of the valley. During events of baselevel fall the river straightens by incision into its own floodplain. The resulting stratigraphy at the end of the simulation is illustrated in figure 5.4. The stratigraphy is visible through the transparent floodplain surface as three parallel sections, coloured according to the deposition age of the sediment. The oldest sediment occupies the margins of the floodplain as terraces (blue), while valley centre is dominated by younger sediment positioned upon older channel lags (red).

### 5.2.3 Basin fill

The last example of a modelled stratigraphy is of relatively large temporal and spatial scale for a CHILD simulation (10 x 10 km, 40 x 40 nodes, simulation time ~ 2.0 Myr, Figure 5.5). The modelled setting consists of a depositional basin confined by two uplifting fault blocks. The fault blocks are eroded and deliver two grainsize fractions to the small inter-montane basin. During the steepest descent routing of the sediment into the basin the sediment carried by the flow is sorted using the two-fraction model of Wilcock (1998). An extra sediment source is entering the basin in the form of an axial flowing river, which is instructed to spread fine-grained floodplain sediments (blue). Initially the river occupies the centre of the intermontane basin, but its position gradually shifts by the progradation of the right-hand side alluvial fans (Figure 5.5).

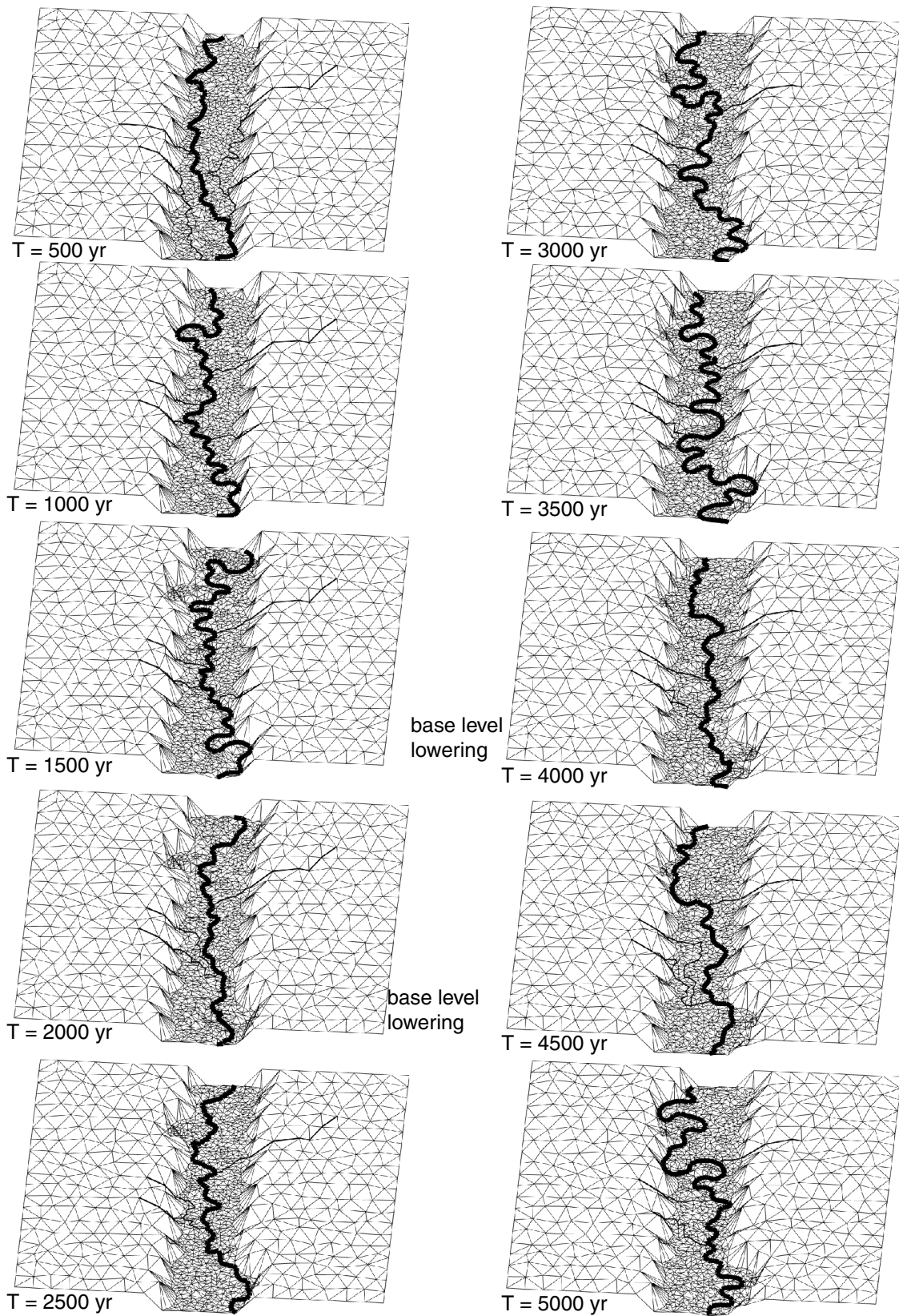


Figure 5.3 Simulation of a meandering river depicted in successive timesteps of 500 yrs. Intervals of meandering and alluviation of the valley correspond to phases of base-level rise, while straightening by incision occur during base-level fall ( $t=2000$  and  $t=4000$  yrs).

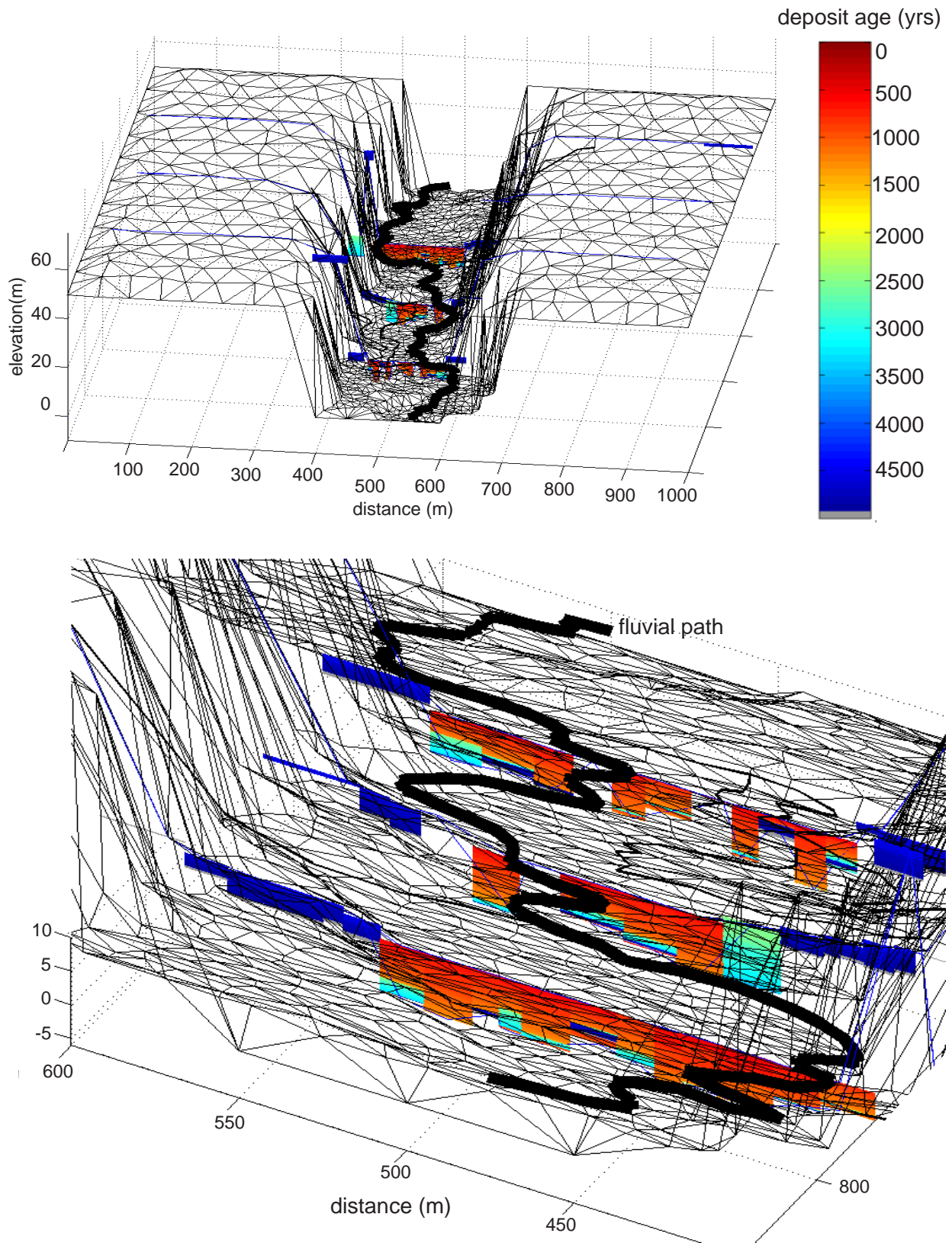


Figure 5.4 TIN representation the floodplain occupied by the meandering channel. The TIN is made transparent in order to visualize three stratigraphic sections of the floodplain subsurface. The sections are coloured according to the depositional age of the strata, showing older sediment at the sides of the valley as fluvial terraces, and younger strata occupying the valley centre.

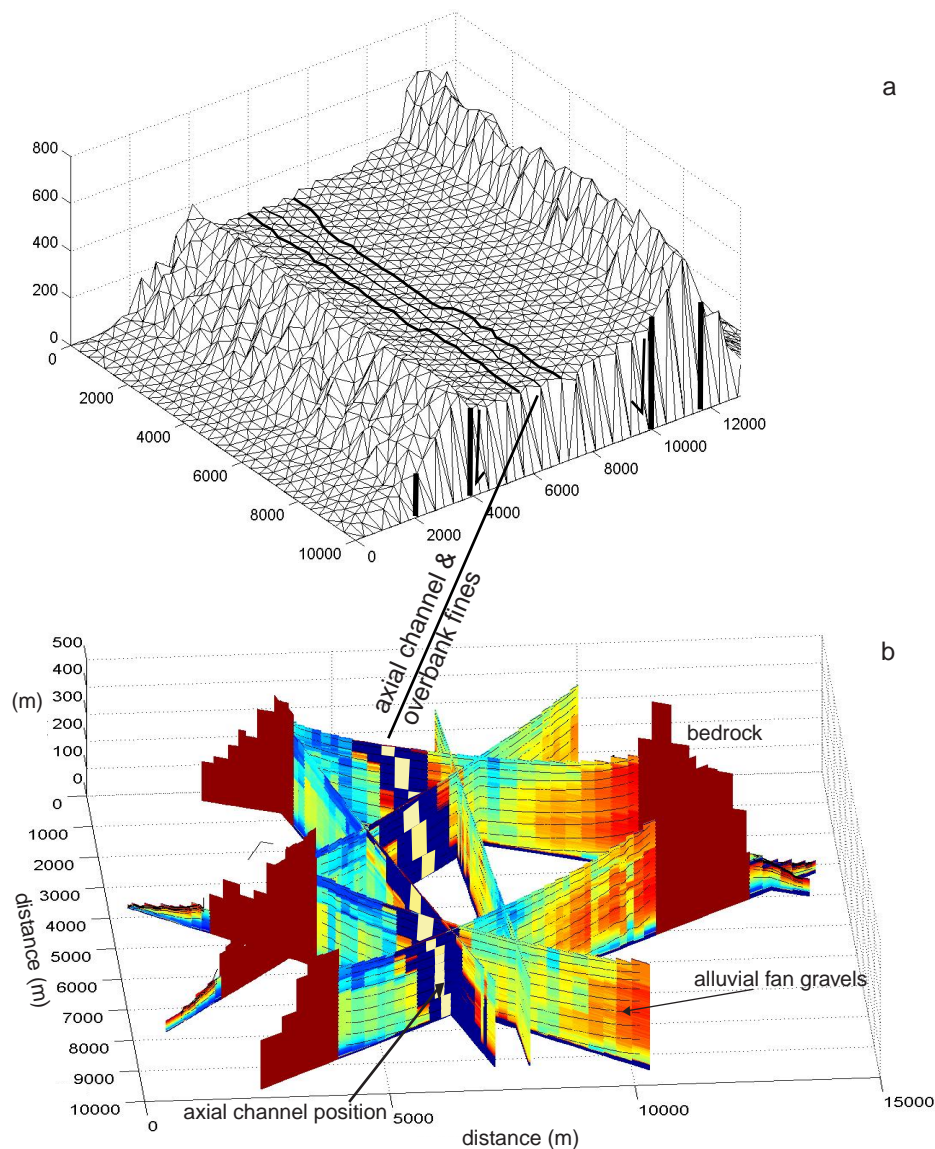


Figure 5.5 (a) Surface TIN showing the uplifted fault blocks and the axial river in the inter-montane basin. (b) Fence diagram through the inter-montane basin fill accumulated after 2.0 Myr. It shows the progradation of the alluvial fan gravels (red) and the gradual shift of the axial floodplain sediments (blue).

### 5.3 Conclusions

The above model examples demonstrate that it is possible to simulate alluvial fans, a meandering river and a small basin including their 3D stratigraphy using the TIN-based CHILD software. At present, evaluation of the effect of multiple variables or model development at geologic time scales ( $> 0.5$  Myr) is limited by the capacity of today's computers. It is to be expected, that due to the steady increase in available computer speed and memory, and the advantages TINs have in solving geological problems, this discretisation method will be the standard for stratigraphic simulation in 5 to 10 years time.



## Conclusions

In this thesis a tectono-sedimentary forward model has been presented, devised to simulate sediment erosion and deposition in a coupled drainage basin - foreland system, as well as accumulating a three-dimensional stratigraphy.

The aim of the research was to investigate which features recorded in the foreland basin architecture are diagnostic of the balance and interplay between two main external forcings: repeated tectonic activity and eustatic sea-level variation.

Special attention has been paid to differences in stacking patterns of the depositional systems and the character of the sequence-bounding unconformities. Throughout the chapters of this thesis, the complexity of the tectono-sedimentary foreland configuration was stepwise increased, from a linear thrust front to a segmented foreland containing a thrust-sheet top basin, while the intensity and frequency of tectonic activity and sea-level variation remained similar. The general conclusions resulting from the numerical simulations in this thesis are presented in this chapter.

### 6.1 Drainage basins

The aspect ratios of modelled drainage basins on an actively deforming fault–bend fold and the consequent spacing between alluvial fans approximate those of natural basins along linear mountain fronts. This resemblance is the result of the steepest-descent cellular routing scheme that dominates the catchments during active erosion and which leads to convergent drainage patterns. The experiments described in Chapter 2 also indicate that this spacing is not just a static characteristic, but is influenced by change of the tectonic displacement rate and to a lesser degree by bedrock erodability.

Higher erodability of the bedrock substratum results in a more rapid and elaborate sideways drainage network development, and increased synchronization of the catchments yield curves during the interval of tectonic activity (Figures 2.6 and 2.12). Directly after cessation of tectonic activity, catchments with higher erodability are more mature and closely spaced. During subsequent quiescence, drainage basins strive to a comparable configuration (Figure 2.6).

Tectonic displacement rate is the more important factor influencing the spacing. Rapid propagation of the thrust-tip onto the foreland leads to ponding of hinterland drainage and results in larger fan spacing (Figure 2.7).

## 6.2 Alluvial fans

The sediment yield generated by fluvial bedrock erosion in the drainage basins has the typically asymmetrical shape of a response curve (Figures 2.12 and 3.6). Yield gradually increases during tectonic activity, and declines exponentially during tectonic quiescence. Syn-tectonic yields are increasing, but they are not sufficient to completely fill the accommodation space created in the adjacent foreland basin due to flexural response upon active tectonic thrust loading. As a result and counter-intuitively, deposition of alluvial fan gravels in the foreland basin retreats during tectonic activity, whereas progradation is characteristic of phases of tectonic quiescence and reduced flexural subsidence. A history of pulsating tectonic activity is reflected in the alluvial architecture of the basin as a succession of coarsening-up, prograding gravel sheets that laterally connect during quiescence, and alternate with basin-wide onlap of fine-grained sediments marking renewed tectonic activity (Figures 2.11 and 3.10).

## 6.3 Axial fluvio-deltaic system

Alternating phases of tectonic activity and resulting variations in accommodation space are reflected in the sequences deposited by axial fluvio-deltaic systems in the foreland basin model (Figure 3.9). Here, progradation is also characteristic of tectonic quiescence with the difference that the progradation of the axial system upon reduction of accommodation space is a factor 10 faster than that of the alluvial fans. As a consequence, the axial system first occupies the zone around the basin margin fans during transition from activity to quiescence, followed by a delayed progradation and offlap of the alluvial fans over the axial-fluvial sediments (Figures 3.10 and 3.11)

During renewed tectonic activity (and subsidence) the basin is rapidly flooded within a few kyrs. The transgression encroaches the alluvial plain in the area, close to the thrust front, now characterized by maximal flexural subsidence. Therefore, the best time marker for the onset of tectonic activity is the fine-grained, marine onlap found here. The retreating syn-tectonic axial system takes the form of a conical delta surface constructed by bifurcating channel belts that swiftly relocate in response to the rise in relative sea level (Figure 3.7).

The model experiments of Chapter 3 show that there are two contrasting types of sequence boundaries developed in the alluvial stratigraphy when an eustatic sea-level variation is superposed upon the alternation of tectonic activity and subsidence (Figures 3.9, 3.10 and 3.11).

A) During intervals of tectonic activity, eustatic fall and rise of sea level form prograding, shallowing-up sequences, which are bounded by Type-2 unconformities and subsequent flooding surfaces. The syn-tectonic, high flexural subsidence rates prohibit the sea level to drop below the delta break in slope, safeguarding the stratigraphy from severe incision.

B) During intervals of tectonic quiescence, Type-1 unconformities are formed, because eustatic falls now drop below the delta break in slope, as they are no longer compensated by the subsidence component in relative sea level. Because multiple eustatic sea-level cycles may occur during a quiescence interval, the resulting Type-1 unconformity at the base of the delta-top sheet sandstone can be a composite and therefore poor time marker.

The suites of amalgamating, axial channel belts that characterise this delta top sheet sandstone have a preference for the depression between the basin-margin alluvial fans and the conical delta surface that was formed during a previous tectonic phase (Figure 3.12).

Similar suites of amalgamating axial channel belts are created when the foreland basin is detached from its substratum by a hinterland-dipping sole thrust and transformed into a thrust-sheet top basin (Figures 4.5 and 4.6). In contrast to channel belts in the asymmetrical foreland basin of Chapter 3, the belts in this configuration show no clear preference for a location close to the thrust-fault front. This is because the translation of the basin over the detachment fault causes equal uplift along the entire width of the basin. The experiments show that displacement over low-angle faults ( $2\sim 6^\circ$ ) with moderate rates ( $\sim 5.0$  m/kyr) results in a vertical uplift component sufficient to counteract the background flexural subsidence rate. Consequently, the evolution of accommodation space and therefore the basin architecture are extremely sensitive to the dip angle of the detachment fault. The interconnectedness of the channel belts, the rate of the tectonically forced regression, the sensitivity to incised valley formation and bypass of sediment to adjacent basins increases with the dip angle of the detachment fault. In the light of these model results the Eocene Castissent Formation in the Pyrenean Tresp Basin, previously interpreted as a classical incised valley system (Marzo *et al.*, 1988) or highstand sequence (Nijman, 1998), is explained as a phase of moderate tectonic reduction of the accommodation space. This mechanism explains the continuous marine influence on the delta plain simultaneous with a forced regression and increased sandstone interconnectedness at the cost of fine-grained intervals.



## References

- Aigner, T., Doyle, M. and Lawrence, D.T.** 1989. Quantitative Modelling of Carbonate Platforms: Some Examples. In: *Controls on carbonate platform and basin development* (Ed J. Read), *Society of Economic Paleontologists and Mineralogists Special Publication*, **44**, pp. 27-37.
- Alexander, J. and Leeder, M.R.** 1987. Active tectonic control on alluvial architecture. *Recent developments in fluvial sedimentology: Society of Economic Paleontologists and Mineralogists Special Publication*, **39**: 245-252.
- Allen, J.R.L.** 1965. A review of the origin and characteristics of recent alluvial sediments. *Sedimentology*, **5**: 89-191.
- Allen, P.A. and Densmore, A.L.** 2000. Sediment flux from an uplifting fault block. *Basin Research*, **12**: 367-380.
- Anderson, D.S. and Cross, T.A.** 2001. Large-scale cycle architecture in continental strata, Hornelen basin (Devonian), Norway. *Journal of Sedimentary Research*, **71**: 225-271.
- Anderson, R.S. and Humprey, N.F.** 1990. Interaction of weathering and transport processes in the evolution of arid landscape. In: *Quantitative Dynamic Stratigraphy* (Ed T.A. Cross), pp. 349-361. Prentice-Hall, Englewood Cliffs.
- Ardevol, L., Klimowitz, J., Malagon, J. and Nagtegaal, P.J.C.** 2000. Depositional Sequence Response to Foreland Deformation in the Upper Cretaceous of the Southern Pyrenees, Spain. *American Association of Petroleum Geologists Bulletin*, **84**: 566-587.
- Bagirov, E. and Lerche, I.** 1999. Probability and sensitivity analysis of two-dimensional modelling results. In: *Numerical Experiments in Stratigraphy: Recent Advances in Stratigraphic and Sedimentological Computer Simulations* (Ed R.H. Goldstein), *Society for Sedimentary Geology Special Publication*, **62**, pp. 35-68.
- Bagnold, R.A.** 1980. An empirical correlation of bedload transport rates in flumes and natural rivers. *Proceedings of the Royal Society*, **372A**: 453-473.
- Baltzer, F. and Purser, B.H.** 1990. Modern alluvial fan and deltaic sedimentation in a foreland tectonic setting: the Lower Mesopotamian Plain and Arabian Gulf. *Sedimentary Geology*, **67**: 175-197.
- Barrel, J.** 1917. Rhythms and the measurement of Geologic time. *Geological Society of America Bulletin*, **28**: 745-904.
- Beck, R.A. and Vondra, C.F.** 1985. *Syntectonic sedimentation and Laramide basement thrusting*. Abstracts, International Symposium on Foreland Basins, Fribourg, Switzerland, 36 pp.
- Beer, J.A., Allmendinger, R.W., Figueroa, D.E. and Jordan, T.E.** 1990. Seismic stratigraphy of a neogene piggyback basin, Argentina. *American Association of Petroleum Geologists*, **74**: 1183-1202.
- Bentham, P. and Burbank, D.W.** 1996. Chronology of the Eocene Foreland Basin Evolution Along the Western Oblique Margin of the South-Central Pyrenees. In: *Tertiary basins of Spain, the stratigraphic record of Crustal Kinematics* (Ed C.J. Dabrio), pp. 144-152. Cambridge University Press, Cambridge.
- Bentham, P.A., Burbank, D.W. and Puigdefabregas, C.** 1992. Temporal and spatial controls on the alluvial architecture of an axial drainage system: late Escanilla Formation, southern Pyrenean Foreland Basin, Spain. *Basin Research*, **4**: 335-352.
- Bernal, A. and Hardy, S.** 2002. Syn-tectonic sedimentation associated with three-dimensional fault-bend fold structures. *Journal of Structural Geology*, **24**: 609-635.
- Bezemer, T.** 1998. *Numerical modelling of fault-related sedimentation*. Ph.D. Thesis, Vrije Universiteit, Amsterdam, Amsterdam, 161 pp.
- Bhattacharya, J.** 1991. Regional to sub-regional facies architecture of river-dominated deltas, Upper Cretaceous Dunvegan Formation, Alberta sub-surface. In: *The Three-dimensional Facies Architecture of Terrigenous Clastic sediments and its implications for Hydrocarbon Discovery and Recovery* (Ed N. Tyler), *Special Publication of the Society for Sedimentary Geology, "Concepts and Models in Sedimentology and Paleontology"*, **3**, pp. 189-206.
- Bierman, P.R.** 1994. Using in situ produced cosmogenic isotopes to estimate rates of landscape erosion, a review from the geomorphic perspective. *Journal of Geophysical Research*, **99**: 13885-13896.
- Bitzer, K. and Plug, R.** 1989. DEPO3D: A three-dimensional Model for Simulating Clastic sedimentation and Isostatic Compensation in Sedimentary basins. In: *Quantitative Dynamic Stratigraphy* (Ed T.A. Cross), pp. 335-348. Prentice Hall, Englewood Cliffs, New Jersey.
- Blair, T.C.** 1999. Alluvial fan and catchment initiation by rock avalanching, Owens Valley, California. *Geomorphology*, **28**: 201-221.
- Blair, T.C. and Bildeau, W.** 1988. Development of tectonic cyclothems in rift pull-apart and foreland basins: sedimentary response to episodic tectonism. *Geology*, **16**: 517-520.
- Blair, T.C. and McPherson, J.G.** 1994a. Alluvial fan processes and forms. In: *Geomorphology of desert environments* (Ed A.J. Parsons), pp. 354-402. Chapman and Hall, London.
- Blair, T.C. and McPherson, J.G.** 1994b. Alluvial fans and their distinction from rivers based on morphology, hydraulic processes, and facies assemblages. *Journal of Sedimentary Research*, **A64**: 450-489.
- Bornholdt, S., Nordlund, U. and Westphal, H.** 1999. Inverse stratigraphic modelling using genetic algorithms. In: *Numerical Experiments in Stratigraphy: Recent Advances in Stratigraphic and Sedimentological Computer Simulations* (Ed R.H. Goldstein), *Society for Sedimentary Geology Special Publication*, **62**, pp. 85-90.

- Boscher, H. and Schlager, W.** 1992. Computer simulation of reef growth. *Sedimentology*, **39**: 503-512.
- Bowman, S.A. and Vail, P.R.** 1999. Interpreting the stratigraphy of the Baltimore Canyon section, offshore New Jersey with PHIL, a stratigraphic simulator. In: *Numerical Experiments in Stratigraphy: Recent Advances in Stratigraphic and Sedimentological Computer Simulations* (Ed R.H. Goldstein), *Society for Sedimentary Geology Special Publication*, **62**, pp. 117-138.
- Braun, J. and Sambridge, M.** 1997. Modelling landscape evolution on geological timescales: a new method based on irregular spatial discretization. *Basin Research*, **9**: 27-52.
- Bridge, J.S.** 1979. A FORTRAN IV program to simulate alluvial stratigraphy. *Computers and Geosciences*, **5**: 335-348.
- Brozovic, N. and Burbank, D.W.** 2000. Dynamic fluvial systems and gravel progradation in the Himalayan foreland. *GSA Bulletin*, **112**: 394-412.
- Bryant, M., Falk, P. and Paola, C.** 1995. Experimental study of avulsion frequency and rate of deposition. *Geology*, **23**: 365-368.
- Bull, W.B.** 1977. The Alluvial Fan environment. *Progress in Physical Geography*, **1**: 222-270.
- Burbank, D.W.** 1992. Causes of recent Himalayan uplift, deduced from the depositional patterns in the Ganges basin. *Nature*, **357**: 680-682.
- Burbank, D.W., Meigs, A. and Brozovic, N.** 1996. Interactions of growing folds and coeval depositional systems. *Basin Research*, **8**: 199-223.
- Burbank, D.W. and Reynolds, R.G.H.** 1988. Stratigraphic keys to the timing of thrusting in terrestrial foreland basins: Applications to the Northwestern Himalaya. In: *New Perspectives in Basin Analysis* (Ed C. Paola), pp. 331-351. Springer Verlag, New York.
- Burbank, D.W., Verges, J., Muñoz, J.A. and Bentham, P.** 1992. Coeval hindward- and forward imbricating thrusting in the south-central Pyrenees, Spain: Timing and rates of shortening and deposition. *Geological Society of America Bulletin*, **104**: 3-17.
- Burgess, P.M. and Hovius, N.** 1998. Rates of delta progradation during highstands: consequences for the timing of deposition in deep-marine systems. *Journal of the Geological Society of London*, **155**: 217-222.
- Burgess, P.M., Wright, V.P. and Emery, D.** 2001. Numerical forward modelling of peritidal carbonate parasequences development: implications for outcrop interpretation. *Basin Research*, **13**: 1-16.
- Burns, B.A., Heller, P.L., Marzo, M. and Paola, C.** 1997. Fluvial response in a sequence stratigraphic framework: Example from the Montserrat fan-delta, Spain. *Journal of Sedimentary Research*, **67**: 310-320.
- Burrough, P.A. and McDonnell, R.A.** 1998. *Principles of Geographical Information Systems*. Oxford University Press, Oxford, 346 pp.
- Butler, R.W.H. and Grasso, M.** 1993. Tectonic controls on base level variations and depositional sequences within thrust-top and foredeep basins: examples from the Neogene thrust belt of central Sicily. *Basin Research*, **5**: 137-151.
- Cant, D.J.** 1991. Geometric modelling of facies migration: theoretical development of facies succession on local unconformities. *Basin Research*, **3**: 51-62.
- Carle, S.F., Labolle, E.M., Weissmann, G.S., van Brocklin, D. and Fogg, G.E.** 1998. Conditional simulation of hydrofacies architecture: a transition probability/Markov approach. In: *Hydrogeological models of Sedimentary Aquifers: Concepts in Hydrogeology and Environmental Geology* (Ed J.M. Davis), *Society for Sedimentary Geology Special Publication*, **1**, pp. 147-170.
- Chaleron, E. and Mugnier, J.-L.** 1993. Sequence de propagation des failles dans un prisme d'accrétion: une modélisation numérique. *Bulletin Société Géologique de France*, **164**.
- Chase, C.G.** 1992. Fluvial land sculpting and the fractal dimension of topography. *Geomorphology*, **5**: 39-57.
- Chen, W.S., Ridgway, K.D., Horng, C.S., Chen, Y.G., Shea, K.S. and Yeh, M.G.** 2001. Stratigraphic architecture, magnetostratigraphy and incised-valley systems of the Pliocene-Pleistocene collisional marine foreland basin of Taiwan. *Geological Society of America Bulletin*, **113**: 1249-1271.
- Clements, R., Hurst, A.R., Knarud, R. and Omre, H.** 1990. A computer program for evaluation of fluvial reservoirs. In: *North Sea oil and gas reservoirs -II* (Ed J.O. Aasen), pp. 373-385. Graham and Trotman, London.
- Colman, S.M. and Watson, K.** 1983. Ages estimated from a diffusion equation model for scarp degradation. *Science*, **221**: 263-265.
- Coulthard, T.J., Kirby, M.J. and Macklin, M.G.** 1999. Modelling the impacts of Holocene environmental change on the fluvial and hillslope morphology of an upland landscape, using a cellular automaton approach. In: *Fluvial processes and environmental change* (Ed T.M. Quine), pp. 31-46. Wiley and Sons, Chichester.
- Coulthard, T.J., Macklin, M.G. and Kirkby, M.J.** 2002. A cellular model of Holocene upland river basin and alluvial fan evolution. *Earth Surface Processes and Landforms*, **27**: 269-288.
- Covey, M.** 1986. The evolution of foreland basins to steady state: evidence from the western Taiwan foreland basin. In: *Foreland Basins* (Ed G.P. Allen), *Special Publication of the International Association of Sedimentologists*, **8**, pp. 77-90.
- Cowell, P.J., Roy, P.S. and Jones, R.A.** 1995. Simulation of large-scale coastal change using a morphological behaviour model. *Marine Geology*, **126**: 45-61.
- Crave, A. and Davy, P.** 2001. A stochastic "precipitation" model for simulating erosion/sedimentation dynamics. *Computers and Geosciences*, **27**: 815-827.

- Cross, T.A. and Harbaugh, J.W.** 1990. Quantitative Dynamic Stratigraphy: A Workshop, A Philosophy, A Methodology. In: *Quantitative Dynamic Stratigraphy* (Ed T.A. Cross), pp. 3-20. Prentice Hall.
- Cross, T.A. and Lessenger, M.A.** 1999. Construction and application of a stratigraphic inverse model. In: *Numerical Experiments in Stratigraphy: Recent Advances in Stratigraphic and Sedimentological Computer Simulations* (Ed R.H. Goldstein), *Society for Sedimentary Geology Special Publication*, pp. 69-83.
- Davis, W.M.** 1912. *Die erklärende beschreibung der Landformen*. B.G. Teubner, Leipzig, 565 pp.
- De Chant, L.J., Pease, P.P. and Tchakerian, V.P.** 1999. Modelling alluvial fan morphology. *Earth Surface Processes and Landforms*, **24**: 641-652.
- DeCelles, P.G., Gray, M.B., Ridgway, K.D. and Cole, R.B.** 1991a. Kinematic history of foreland uplift from Paleocene synorogenic conglomerate, Beartooth Range, Wyoming and Montana. *Geological Society of America Bulletin*, **103**: 1458-1475.
- Demicco, R.V.** 1998. Cyclopath 2D - A two-dimensional, forward model of cyclic sedimentation on carbonate platforms. *Computers and Geosciences*, **24**: 405-423.
- Den Bezemer, T., Kooi, H., Podlachikov, Y. and Cloetingh, S.** 1998. Numerical modelling of growth strata and grain-size distributions associated with fault-bend folding. In: *Cenozoic Foreland Basins of Western Europe* (Ed M. Fernandez), *Special Publication of the Geological Society*, **134**, pp. 381-401.
- Densmore, A.L., Ellis, M.A. and Anderson, R.S.** 1998. Landsliding and the evolution of normal fault bounded mountains. *Journal of Geophysical Research*, **103**: 15203-15219.
- Desegaulx, P., Kooi, H. and Cloetingh, S.** 1991. Consequences of foreland basin development on thinned continental lithosphere: Application to the Aquitaine basin (SW France). *Earth Planetary Science Letters*, **106**: 116-132.
- Deutsch, C.V. and Journel, A.G.** 1997. *GSLIB geostatistical software library and user's guide*. Oxford University Press, New York, 384 pp.
- Dickinson, W.R.** 1974. Plate tectonics and sedimentation. In: *Tectonics and Sedimentation* (Ed W.R. Dickinson), *Special Publication of the Society of Economic Paleontologists and Mineralogists (SEPM)*, **22**, pp. 1-27.
- Doligez, B., Granjeon, D., Joseph, P., Escard, R. and Beucher, H.** 1999. How can stratigraphic modelling help constrain geostatistical reservoir simulations. In: *Numerical Experiments in Stratigraphy: Recent Advances in Stratigraphic and Sedimentological Computer Simulations* (Ed R.H. Goldstein), *Society for Sedimentary Geology Special Publication*, **62**, pp. 239-244.
- Dreyer, T.** 1993. Quantified fluvial architecture in ephemeral stream deposits of the Esplugafreda Formation (Paleocene), Tremp-Graus basin, northern Spain. In: *Alluvial Sedimentation* (Ed C. Puigdefabregas), *International Association of Sedimentologists Special Publication*, **17**, pp. 337-362.
- Dreyer, T., Corregidor, J., Arbues, P. and Puigdefabregas, C.** 1999. Architecture of the tectonically influenced Sobrarbe deltaic complex in the Ainsa Basin, northern Spain. *Sedimentary Geology*, **127**: 127-169.
- Dreyer, T. and Falt, L.M.** 1993. Sedimentary architecture of field analogues for reservoir modelling (SAFARI): a case study of the fluvial Escanillia Formation, Spanish Pyrenees. In: *The Geological Modelling of hydrocarbon reservoirs and outcrop analogues*, *Special Publication of the International Association of Sedimentologists*, **17**, pp. 57-80.
- Dubrule, O.** 1989. A review of stochastic models for petroleum reservoirs. In: *Geostatistics* (Ed M. Armstrong), **2**, pp. 493-506. Kluwer Academic Publishers, Dordrecht, Netherlands.
- Ellis, M.A., Densmore, A.L. and Anderson, R.S.** 1999. Development of mountainous topography in the Basin Ranges, USA. *Basin Research*, **11**: 21-41.
- Emery, D. and Myers, K.J.** 1996. *Sequence Stratigraphy*. Blackwell Science, Oxford, 297 pp.
- Erslev, E.A.** 1991. Trishear fault-propagation folding. *Geology*, **19**: 617-620.
- Flemings, P.B. and Grotzinger, J.P.** 1996. STRATA: Freeware for analysing stratigraphic problems. *GSA Today*, **12**: 1-7.
- Flemings, P.B. and Jordan, T.E.** 1990. Stratigraphic modelling of foreland basins: Interpreting thrust deformation and lithosphere rheology. *Geology*, **18**: 430-434.
- Forman, S.L.** 1990. Post-glacial relative sea level history of northwestern Spitsbergen. *Geological Society of America Bulletin*, **102**: 1580-1590.
- Fortune, S.** 1995. *Voronoi Diagrams and Delauney Triangulations*. Computing in Euclidan Geometry. World Scientific, Singapore, 225-265 pp.
- Fraser, G.A. and DeCelles, P.G.** 1992. Geomorphic controls on sediment accumulation at margins of foreland basins. *Basin Research*, **4**: 233-252.
- Freeman, G.T.** 1991. Calculating catchment area with divergent flow based on a rectangular grid. *Computers and Geosciences*, **17**: 413-422.
- Friend, P.F., Marzo, M., Nijman, W. and Puigdefabregas, C.** 1981. Fluvial sedimentology in the Tertiary South Pyrenean and Ebro basins. In: *Field guide to the Modern Ancient Fluvial systems in Britain and Spain* (Ed T. Elliot), pp. 4.1-4.50, Keele University.
- Galloway, W.E.** 1989. Genetic stratigraphic sequences in basin analysis; architecture and genesis of flooding surfaces bounded depositional units. *American Association of Petroleum Geologists Bulletin*, **73**: 125-142.
- Garcia-Castellanos, D.** 2002. Interplay between lithospheric flexure and river transport in foreland basins. *Basin Research*, **14**: 89-104.

- Garcia-Castellanos, D., Fernandez, M. and Torne, M.** 1997. Numerical modelling of foreland basin formation: a program relating thrusting, flexure, sediment geometry and lithosphere rheology. *Computers and Geosciences*, **23**: 993-1003.
- Gasparini, N.M., Tucker, G.E. and Bras, R.L.** 1999. Downstream fining through selective particle sorting in an equilibrium drainage network. *Geology*, **27**: 1079-1082.
- Gawthorpe, R.L., Hall, M., Sharp, I. and Dreyer, T.** 2000. Tectonically enhanced forced regressions: examples from growth folds in extensional and compressional settings, the Miocene of the Suez rift and the Eocene of the Pyrenees. In: *Sedimentary Responses to Forced Regressions* (Ed D. Hunt), *Special Publication of the Geological Society of London*, **172**, pp. 177-191.
- Gawthorpe, R.L. and Hardy, S.** 2002. Extensional fault-propagation folding and base-level change as controls on growth strata geometries. *Sedimentary Geology*, **146**: 47-56.
- Geddes, A.** 1960. The alluvial morphology of the Indo-Gangetic plain, Its mapping and geographical significance. *Institute of British Geographers, Transactions and Papers*, **28**: 253-276.
- Gomez, B., and Church, M.** 1989. An assesment of bedload sediment transport formulae for gravel rivers. *Water Resources Research*, **25**: 1161-1186.
- Gomez, B. and Sims, P.C.** 1981. Temporal variations in bedload transport rates: the effect of progressive bed armouring. *Earth Surface Processes and Landforms*, **8**: 41-54.
- Goodchild, M.F. and Mark, D.M.** 1987. The fractal nature of geographic phenomena. *Annales of Association of American Geographers*, **77**: 265-278.
- Granjeon, D. and Joseph, P.** 1999. Concepts and applications of a 3-D multiple lithology, diffusive model in stratigraphic modelling. In: *Numerical Experiments in Stratigraphy: Recent Advances in Stratigraphic and Sedimentological Computer Simulations* (Ed R.H. Goldstein), *Society for Sedimentary Geology Special Publication*, **62**, pp. 197-210.
- Griffiths, C.M., Dyt, C., Paraschivoiu, E. and Liu, K.** 2001. SEDSIM in hydrocarbon exploration. In: *Geological Modeling and Simulation: Sedimentary Systems* (Ed J.C. Davis), pp. 71-117.
- Gupta, S.** 1997. Himalayan drainage patterns and the origin of fluvial megafans in the Ganges foreland basin. *Geology*, **25**: 11-14.
- Hack, J.T.** 1957. Studies of longitudinal stream profiles in Virginia and Maryland. *USGS Professional paper*, **294-B**.
- Hardy, S. and Poblet, J.** 1995. The velocity description of deformation. Paper 2: Sediment geometries and fault-bend folding. *Marine and Petroleum Geology*, **12**: 165-176.
- Hardy, S., Poblet, J., McClay, K.R. and Waltham, D.** 1996. Mathematical modelling of growth strata associated with fault-related fold structures. In: *Buchanan, P.G. Nieuwland, D.A., Geological Society of London Special Publication*, **99**, pp. 265-282.
- Harvey, A.M.** 1997. The role of alluvial fans in arid zone fluvial systems. In: *Arid zone geomorphology* (Ed D.S.G. Thomas), pp. 231-259. Wiley, Chichester.
- Haupt, B.J., Seidov, D. and Statteger, K.** 1999. SEDLOB and PATLOB: Two numerical tools for modelling climatically forced sediment and water volume transport in large ocean basins. In: *Computerized Modelling of Sedimentary Systems* (Ed Statteger), pp. 115-147.
- Heimsath, A.M., Dietrich, W.E., Nishiizumi, K. and Finkel, R.C.** 1997. The soil production function and landscape equilibrium. *Nature*, **388**: 358-361.
- Helland-Hansen, W., Kendal, C.G.S., Lerche, I. and Nakayama, K.** 1988. A simulation of continental basin margin sedimentation in response to crustal movements, eustatic sea-level changes and sediment accumulation rates. *Mathematical Geology*, **20**: 777-802.
- Heller, P.L., Angevine, C.L. and Wilson, N.S.** 1988. Two phase stratigraphic model of foreland basin sequences. *Geology*, **16**: 501-504.
- Heller, P.L., Burns, B.A. and Marzo, M.** 1993. Stratigraphic solution sets for determining the roles of sediment supply, subsidence and sealevel on transgressions and regressions. *Geology*, **21**: 747-750.
- Heller, P.L. and Jones, M.A.** 2001. Time Lag of syntectonic Indicators in Foreland Basin Deposits (abstract). In: *AAPG Annual Meeting*, Denver.
- Hirst, J.P.P. and Nichols, G.J.** 1986. Thrust tectonic controls on Miocene alluvial fan distribution patterns, southern Pyrenees. In: *Foreland Basins: International Association of Sedimentologists Special Publication* (Ed P. Homewood), **8**, pp. 247-258.
- Hockney, R.W. and Eastwood, J.W.** 1981. *Computer simulation using particles*. McGraw-Hill Book Co, New York, 523 pp.
- Hodgetts, D., Egan, S.S. and Williams, G.D.** 1998. Flexural modelling of continental lithosphere deformation: A comparison of 2D and 3D techniques. *Tectonophysics*, **294**: 1-20.
- Hogan, P.J. and Burbank, D.W.** 1996. Evolution of the Jaca Piggyback Basin and Emergence of the External Sierra, Southern Pyrenees. In: *Tertiary Basins of Spain, the Stratigraphic Record of Crustal Kinematics* (Ed C.J. Dabrio), pp. 153-160. Cambridge University Press, Cambridge.
- Holl, J.E. and Anastasio, D.J.** 1995. Kinematics around large-scale oblique ramp, southern Pyrenees, Spain. *Tectonics*, **14**: 1368-1379.



- Hooke, R.L.** 1968. Steady state relationships on arid-region alluvial fans in closed basins. *American Journal of Science*, **266**: 609-629.
- Horton, B.K. and DeCelles, P.G.** 2001. Modern and ancient fluvial megafans in the foreland basin system of the central Andes, southern Bolivia: implications for drainage network evolution in fold-thrust belts. *Basin Research*, **13**: 43-63.
- Horton, R.E.** 1945. Erosional development of streams and their drainage basins; hydrophysical approach to quantitative morphology. *Geological Society of America Bulletin*, **56**: 275-370.
- Houston, W.S., Huntoon, J.E. and Kamola, D.L.** 2000. Modelling of Cretaceous foreland-basin parasequences, Utah, with implications for timing of Sevier thrusting. *Geology*, **28**: 267-270.
- Hovius, N.** 1996. Regular spacing of drainage outlets from linear mountain belts. *Basin Research*, **8**: 29-44.
- Hovius, N., Stark, C.P. and Allen, P.A.** 1997. Sediment flux from a mountain belt derived by landslide mapping. *Geology*, **25**: 231-234.
- Howard, A.D.** 1994. A detachment limited model of drainage basin evolution. *Water Resources Research*, **30**: 739-752.
- Howard, A.D.** 1996. Modelling channel evolution and floodplain morphology. In: *Floodplain processes*, pp. 15-62. John Wiley and Sons, New York.
- Howard, A.D., Dietrich, W.E. and Seidl, M.A.** 1994. Modeling fluvial erosion on regional to continental scales. *Journal of Geophysical Research*, **99**: 19971-13986.
- Howard, A.D. and Kerby, G.** 1983. Channel changes in badlands. *Geological Society of America Bulletin*, **94**: 739-752.
- Humphrey, N.F. and Heller, P.L.** 1995. Natural oscillations in coupled geomorphic systems: an alternative origin for cyclic sedimentation. *Geology*, **23**: 499-502.
- Hutchinson, M.F.** 1989. A new procedure for gridding elevation and streamline data with automatic removal of spurious pits. *Journal of Hydrology*, **106**: 211-232.
- Huyghe, P., J.-L., M., Griboulard, R., Deniaud, Y., Gonthier, E. and Faugeres, J.-C.** 1999. Review of the tectonic control and sedimentary pattern in late Neogene Piggyback Basins on the Barbados Ridge Complex. In: *Sedimentary basins of the world* (Ed P. Mann), **4**, pp. 367-386.
- Ikeda, S., Parker, G. and Sawai, K.** 1981. Bend theory of river meanders. Part 1. Linear development. *Journal of Fluid Mechanics*, **112**: 363-377.
- Jervey, M.T.** 1988. Quantitative geological modelling of siliciclastic rock sequences and their seismic expression. In: *Sea-level changes, an integrated approach* (Ed J.C. Van Wagoner), *Society for Sedimentary Geology Special Publication*, **42**, pp. 47-69.
- Jin, J., Aigner, T., Bachman, G.H., Luterbacher, H.P. and Muller, M.** 1995. Sequence stratigraphy and depositional history in the south-eastern German Molasse Basin. *Marine and Petroleum Geology*, **12**: 929-940.
- Johnson, D. and Beaumont, C.** 1995. Preliminary results from a planform kinematic model of orogen evolution, surface processes and the development of clastic foreland basin stratigraphy. In: *Stratigraphic Evolution of Foreland Basins* (Ed G. Ross), *Society for Sedimentary Geology Special Publication*, **52**, pp. 3-24.
- Jones, P.B. and Linsser, H.** 1986. Computer synthesis of balanced cross-sections by forward modelling (abstract). *American Association of Petroleum Geologist Bulletin*, **70**: 605.
- Jordan, T.E. and Flemings, P.B.** 1991. Large-Scale Stratigraphic Architecture, Eustatic Variation, and Unsteady Tectonism: A Theoretical Evaluation. *Journal of Geophysical Research*, **96**: 6681-6699.
- Kamola, D.L. and Huntoon, J.E.** 1995. Repetitive stratal patterns in a foreland basin sandstone and their possible tectonic significance. *Geology*, **23**: 177-180.
- Karner, G.D.** 1982. Spectral representation of isostatic models. *BMR Journal Australian Geology and Geophysics*, **7**: 55-62.
- Karssenbergh, D.** 2002. *Building dynamic spatial environmental models*. Ph.D Thesis, Utrecht University, Utrecht, 222 pp.
- Karssenbergh, D., Tornqvist, T. and Bridge, J.S.** 2001. Conditioning a process-based model of sedimentary architecture to well data. *Journal of Sedimentary Research*, **71**: 868-879.
- Kaufman, P., Grotzinger, J.P. and McCormick, D.S.** 1991. Depth-dependent diffusion algorithm for simulation of shallow marine depositional systems. In: *Sedimentary modelling: computer simulations and methods for improved parameter definitions* (Ed W. Ross), *Kansas Geological Survey Bulletin*, **233**, pp. 489-508.
- Kenyon, P.M. and Turcotte, D.L.** 1985. Morphology of delta prograding by bulk sediment transport. *Geological Society of America Bulletin*, **84**: 1457-1465.
- Kirkby, E. and Whipple, K.X.** 2001. Quantifying differential rock-uplift rates via stream profile analysis. *Geology*, **29**: 415-418.
- Kirkby, M.J.** 1992. An erosion-limited hillslope evolution model. In: *Functional geomorphology: Landform analysis and models* (Ed J. Ploey), *Catena Supplement*, **23**, pp. 157-188.
- Kirky, E., Reiners, P.W., Krol, M.A., Whipple, K.X., Hodges, K.V., Farley, K.A., Tang, W. and Chen, Z.** 2002. Late Cenozoic evolution of the eastern margin of the Tibetan Plateau: Inferences from  $^{40}\text{Ar}/^{39}\text{Ar}$  and (U-Th)/He thermochronology. *Tectonics*, **21**.
- Knighton, D.** 1998. *Fluvial Forms and Processes*. Oxford University Press, London, 383 pp.

- Kooi, H. and Beaumont, C.** 1994. Escarpment evolution on high-elevation rifted margins: insight derived from surface processes model that combines diffusion, advection and reaction. *Journal of Geophysical Research*, **99**: 12191-12209.
- Kraus, M.J. and Middleton, L.T.** 1987. Contrasting architecture of two alluvial suites in different structural settings. In: *Special Publication of the Society of Economic Paleontologists and Mineralogists* (Ed M.D. Harvey), **39**, pp. 253-262, Tulsa.
- Kuenen, P.H.** 1957. Longitudinal filling of oblong sedimentary basins. *Verhandelingen van het Koninklijk Nederlandsch Geologisch - Mijnbouwkundig Genootschap Gedenkboek F.A. Vening Meinesz*, **18**: 189-195.
- Lancaster, S.T.** 1998. *A nonlinear river meander model and its incorporation in a landscape evolution model*. Ph.D., Massachusetts Institute of Technology (MIT), Cambridge, MA, 177 pp.
- Lawrence, D.T., Doyle, M. and Aigner, T.** 1990. Stratigraphic Simulation of Sedimentary Basins. *American Association of Petroleum Geologists Bulletin*, **74**: 273-295.
- Lawton, T.F., and Robinson, R.A.J.** 2003. Implications of Nonmarine Sequence Architecture for Foreland Basin Dynamics, Central and southern Utah. In: *American Association of Petroleum Geologists Annual Meeting, Annual Meeting 2003*, Salt Lake City, Utah.
- Leeder, M.R.** 1999. *Sedimentology and sedimentary basins; from turbulence to tectonics*. Blackwell Science, Oxford, 592 pp.
- Leopold, L.B. and Maddock, T.J.** 1953. *The hydraulic geometry of stream channels and some physiographic implications*. United States Geological Survey Professional Paper, **252**, 57 pp.
- Lessenger, M. and Lerche, I.** 1999. Inverse Modelling. In: *Numerical Experiments in Stratigraphy: Recent Advances in Stratigraphic and Sedimentological Computer Simulations* (Ed R.H. Goldstein), *Society for Sedimentary Geology Special Publication*, **62**, pp. 29-31.
- Lewin, J. and Brewer, P.A.** 2001. Predicting channel patterns. *Geomorphology*, **40**: 329-339.
- Lin, C. and Harbaugh, J.W.** 1984. *Graphic display of two and three-dimensional Markov computer models in geology*. Van Nostrand Reinhold, New York, 180 pp.
- Lopez-Blanco, M., Marzo, M., Burbank, D., Vergez, J., Roca, E., Anadon, P. and Pina, J.** 2000. Tectonic and climatic controls on the development of large foreland fan-deltas: Montserrat and Sant Llorenç de Munt Systems (Middle Eocene, Ebro Basin, NE Spain). *Sedimentary Geology*, **138**: 17-39.
- Lopez-Blanco, M., Marzo, Pina, J.** 2000. Transgressive-regressive sequence hierarchy of foreland fan-delta clastic wedges (Montserrat and Sant Llorenç del Munt, Middle Eocene, Ebro basin, NE Spain). *Sedimentary Geology*, **138**: 41-69.
- Loseth, T.M.** 1999. *Submarine Mass flow sedimentation: Computer Modelling and Basin Fill Stratigraphy*. Lecture Notes in Earth Sciences, **82**. Springer Verlag, Berlin, 156 pp.
- Mackey, S.D. and Bridge, J.S.** 1995. Three-dimensional model of alluvial stratigraphy: theory and application. *Journal of Sedimentary Research*, **B65**: 7-31.
- Marr, J.G., Swenson, J.B., Paola, C. and Voller, V.R.** 2000. A two diffusion model of fluvial stratigraphy in closed depositional basins. *Basin Research*, **12**: 381-398.
- Marzo, M., Nijman, W. and Puigdefabregas, C.** 1988. Architecture of the Castissent fluvial sheet sandstones, Eocene South Pyrenees, Spain. *Sedimentology*, **35**: 719-738.
- Matter, A., Homewood, P., Caron, C., Van Stuyvenberg, J., Weidmann, M. and Winkler, W.** 1980. Flysch and Molasse of central and western Switzerland. In: *Geology of Switzerland, a guide book* (Ed R. Trumphy).
- Meigs, A., Brozovic, N. and Johnson, M.L.** 1999. Steady, balanced rates of uplift and erosion of the Santa Monica Mountains, California. *Basin Research*, **11**: 59-73.
- Meigs, A.J.** 1997. Sequential development of a selected Pyrenean thrust fault. *Journal of Structural Geology*, **19**: 481-502.
- Meijer, X.D.** 2002. Modelling the drainage evolution of a river-shelf system forced by Quaternary glacio-eustasy. *Basin Research*, **14**: 361-379.
- Miall, A.D.** 1981. Alluvial sedimentary basins: tectonic setting and basin architecture. In: *Sedimentation and Tectonics in Alluvial Basins* (Ed A.D. Miall) 23 edn, *Special Paper, Geological Association of Canada*, pp. 1-33, Waterloo, Ontario.
- Milana, J.P. and Ruzycski, L.** 1999. Alluvial-fan slope as a function of sediment transport efficiency. *Journal of Sedimentary Research*, **69**: 553-562.
- Milliman, J.D. and Syvitski, J.P.M.** 1992. Geomorphic/tectonic control of sediment discharge to the oceans: the importance of small mountainous rivers. *Journal of Geology*, **100**: 525-544.
- Molenaar, N. and Martinus, A.W.** 1996. Fossiliferous intervals and sequence boundaries in shallow marine fan-deltaic deposits (Early Eocene, southern Pyrenees, Spain). *Paleogeography, Paleoclimatology, Paleoecology*, **121**: 147-168.
- Morris, R.G. and Sinclair, H.D.** 1997. Exhumation of the Pyrenean Orogen: implications for sediment discharge. *Basin Research*, **101**: 69-85.
- Munoz, J.** 1992. Evolution of a continental collisional belt: ECORS-Pyrenees crustal balanced section. In: *Thrust Tectonics* (Ed K.R. McKlay), pp. 235-246. Chapman and Hall, London.

- Murray, A.B. and Paola, C.** 1997. Properties of a cellular braided-stream model. *Earth Surface Processes and Landforms*, **22**: 1001-1025.
- Mutti, E.** 1985. Turbidite systems and their relation to depositional sequences. In: *Provenance of Arenites* (Ed G.G. Zuffa), pp. 65-93. Reidel Publ. Co.
- Mutti, E., Seguret, M. and Sgavetti, M.** 1988. Sedimentation and deformation in the Tertiary Sequences of the Southern Pyrenees. In: *AAPG Mediterranean Basin Conference, Special Publication of Geology, Parma University*, pp. 153, 51 fig., Field Trip 7.
- Nijman, W.** 1989. The South Pyrenean Tertiary basin configuration reconsidered. *Geodinamica Acta (Paris)*, **3**: 17-42.
- Nijman, W.** 1998. Cyclicity and basin axis shift in a piggyback basin: towards modelling of the Eocene Tresp - Ager Basin, South Pyrenees, Spain. In: *Cenozoic Foreland Basins of Western Europe, Geological Society Special Publication* (Ed M. Fernandez), **134**, pp. 135-162, London.
- North, C.P. and Halliwell, D.I.** 1994. Bias in estimating fractal dimension with the rescaled range (R/S) technique. *Mathematical Geology*, **26**: 531-555.
- Odgaard, J.** 1986. Meander Flow model I: development. *Journal of Hydraulic Engineering*, **112**: 1117-1133.
- Olsen, T., Steel, R., Hogseth, K., Skar, T. and Roe, S.L.** 1995. Sequential architecture in a fluvial succession: sequence stratigraphy in the Upper Cretaceous Mesaverde Group, Price Canyon, Utah. *Journal of Sedimentary Research*, **B65**: 265-280.
- Oreskes, N., Shrader-Frechette, K. and Belitz, K.** 1994. Verification, validation and conformation of numerical models in earth sciences. *Science*, **263**: 641-646.
- Ori, G.G.** 1993. Continental depositional systems of the Quaternary of the Po Plain (northern Italy). *Sedimentary Geology*, **83**: 1-14.
- Ori, G.G. and Friend, P.** 1984. Sedimentary basins formed and carried piggy-back on active thrust sheets. *Geology*, **12**: 475-478.
- Oualine, S.** 1997. *Practical C Programming, Third Edition*. O'Reilly, Cambridge, 428 pp.
- Paola, C., Heller, P.L. and Angevine, C.L.** 1992. The large-scale dynamics of grain size variations in alluvial basins I: Theory. *Basin Research*, **4**: 73-90.
- Peltier, W.R.** 1990. *Glacial isostatic adjustment and relative sealevel change*. National Academy Press, Washington, D.C, p.73-87 pp.
- Peper, T.** 1993. *Tectonic control on the sedimentary record in foreland basins*. PhD-thesis, Free University, Amsterdam, 178 pp.
- Peper, T., Beekman, F. and Cloetingh, S.** 1992. Consequences of thrusting and intraplate stress fluctuations for vertical motions in foreland basins and peripheral areas. *Geophysical Journal International*, **111**: 104-126.
- Peper, T. and de Boer, P.L.** 1995. Intrabasinal thrust-tectonic versus climate control on rhythmicities in the Eocene South Pyrenean Tresp-Graus foreland basin: inferences from forward modelling. *Tectonophysics*, **249**: 93-107.
- Pfiffner, O.A.** 1986. Evolution of the north Alpine foreland basin in the central Alps. In: *Foreland Basins* (Ed P. Homewood), *International Association of Sedimentologists Special Publication*, **8**, pp. 219-229.
- Pickering, K.T., Hiscott, R.N., Kenyon, N.H., Ricci Lucchi, F. and Smith, R.D.A.** 1995. *Atlas of Deep Water Environments: Architectural style in turbidite systems*. Chapman & Hall, 333 pp.
- Pieri, M.** 1983. Three seismic sections through the Po Plain. In: *Seismic expression of structural styles* (Ed. Bally, E.W.), *American Association of Petroleum Geologists Course Note Series* Vol. 3, pp. 3.4.1/ 8-26.
- Playfair, J.** 1802. *Illustrations of the Huttonian Theory of the Earth, Cadel and Davis (London) and Creech (Edinburgh)*. Reprinted in 1964 by the University of Illinois, Dover Publications, New York, 528 pp.
- Plint, A.G., McCarthy, P.J. and Faccini, U.F.** 2001. Nonmarine sequence stratigraphy; updip expression of sequence boundaries and system tracts in a high-resolution framework, Cenomanian Dunvegan Formation, Alberta foreland basin, Canada. *American Association of Petroleum Geologists Bulletin*, **85**: 1967-2001.
- Poblet, J., Muñoz, J.A., Trave, A. and Serra-Kiel, J.** 1998. Quantifying the kinematics of detachment folds using three-dimensional geometry: Application to the mediano anticline (Pyrenees, Spain). *Geological Society of America Bulletin*, **110**: 111-125.
- Posamentier, H.W., and Allen, G.P.** 1999. Siliciclastic sequence stratigraphic-concepts and applications, *SEPM Concepts in Sedimentology and Paleontology*, **7**, pp. 210.
- Posamentier, H.W. and Vail, P.R.** 1988. Eustatic controls on clastic deposition I - sequence and system tracts models. In: *Sea-level Changes: An Integrated Approach* 42 edn, *Special Publication, Society of Economic Paleontologists and Mineralogists*, pp. 109-124, Tulsa, USA.
- Postma, G.** 1995. Sea-level changes and the architectural response on coarse-grained delta architecture. In: *Fan Deltas: Depositional styles and controls* (Ed G.J. Orton), *Journal of Sedimentary Geology*, **98**, pp. 3-12.
- Press, W.H., Teukolsky, S.A., William, T.V. and Flannery, B.P.** 1992. *Numerical Recipes in Fortran 77*. Cambridge University Press, Cambridge.
- Price, R.A.** 1973. Large-scale gravitational flow of supracrustal rocks, Southern Canadian Rockies. In: *Gravity and Tectonics* (Ed R. Scholten), pp. 491-502. Wiley and Sons, New York.
- Puigdefabregas, C., Munoz, J.A., and Vergez, J.** 1992. Thrusting and foreland evolution in the southern Pyrenees. In: *Thrust Tectonics* (Ed K.R. McClay), pp. 247-255. Chapman and Hall, London.

- Puigdefabregas, C. and Souquet, P.** 1986. Tectono - sedimentary cycles and depositional sequences of the Mesozoic and Tertiary from the Pyrenees. *Tectonophysics*, **129**: 173-203.
- Quinlan, G.M. and Beaumont, C.** 1984. Appalachian thrusting, lithospheric flexure and the Paleozoic stratigraphy of the eastern Interior of North America. *Canadian Journal of Earth Sciences*, **21**: 973-996.
- Quiquerez, A., Allemand, P. and Dromart, G.** 2000. Dibafill; a 3-D two-lithology diffusive model for basin infilling. *Computers and Geosciences*, **26**: 1029-1042.
- Ramos, E., Busquets, P. and Vergez, J.** 2002. Interplay between longitudinal fluvial and transverse alluvial fan systems and growing thrusts in a piggyback basin (SE Pyrenees). *Sedimentary Geology*, **146**: 105-131.
- Remacha, E., Fernandez, L.P., Meastro, E., Oms, O., Estrada, and Teixell, A.** 1998. The upper Hecho Group turbidites and their vertical evolution to deltas. In: *Field Trip Guidebook of the 15th International Sedimentological Congress* (Ed A.M. Hevia, Soria, A.R), Alicante, Spain.
- Ricci-Lucchi, F.** 1986. The Oligocene to Recent foreland basins of the northern Apennines. In: *Foreland Basins* (Ed P.A. Allen), *Special Publication of the International Association of Sedimentologists*, **8**, pp. 105-139.
- Ritchie, B.D., Hardy, S. and Gawthorpe, R.L.** 1999. Three-dimensional modelling of coarse-grained clastic deposition in sedimentary basins. *Journal of Geophysical Research B, Solid Earth Sciences and Planets*, **104**: 17759-17780.
- Riveneas, J.** 1997. Impact of sediment transport efficiency on large-scale sequence architecture: results from computer simulation. *Basin Research*, **9**: 91-106.
- Riveneas, J.C.** 1992. Application of a dual lithology, depth-dependent diffusion equation in stratigraphic simulation. *Basin Research*, **4**: 133-146.
- Robinson, R.A.J. and Slingerland, R.L.** 1998. Origin of grain-size trends in a foreland basin: the Ponoco Formation of the Central Appalachian basin. *Journal of Sedimentary Research*, **68**: 473-486.
- Rust, B.R. and Koster, E.H.** 1984. Coarse alluvial deposits. In: *Facies Models, Geoscience Canada Reprint Series*, **1**, pp. 53-69.
- Schlager, W.** 1993. Accommodation and supply - a dual control on stratigraphic sequences. *Sedimentary Geology*, **86**: 111-136.
- Schlunegger, F., Jordan, T.E. and Klaper, E.M.** 1997. Controls of erosional denudation in the orogen on foreland basin evolution; the Oligocene central Swiss Molasse basin as an example. *Tectonics*, **16**: 823-840.
- Schmidt, K.M. and Montgomery, D.R.** 1995. Limits to relief. *Science*, **270**: 617-620.
- Schumm, S.A.** 1963. Disparity between present rates of denudation and orogeny. *U.S. Geological Survey Professional Paper 454-HH1-H13*.
- Schumm, S.A.** 1977. *The fluvial system*. John Wiley and Sons, New York, 338 pp.
- Schumm, S.A.** 1981. Evolution and response of the fluvial system: sedimentologic implications. *Society of Economic Paleontologists and Mineralogists Special Publication*, **31**: 19-29.
- Schumm, S.A.** 1998. *To interpret the Earth: Ten Ways to be Wrong*. Cambridge University Press, Cambridge, 133 pp.
- Schwans, P.** 1995. Controls on sequence stacking and fluvial to shallow-marine architecture in a foreland basin. *American Association of Petroleum Geologists Bulletin*, **64**: 55-102.
- Shanley, K.W. and McCabe, P.J.** 1994. Perspectives on the sequence stratigraphy of continental strata. *American Association of Petroleum Geologists Bulletin*, **78**: 544-568.
- Sinclair, H.D., Coackley, D.P., Allen, P.A. and Watts, A.B.** 1991. Simulation of foreland basin stratigraphy using a diffusion model of mountain belt uplift and erosion: an example of the Central Alps, Switzerland. *Tectonics*, **10**: 599-620.
- Sinha, R. and Friend, P.F.** 1994. River systems and their sediment flux, Indo - Gangetic plains, north Bihar, India. *Sedimentology*, **41**: 825-845.
- Slingerland, R.L., Harbaugh, J.W. and Furlong, K.P.** 1993. *Simulating Clastic Sedimentary Basins*. Prentice-Hall, New York, 220 pp.
- Small, E.E., Anderson, R.S., Hancock, G.S. and Finkel, R.C.** 1999. Estimates of regolith production from <sup>10</sup>Be and <sup>26</sup>Al: Evidence for steady state alpine hillslopes. *Geomorphology*, **27**: 131-150.
- Snyder, N.P., Whipple, K.X., Tucker, G.E. and Merritts, D.** 2000. Landscape response to tectonic forcing; DEM analysis of stream profiles in the Medocino Triple Junction region, northern California. *Geol. Soc. Am. Bull.*, **112**: 1250-1263.
- Spangler, M.G. and Handy, R.L.** 1982. *Soil Engineering*. Harper and Row Publishing, New York, 819 pp.
- Steckler, M.S., Reynolds, D.J., Coakley, B.J., Swift, B.A. and Jarrard, R.D.** 1993. Modelling passive margin sequence stratigraphy. In: *Sequence stratigraphy and facies associations* (Ed G.P. Allen), *International Association of Sedimentologists Special Publication*, **18**, pp. 19-41.
- Steel, R.J., Meahle, S., Nilsen, H., Roe, S.L. and Spinnangr, A.** 1977. Coarsening upward cycles in the alluvium of Hornelen Basin (Devonian), Norway: Sedimentary response to tectonic events. *Geological Society of America Bulletin*, **88**: 1124-1134.
- Stock, J.D. and Montgomery, D.R.** 1999. Geologic constraints on bedrock river incision using the streampower law. *Journal of Geophysical Research*, **104**: 4983-4993.

- Stockmal, G.S., Beaumont, C. and Boutilier, R.** 1986. Geodynamic models of convergent tectonics: the transition from rifted margin to overthrust belt and consequences for foreland basin development. *Bulletin American Association of Petroleum Geologists*, **70**: 181-190.
- Storms, J.E.A., Weltje, G.J., van Dijke, J.J., Geel, C.R. and Kroonenberg, S.B.** 2002. Process-response modelling of wave-dominated coastal systems: simulating evolution and stratigraphy on geological time scales. *Journal of Sedimentary Research*, **72**: 226-239.
- Strobel, J., Soewito, F., Kendall, C.G.S., Biswas, G., Bezedk, J. and Cannon, R.** 1989. Interactive (SEDPACK) simulation of clastics and carbonate sediments in shelf to basin settings. *Computers and Geosciences*, **15**: 1279-1290.
- Suppe, J.** 1983. Geometry and kinematics of fault-bend folding. *American Journal of Science*, **283**: 684-721.
- Syvitski, J.P.M. and Daughney, S.** 1992. Delta2: Delta progradation and basin filling. *Computers and Geosciences*, **18/7**: 839-879.
- Syvitski, J.P.M., Skene, K.I., Nicholson, M. and Morehead, M.** 1998. Plume 1.1; deposition of sediment from an alluvial plume. *Computers and Geosciences*, **24**: 159-171.
- Talling, P., Stewart, M.D., Stark, C.P., King, K., Gupta, S., Vincent, S.J. and Wilkin, J.** 1997. Regular spacing of drainage outlets from linear fault blocks. *Basin Research*, **9**: 275-302.
- Talling, P.J.M., Lawton, T.F., Burbank, D.W. and Hobbs, R.S.** 1995. Evolution of latest Cretaceous-Eocene nonmarine deposystems in the Axhandle Piggyback basin of central Utah. *Geological Society of America Bulletin*, **107**: 297-315.
- Tankard, A.J.** 1986. On the depositional response to thrusting and lithospheric flexure: examples from the Appalachian and Rocky Mountain Basins. In: *Foreland Basins* (Ed H. P.), *Special Publication of the International Association of Sedimentologists*, **8**, pp. 369-394.
- Tetzlaff, D. and Harbaugh, J.** 1989. *Simulating clastic sedimentation*. Van Nostrand Reinhold, New York, 202 pp.
- Tetzlaff, D. and Priddy, G.** 2001. Sedimentary process modelling: from academia to industry. In: *Geological Modelling and Simulation: Sedimentary Systems* (Ed J.C. Davis), *Computer Applications in Earth Sciences*, pp. 45-69. Kluwer.
- Tucker, G.E.** 1996a. *Modeling the large-scale interaction of climate, tectonics and topography*. Ph.D. thesis, Pennsylvania State University, University Park, PA.
- Tucker, G.E.** 2003. Drainage basin sensitivity to tectonic and climatic forcing: implications of a stochastic model for the role of entrainment and erosion thresholds. *Earth Surface Processes and Landforms*, **(submitted)**: 48.
- Tucker, G.E., and Bras, R.L.** 2000. A Stochastic Approach to Modelling the Role of Rainfall Variability in Drainage Basin Evolution. *Water Resources Research*, **36**: 1953-1964.
- Tucker, G.E., and Slingerland, R.** 1996b. Predicting sediment flux from fold and thrust belts. *Basin Research*, **8**: 329-350.
- Tucker, G.E., Gasparini, N.M., Bras, R.L. and Lancaster, S.T.** 1999. Modeling Floodplain Dynamics and Stratigraphy: Implications for Geoarcheology. Part II-c, Department of Civil and Environmental Engineering, Massachusetts Institute of Technology, submitted to U.S. Army Corps of Engineers Construction Engineering Research Laboratory, Cambridge, Massachusetts.
- Tucker, G.E., Lancaster, S.T., Gasparini, N.M. and Bras, R.L.** 2002. The Channel-Hillslope Integrated Landscape Development Model (CHILD). In: *Landscape Erosion and Sedimentation Modelling* (Ed W.W. Doe), pp. 349-388. Kluwer Press.
- Turcotte, D.L. and Schubert, G.** 1982. *Geodynamic applications of continuum physics to geological problems*. John Wiley & Sons, New York, 450 pp.
- Tuttle, K.J. and Wendebourg, J.** 1999. Applying sedimentary process simulation to assess the spatial distribution of hydraulic conductivities. In: *Numerical Experiments in Stratigraphy: Recent Advances in Stratigraphic and Sedimentological Computer Simulations* (Ed R.H. Goldstein), *Society for Sedimentary Geology Special Publication*, **62**, pp. 323-336.
- Tyler, K., Henriquez, A., Georgsen, F., Holden, L. and Tjemeland, H.** 1992. A program for 3-D modelling of heterogeneties in a fluvial reservoir. In: *ECMOR III: Proceedings of the third European conference on the mathematics of oil recovery* (Ed C.L. Farmer), pp. 31-40, Delft, The Netherlands.
- van der Beek, P., Chambel, B. and Mugnier, J.L.** 2002. Control of detachment dip on drainage development of active fault-propagation folding. *Geology*, **30**: 471-474.
- van Heijst, M.W.I.M. and Postma, G.** 2001. Fluvial response to sea-level changes; a quantitative analogue experimental approach. *Basin Research*, **13**: 269-292.
- Van Wagoner, J.C., Posamentier, H.W., Mitchum, R.M., Vail, P.R., Sarg, J.F., Loutit, T.S. and Hardenbol, J.** 1988. An overview of the fundamentals of sequence stratigraphy and key definitions. In: *Sea-level changes: an integrated approach* (Ed J.C. Van Wagoner), *Society of Economic Paleontologists and Mineralogists Special Publication*, **42**, pp. 39-45.
- Vergez, J. and Burbank, D.W.** 1996. Eocene-Oligocene Thrusting and basin configuration in the Eastern and Central Pyrenees (Spain). In: *Tertiary Basins of Spain, the Stratigraphic Record of Crustal Kinematics* (Ed C. Dabrio, J.), pp. 120-133. Cambridge University Press, Cambridge.
- Vergez, J., Fernandez, M. and Martinez, A.** 2002. The Pyrenean orogen: pre-, syn-, and post collisional evolution. *Journal of the Virtual Explorer*, **8**: 57-76.

- Wagreich, M.** 2001. A 400-km-long piggyback basin (Upper Aptian-Lower Cenomanian) in the Eastern Alps. *Terra Nova*, **13**: 401-406.
- Waltham, D.** 1992. Mathematical modelling of sedimentary basin processes. *Marine and Petroleum Geology*, **9**: 265-273.
- Warrlich, G.M.D., Waltham, D.A. and Bosence, D.W.J.** 2002. Quantifying the sequence stratigraphy and drowning mechanisms of atolls using a 3-D forward stratigraphic modelling program ( CARBONATE 3D). *Basin Research*, **14**: 379-400.
- Warwick, P.D. and Flores, R.M.** 1987. Evolution of fluvial styles in the Eocene Wasatch Formation, Powder River Basin Wyoming, *Recent developments in fluvial sedimentology: Society of Economic paleontologists and Mineralogists Special Publication*, **39**, pp. 303-310.
- Watney, W.L., Rankey, E.C. and Harbaugh, J.** 1999. Perspectives on stratigraphic simulation models: current approaches and future opportunities. In: *Numerical Experiments in Stratigraphy: Recent Advances in Stratigraphic and Sedimentological Computer Simulations* (Ed R.H. Goldstein), *Society for Sedimentary Geology Special Publication*, **62**, pp. 3-21.
- Watts, A.B.** 2001. *Isostasy and Flexure of the Lithosphere*. Cambridge University Press, Cambridge, 458 pp.
- Webb, E.K.** 1994. Simulating the three-dimensional distribution of sediment units in braided stream deposits. *Journal of Sedimentary Research*, **B64**: 219-231.
- Wees, J.D. and Cloetingh, S.** 1994. A finite-difference technique to incorporate spatial variations in rigidity and planar faults into 3-D models for lithospheric flexure. *Geophysical Journal International*, **117**: 179-195.
- Wells, N.A. and Dorr, J.A.** 1987. A reconnaissance of sedimentation on the Kosi alluvial fan of India. In: *Recent developments in Fluvial Sedimentology* (Ed M.D. Harvey), *Society of Economic Paleontologists and Mineralogists Special Publication*, **39**, pp. 51-62.
- Weltje, G.J., van Ansenwoude, S.O.K.J. and de Boer, P.L.** 1996. High-frequency detrital signals in Eocene fan-delta sandstones of mixed parentage (South-Central Pyrenees, Spain): a reconstruction of chemical weathering in transit. *Journal of Sedimentary Research*, **66**: 119-131.
- Wendebourg, J., and Harbaugh, J.W.** 1997. *Simulating oil entrapment in clastic sequences*. Computer methods in geosciences, **16**. Pergamon Press, Oxford, 199 pp.
- Wendebourg, J. and Harbaugh, J.W.** 1996. Sedimentary process simulation: a new approach for describing petrophysical properties in three dimensions for subsurface flow simulation. In: *Geological modelling and mapping* (Ed F. Merriam), pp. 1-25. Plenum Press, New York.
- Wheeler, H.E.** 1958. Time - Stratigraphy. *Bulletin American Association of Petroleum Geologists*, **42**: 640-655.
- Wheeler, H.E.** 1964. Baselevel, lithosphere surface and time-stratigraphy. *Geological Society of America Bulletin*, **75**: 599-610.
- Whipple, K.X.** 2001. Fluvial landscape response time: How plausible is steady state denudation ? *American Journal of Science*, **301**: 313-325.
- Whipple, K.X., and Tucker, G.E.** 1999. Dynamics of the streampower river incision model: Implications for the height limits of mountain ranges, landscape response timescales, and research needs. *Journal of Geophysical Research*, **104**: 17661-17674.
- Whipple, K.X., Parker, G., Paola, C. and Mohrig, D.** 1998. Channel dynamics, sediment transport, and the slope of alluvial fans: experimental study. *Journal of Geology*, **106**: 677-693.
- Whipple, K.X. and Trayler, C.R.** 1996. Tectonic control on fan size: The importance of spatially variable subsidence rates. *Basin Research*, **8**: 351-366.
- Whipple, K.X. and Tucker, G.E.** 1999. Dynamics of the stream-power river incision model: Implications for the height limits of mountain ranges, landscape response timescales, and research needs. *Journal of Geophysical Research*, **104**: 17661-17674.
- Whipple, K.X. and Tucker, G.E.** 2002. Implications of sediment-flux-dependent river incision models for landscape evolution. *Journal of Geophysical Research*, **107**.
- Wilcock, P.R.** 1998. Two-fraction model of initial sediment motion in gravel bed rivers. *Science*, **280**: 410-412.
- Willgoose, G.R., Bras, R.L. and Rodriguez-Iturbe, I.** 1991. A physically coupled network and hillslope evolution model. *Water Resources Research*, **27**: 1671-1684.
- Yang, C.T.** 1996. *Sediment transport; theory and practice*. McGraw Hill, New York, 396 pp.
- Yoshida, S., Willis, A. and Miall, A.D.** 1996. Tectonic control of nested sequence architecture in the Castlegate Sandstone (Upper Cretaceous), Book Cliffs, Utah. *Journal of Sedimentary Research*, **66**: 737-748.
- Zoetemeijer, R.** 1991. *Tectonic modelling of foreland basins*, Free University, Amsterdam, 148 pp.
- Zoetemeijer, R., Cloetingh, S., Sassi, W. and Roure, F.** 1993. Modelling of a piggyback-basin: record of tectonic evolution. *Tectonophysics*, **226**: 253-269.
- Zweigel, J., Aigner, T. and Luterbacher, H.P.** 1998. Eustatic versus tectonic controls on Alpine foreland fill, sequence stratigraphy and subsidence analysis in the SE German Molasse. In: *Cenozoic Foreland basins in Western Europe* (Ed M. Fernandez), *Geological Society of London Special Publication*, **134**, pp. 299-323, London.

## Samenvatting

Gebergteketens ontstaan als gevolg van plaattektoniek. Delen van de aardkorst botsen tegen elkaar of schuiven onder elkaar waardoor gebergtes als grootschalige kreukelzones worden gevormd. Gebergteketens worden omringd door depressies in de aardkorst, zogenaamde voorlandbekkens. Deze voorlandbekkens ontstaan tegelijk met de gebergteketen door het doorbuigen van de aardkorst onder het gewicht van het zich vormende gebergte. Voorbeelden van voorlandbekkens zijn het zuid-Duitse Molasse Bekken geassocieerd met de Alpen, het Ebro Bekken als gevolg van het ontstaan van de Pyreneeën, de Po Vlakte behorende tot de Apennijnen en het Indo-Ganges Bekken gerelateerd aan de Himalaya.

Voorlandbekkens zijn asymmetrisch in doorsnede en worden gevuld met afbraakmateriaal van het gebergte. Dit afbraakmateriaal (sediment) wordt doorgaans aangevoerd door fluviaatiele puinwaaiers en door parallel aan het gebergte lopende riviersystemen. De hoeveelheid en de korrelgrootte van het sediment worden beïnvloed door de opheffingsgeschiedenis van het gebergte, de erodeerbaarheid van het gesteente en het klimaat.

Deze factoren en ook de daling van het voorlandbekken, sturen de afzetting van dit sediment in het voorland bekken. Verschillen tussen en veranderingen van deze factoren maken dat de aard en de ruimtelijke verdeling van de sedimentlagen en de korrelgroottes voor ieder bekken anders is. Een fase van actieve gebergtevorming en daarmee belasting van de aardkorst leidt tot een toename van de bodemdaling in het bekken en daarmee tot een toename van de ruimte waarin sediment kan worden opgeslagen, de accommodatie ruimte. Indien het voorlandbekken grenst aan een zee, wordt de ruimte om sediment op te slaan mede bepaald door veranderingen van de zeespiegel. De opeenstapeling van sedimentlagen in het voorlandbekken is dus een afspiegeling van de verhouding tussen en interactie van de factoren tektoniek in de vorm van groei van het gebergte en daling van de bekkenbodem en zeespiegelbewegingen.

Een klassieke benadering binnen de geologie is om op basis van de geometrie van fossiele sedimentaire afzettingen in voorlandbekkens te herleiden wat de relatieve invloed van ieder van deze factoren is geweest. Aldus wordt de geschiedenis van gebergtevorming gereconstrueerd en worden conceptuele (denk)modellen ontwikkeld. De moeilijkheid is dat de sedimentlagen niet volledig in drie dimensies kunnen worden bestudeerd en dat de geoloog conclusies moet baseren op boringen (1D), seismiek (2D) en/of veldstudies (2.5D). Verder is vaak niet duidelijk of de waargenomen geometrieën het unieke resultaat zijn van één dominante factor of van een combinatie van factoren. De verhoudingen en snelheden van de factoren, en processen die tot de sediment geometrieën hebben geleid, zijn moeilijk te kwantificeren op basis van enkel een geologische reconstructie.

## *Samenvating*

In dit proefschrift wordt een computermodel gepresenteerd waarin de genoemde factoren en de daaraan gerelateerde processen experimenteel kunnen worden gevarieerd. In het model wordt het complexe samenspel van tektoniek, zeespiegelbewegingen en sediment transport, dat zich in werkelijkheid voltrekt op een tijdschaal van miljoenen jaren, gesimuleerd in enkele dagen tot weken. Dit wordt gedaan in vele duizenden rekenstappen. De morfologische ontwikkeling van het gebergte, rivier patronen en de driedimensionale architectuur van de sedimentlagen in het voorlandbekken kunnen worden gevisualiseerd, gekwantificeerd en vergeleken met natuurlijke voorlandbekkens. Zodoende wordt een interactief en dynamisch beeld gegeven van de evolutie van een voorlandbekken systeem. Veldconcepten kunnen daarmee worden getest en aangescherpt. Met het model kunnen de driedimensionale verdeling en de volumes van grofkorrelige sedimentlichamen voor uiteenlopende geologische scenario's worden voorspeld. Grofkorrelige lichamen zijn van economisch belang vanwege hun functie als reservoir voor olie, gas en water.

Het doel van dit onderzoek is het bepalen van kenmerkende patronen in de ontwikkeling van puinwaaiers, riviergordels en de driedimensionale architectuur van de sedimentaire vulling van voorlandbekkens. In hoeverre zijn dergelijke patronen diagnostisch voor de onderlinge verhouding van de factoren pulserende tektonische activiteit en zeespiegel beweging?

### ***Drainage bekkens (Hoofdstuk 2)***

De gemodelleerde lengte-breedte verhoudingen van drainage bekkens in een actief, omhoog komend gebergte en de resulterende spatiëring van fluviaatiele puinwaaiers in het voorlandbekken zijn goed vergelijkbaar met die in echte lineaire gebergte ketens. Het cellulaire, steilste-pad-transport algoritme, dat in het model dominant actief is tijdens erosie in de drainage bekkens, geeft dus een goede representatie van de werkelijkheid. De experimenten laten zien dat deze spatiëring niet een statische eigenschap van drainage bekkens is, maar wordt beïnvloed door veranderingen in de snelheid van tektonische verplaatsing en in mindere mate door de erodeerbaarheid van het gebergte. Een grotere erodeerbaarheid resulteert in een snellere en bredere vertakking van de zich ontwikkelende drainage netwerken en in een toenemende synchronisatie van tektonische activiteit en sediment productie. Gedurende tektonische rust worden drainage bekkens in gemakkelijk te eroderen gebergtes geometrisch snel volwassen en zijn ze dicht gespatieerd. Drainage bekkens die ontstaan in moeilijker te eroderen gebergtes bereiken veel later een vergelijkbare configuratie.

De tektonische verplaatsingssnelheid van het overschuivingsfront is belangrijker voor de ontwikkeling van het drainage gebied en voor de spatiëring van de individuele drainage bekkens dan de erosiegevoeligheid.

Een snelle propagatie van het overschuivingsfront over het voorlandbekken leidt tot een omkering van de gradient in de zone direct achter de breuk. Daardoor worden kleine drainage netwerken aan het front gehinderd in hun ontwikkeling en de spatiëring van puinwaaiers in het voorlandbekken groter.



### ***Fluviatiele puinwaaiers (Hoofdstuk 2 en 3)***

Uitgezet tegen de tijd laten de sediment volumes geproduceerd in de drainagebekkens een typisch asymmetrische ‘respons curve’ zien. De volumes nemen asymptotisch toe tijdens fases van tektonische activiteit en exponentieel af tijdens tektonische rust. Volumes geproduceerd tijdens tektonische activiteit nemen weliswaar toe, maar zijn onvoldoende om de sediment-accommodatie ruimte gecreëerd door flexurele bodemdaling te compenseren. Geheel tegen de verwachting trekken daarom grofkorrelige puinwaaier afzettingen in voorlandbekkens zich terug tijdens fases van tektonische activiteit. Progradatie is daarentegen karakteristiek voor fases van tektonische rust en daarmee samenhangend afnemende flexurele bodemdaling.

Doorgaande pulserende tektonische activiteit wordt in sedimentaire sequenties in voorlandbekkens gekenmerkt door verticaal grover wordende en prograderende gravel eenheden. Deze maken zijdelings contact waar ze synchroon zijn met fases van tektonische rust. In de verticale sequentie worden de distale delen gescheiden door fijnkorrelige afzettingen die fases van hernieuwde tektonische activiteit markeren.

### ***Het axiale rivier systeem (Hoofdstuk 3)***

Afwisselingen van tektonische activiteit en fases van rust en de resulterende variaties in de toename van sediment-accommodatie ruimte zijn herkenbaar in de afzettingen van het axiale rivier systeem in het model. Progradatie van het rivier/delta systeem kenmerkt fases van tektonische rust. De progradatie snelheid van dit systeem tijdens tektonische rust is een factor 10 groter dan die van de puinwaaiers. Gedurende een overgang van tektonische activiteit naar rust wordt daarom de zone rondom de puinwaaiers eerst bezet door het axiale rivier systeem. De afzettingen daarvan worden vervolgens afgedekt door de trager prograderende puinwaaiers.

Gedurende fases van hernieuwde tektonische activiteit en bodemdaling ondervindt het voorlandbekken een mariene transgressie die in enkele duizenden jaren plaats vindt. De zee komt het eerst binnen in de zone vlak voor de puinwaaiers, waar de bodemdaling het grootst is. Een dergelijke tektonische reactivatie kan dus het best worden gedateerd op basis van de bijbehorende mariene fijnkorrelige afzettingen die de puinwaaiers afdekken.

Het axiale rivier systeem trekt zich terug onder invloed van de transgressie en neemt de vorm aan van een delta met een patroon van actief splitsende en lateraal verplaatsende riviergordels. Het verwilderde gedrag van de riviergordels is een reactie op de stijging van de relatieve zeespiegel. Het sediment kan aldus efficiënt worden verdeeld.

De experimenten in hoofdstuk 3 laten zien dat twee contrasterende sequentie overgangen worden gevormd wanneer eustatische zeespiegelbewegingen worden gesuperponeerd op pulserende fases van tektonische activiteit en bodemdaling.

A) Gedurende fases van tektonische activiteit leiden dalingen en stijgingen van de eustatische zeespiegel tot prograderende en verondiepende sequenties, begrensd door Type-2 unconformities en het daaropvolgende transgressie interval. De syn-tektonische, grote flexurele bodemdaling

## Samenvatting

verhindert dat de zeespiegel daalt tot onder het kritische niveau waar de deltatop overgaat in het deltafront. Insnijding van het deltafront door de rivier vindt daarom niet plaats.

- B) Gedurende fases van tektonische rust worden Type-1 unconformities gevormd, omdat dalingen van de eustatische zeespiegel nu wel onder het kritische niveau komen. Eustatische zeespiegel dalingen worden dan niet gecompenseerd door een stijging van de relatieve zeespiegel als gevolg van de bodemdalings component. Meerdere eustatische zeespiegeldalingen kunnen optreden tijdens een fase van tektonische rust. Daarom is het mogelijk dat de resulterende Type-1 unconformity aan de basis van de deltatop zandsteenlaag van samengestelde oorsprong is. Dit type unconformity is daarom een slechte tijdsindicator. De zandsteenlaag in de deltatop wordt gekenmerkt door clusters van in elkaar snijdende axiale rivier lichamen. Deze lichamen hebben een preferente positie tussen de puinwaaiers en de conische delta die werd gevormd tijdens een voorafgaande fase van tektonische activiteit.

### ***Dekblad-top bekken (Hoofdstuk 4)***

Vergelijkbare clusters van dergelijke amalgameerende axiale rivierlichamen worden gevormd wanneer het voorlandbekken van zijn substraat wordt gescheiden door een overschuivingsbreuk en het bekken wordt getransformeerd tot een dekblad-top bekken. In tegenstelling tot de lichamen gevormd in het asymmetrische voorlandbekken uit hoofdstuk 3, hebben deze lichamen geen duidelijke voorkeur voor een locatie dichtbij de begrenzendende overschuivingsbreuk en de daar liggende puinwaaiers. Dit komt omdat de translatie van het bekken over de hellende overschuivingsbreuk leidt tot een uniforme stijging van bekken. Verplaatsing over een licht hellende breuk ( $2-6^\circ$ ) met gemiddelde snelheden ( $\sim 5.0$  m/kyr) resulteert in een verticale opheffingscomponent die voldoende is om de flexurele bodemdaling te compenseren. De ontwikkeling van de accommodatie ruimte en de stratigrafische architectuur zijn extreem gevoelig voor de hoek van de onderliggende overschuivingsbreuk. De mate van amalgamatie, de onderlinge verbondenheid van de rivierlichamen, de snelheid van de tektonisch geforceerde regressie, de gevoeligheid voor incisie en transport van sediment naar aangrenzende bekkens nemen toe met een toename van de hoek van de onderliggende overschuivingsbreuk. In het licht van deze model resultaten wordt de Eocene Castissent Formatie in het Tremp Bekken, Spaanse Pyreneeën, die voorheen werd geïnterpreteerd als een klassiek voorbeeld van een opvulling van een ingesneden riviervallei die werd gevormd als gevolg van een daling en opvolgende stijging van de eustatische zeespiegel, verklaard als het resultaat van *tektonisch* gereduceerde accommodatie ruimte. Dit tektonische mechanisme verklaart de combinatie van doorgaande mariene invloed op de alluviale vlakte, geforceerde regressie en toenemende onderlinge verbondenheid van grove zandsteen lichamen ten koste van het aandeel fijnkorrelige afzettingen.

In het laatste hoofdstuk wordt geïllustreerd hoe, door gebruik van een triangulair in plaats van een rechthoekig grid, modellen zoals gepresenteerd in de eerdere hoofdstukken kunnen worden verbeterd en verfijnd. De capaciteit en snelheid van computers is hiervoor op dit moment nog te gering, maar zal over 5 à 10 jaar naar verwachting voldoende zijn om de modellen van een triangulair grid te voorzien.

*Samenvating*

## Dankwoord – Acknowledgements

Om te beginnen bedank ik mijn promotor Poppe de Boer voor de zijn wetenschappelijke en andere ondersteuning bij de totstandkoming van dit proefschrift, zijn snelle feedback op de manuscripten en de vrijheid waaronder ik mijn ideeën heb kunnen ontwikkelen. Het enthousiasme van mijn co-promoter Wouter Nijman en zijn overtuiging van het belang van modelstudies bij de benadering van geologische vraagstellingen heeft me altijd geïnspireerd. Wout, Tremp is een prachtig gebied en die atlas die komt er wel.

George Postma, Xander Meijer, Paul Meijer en mijn paranimfen Iwan de Lugt en Sjoukje de Vries ben ik dankbaar voor hun constructieve commentaar op de diverse versies van het manuscript en de daarop gebaseerde artikelen. Het leven in N308 met Jelmer Cleveringa, Xander Meijer, Alexander Okx en Bastian van Dijck, met alle wetenschappelijke en minder wetenschappelijke gedachtewisselingen was altijd erg gezellig. De twee *ster*studenten Maarten en Gerben hebben met de door hen aangezette discussies, programmeerwerk en de ongevraagde opsporing van voor mij onbekende bugs in de computer code een substantiële bijdrage geleverd aan dit werk. Verder veel dank aan de promovendi van de vakgroep Sedimentologie, Max van Heijst (vanavond fietsen?), Sjoukje de Vries, Aart-Peter van den Berg van Saparoea, Jan-Berend Stuut, Maarten Prins en Wessel van Kesteren voor de gezellige werkomgeving.

I thank Greg Tucker and Rafeal L. Bras for their hospitality during the working visit at MIT Parson's lab, in autumn 1999, Nicole Gasparini for answering my questions regarding the CHILD model, and Scott, Valeri and Daniel for their helpful presence in the computer lab.

De leden van de leescommissie, P.A Burrough, S.A.P.L. Cloetingh, S.B. Kroonenberg, G.E. Tucker en C.J. van der Zwan ben ik zeer erkentelijk voor hun werk en de snelle goedkeuring van het manuscript. De adviezen van Reini Zoetemeijer, Taco den Bezemer en Gert Jan Weltje in de opstartfase van dit onderzoek waren zeer nuttig. Het Camarassa team, Martyn Drury, Hans de Bresser en Jan ter Heege, bedankt voor de leuke samenwerking, de aansporingen om toch maar weer de San Salvador op te rennen en de 'allerlaatste' ultimos bij de pool van Hotel Terradets.

Ik bedank de staf van de bibliotheek en de tekenkamer en de systeembeheerders van Aardwetenschappen voor hun ondersteuning. Marnella, Marjolein, Paul en Marjan, bedankt voor de hulp en de constante aanvoer van toner cartridges, glossy paper en beschrijfbare cd-roms. Het sociale leven binnen de faculteit zorgde voor de broodnodige ontspanning in de vorm van de vrijdagmiddag struktoborrels en aangename sfeer op de sedi-paleo gang. Bedankt allemaal ! Dank aan mijn ouders, en in het bijzonder Ton Clevis voor het corrigeren van de Engelse tekst. De laatste regels van dit dankwoord zijn natuurlijk voor Saskia. Zonder haar liefde, steun, en doeltreffende hulp in iedere fase van dit onderzoek (debuggen, experimenteren, schrijven en opmaak) was dit nooit mogelijk geweest. De lange afstands wandelingen waren geweldig. Bedankt Sas!



## Curriculum Vitae

Quintijn Clevis was born on the 27<sup>th</sup> of February 1975 in Broekhuizen, the Netherlands. He attended Atheneum-B grammar school from 1987-1993 at Thomas College in Venlo. In 1993 he started his geology studies at Utrecht University. In the course of these studies he developed a strong interest for Basin Analysis and took several specialization courses in the subject. He graduated Cum Laude in 1998 after completing a field-based research project on the relationships between sedimentation and tectonics in the Archean Mosquito Creek Basin, Western Australia. In 1998 he started the Ph.D project described in this thesis. Since May 2003 he is employed as a post-doc at the School of Geography and the Environment, Oxford University, UK.



*The author of this thesis with one of his early modelling studies*